

CHAPTER TWENTY EIGHT

X-RAY ABSORPTION SPECTROSCOPY OF THE ACTINIDES

Mark R. Antonio and Lynda Soderholm

28.1	Introduction	3086	28.4	Future direction	3183
28.2	The terrestrial aquatic environment	3095		Acronyms, abbreviations, and symbols	3184
28.3	Sorption studies	3140		References	3186

28.1 INTRODUCTION

The recent availability of synchrotron radiation has revolutionized actinide chemistry. This is particularly true in environmental studies, where heterogeneous samples add to the already multifaceted chemistry exhibited by these ions. Environmental samples are often inhomogeneous, chemically diverse, and amorphous or poorly crystalline. Even surrogates prepared in the laboratory to simplify the natural complexity are plagued by multiple oxidation state and varied coordination polyhedra that are a reflection of inherent 5f chemistry. For example, plutonium can be found as Pu^{3+} , Pu^{4+} , $\text{Pu}(\text{v})\text{O}_2^+$, and $\text{Pu}(\text{vi})\text{O}_2^{2+}$ within naturally occurring pH–Eh conditions, consequently complex equilibria are found between these oxidation states in one solution. In addition, dissolved actinides have significant affinities for various mineral surfaces, to which they can adsorb with or without concomitant reduction–oxidation (redox) activity, depending on details of the solution and surface conditions.

A molecular level understanding of this diverse chemistry is necessary if predictive modeling of the fate and transport of these biohazardous ions is to be attained. Synchrotron studies are rapidly becoming a workhorse in the effort to chemically characterize 5f, actinide pollutants, their speciation, and their complexation at a molecular level. Synchrotrons are proving ideal for the task for several reasons: (1) they provide a high flux of tunable, high-energy

radiation; (2) highly focused beams allow for small (<1 mg) sample sizes; (3) the energy range permits excitation of the M- and L-adsorption edges of the actinides; (4) the penetrating nature of X-rays allows sample encapsulation and containment; and (5) a wide variety of spectroscopy, scattering, and imaging experiments are available.

Most of the synchrotron studies published to date have focused on X-ray absorption spectroscopy (XAS). This technique has found widespread use as a speciation probe for several reasons: (1) it is a single-ion probe that can be used to study one element from a complex mixture; (2) it is sensitive to both the oxidation state and to the coordination environment of the ion, and (3) it can be used for solution, surface, or solid samples. As a result, XAS has been able to answer a variety of important fundamental chemistry questions about actinide speciation in solution and in the solid-state that have direct relevance to environmentally germane problems. Very recent trends indicate that these studies will expand to include other X-ray techniques and that more studies will focus on transuranics as the scientific community becomes more aware of the vast potential of synchrotron radiation as a molecular-level probe.

XAS itself is often artificially divided into two experiments, X-ray absorption near-edge structure (XANES), and extended X-ray absorption fine structure spectroscopy (EXAFS) because of the two different modes employed for analyses (Koningsberger and Prins, 1988; Bertagnolli and Ertel, 1994; Zubavichus and Slovokhotov, 2001). From a practical perspective they both arise from the same response about an absorption edge as a function of energy, as shown in Fig. 28.1. The absorption about the edge, or XANES data, provides information about the valence of the central ion by comparison to standards of known oxidation states. Often there is a shift of the absorption edge to higher energy that can be correlated to an increase in valence. This shift can be quite pronounced, as seen for example in Fig. 28.2a for Eu, which shows a 8 eV difference in absorption energy between Eu^{2+} and Eu^{3+} (Antonio *et al.*, 1997; Rakovan *et al.*, 2001). Shifts with oxidation state are often less definitive for the actinides and are complicated by the significant change in coordination environment that occurs in the 4+/5+ couple with the formation of the actinyl ion for U–Am (Ankudinov *et al.*, 1998; Conradson *et al.*, 1998; Antonio *et al.*, 2001) as shown in Fig. 28.2b. The dioxo coordination manifests itself as a predominant shoulder on the high-energy side of the absorption edge (Hudson *et al.*, 1995a) and a shift to somewhat lower energy (Soderholm *et al.*, 1999). This feature is even more enhanced for tetraoxo coordination, as seen in $[\text{Np}(\text{VII})\text{O}_4]^-$ (Williams *et al.*, 2001) and demonstrated in Fig. 28.2c. Therefore, although XANES is primarily used for determining oxidation states, in specific situations it can be used to infer something about the absorbing ion's coordination environment.

Detailed coordination information is determined by fitting the EXAFS oscillations above the absorption edge (Lee *et al.*, 1981; Teo, 1986; Filipponi, 2001). The discovery of EXAFS was made in the 1920s (Lytle, 1999); however, it was

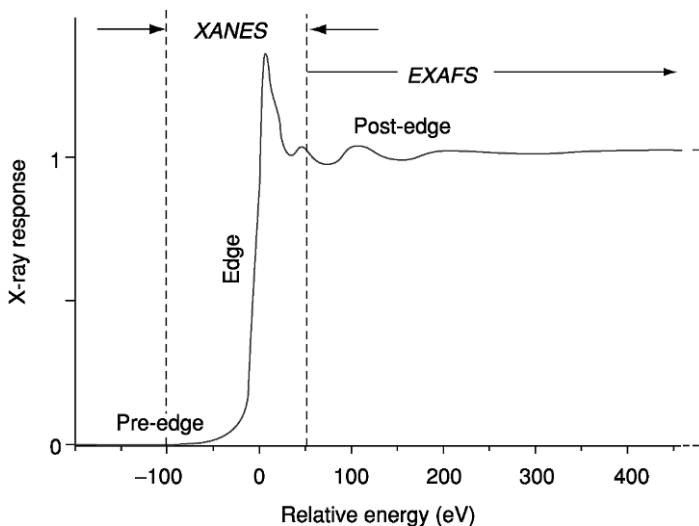


Fig. 28.1 A X-ray absorption spectrum after background subtraction and normalization. The XANES region is usually considered to be the data from about 100 eV below the absorption edge to about 50 eV above the edge. The higher-energy data are considered to be the EXAFS spectrum. This distinction is somewhat arbitrary and reflects the different methods used to analyze the data. The XANES are considered to be electronic in origin and are often plotted as their derivative in order to clearly define the absorption edge for use in oxidation state assignment. The EXAFS data are re-configured into momentum space (\AA^{-1}) (Teo, 1986) and then may be Fourier transformed to obtain a real-space (\AA) spectrum. Data are fit for distances from the central absorbing ion and number of coordinating ligands using either k -space or FT data, as shown in Fig. 28.3.

not until the 1970s that three pivotal developments set the foundation for the practice and acquisition of EXAFS. The first was the direct application of Fourier transform (FT) analysis to invert experimental data to obtain structural information about the near-neighbor coordination environment of a selected absorbing element in amorphous and crystalline materials alike (Sayers *et al.*, 1971). The second was the advent of intense synchrotron radiation of X-ray wavelengths that immensely facilitated the collection of data. Throughout the past three decades, the unique properties of synchrotron radiation available at some 30 operational facilities (as of 2003) throughout the world (Winick and Nuhn, 2003) has been exploited for EXAFS experiments that would be impossible to perform with conventional sources of x-radiation.

One important property – polarization – of the synchrotron radiation, was exploited for what was the first publication (Templeton and Templeton, 1982) about X-ray experiments with an actinide-bearing material, rubidium uranyl nitrate, $\text{RbUO}_2(\text{NO}_3)_3$, at a synchrotron facility. U L_{3-} and L_{1-} edge XANES

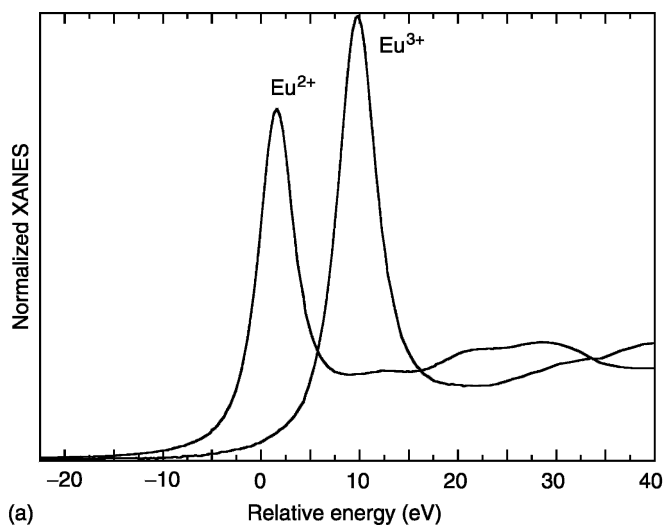


Fig. 28.2 (a) *Eu L₃-edge XANES demonstrating the 8 eV difference between the divalent and trivalent absorption maximum. Less obvious from the spectra is the slightly different FWHMs and integrated intensities of the two spectra, which is important to take into account when determining relative oxidation states from XANES (Antonio et al., 1997; Newville et al., 1999).*

data were acquired for a single-crystal with the electric vector of the linearly polarized synchrotron radiation both parallel and perpendicular to the linear, *trans*-dioxo uranyl {O–U–O} axis. At the time, the interpretation of the ‘substantial dichroism’ effects posed “...a challenge which we hope will stimulate further theoretical work” (Templeton and Templeton, 1982). This theoretical challenge, and the third pivotal development of EXAFS, was largely met in the 1990s with the release of the general-purpose XAS *ab initio* code known as FEFF (de Leon *et al.*, 1991; Rehr *et al.*, 1991, 1992; Zabinsky *et al.*, 1995). The theoretical algorithms available with FEFF6 were first brought to bear upon spectroscopic features in U L₃-edge XANES of oxides and intermetallics (Hudson *et al.*, 1995a). Together with other results, this benchmark study established the origin – a localized multiple-scattering resonance attributable to the linear [O=U=O]²⁺ group – of the absorption resonance observed some 15 eV above the U edge peak in uranyl fluoride, UO₂F₂, in particular, and for uranyl compounds, in general. The calculations provided the initial successful interpretation of the substantial linear X-ray dichroism effects observed some 13 years earlier in the original U L₁- and L₃-edges XANES (Templeton and Templeton, 1982) and the subsequent U L₃-edge XANES and EXAFS of uranyl acetate dihydrate, [UO₂(OOCCH₃)₂] \cdot 2H₂O (Hudson *et al.*, 1996).

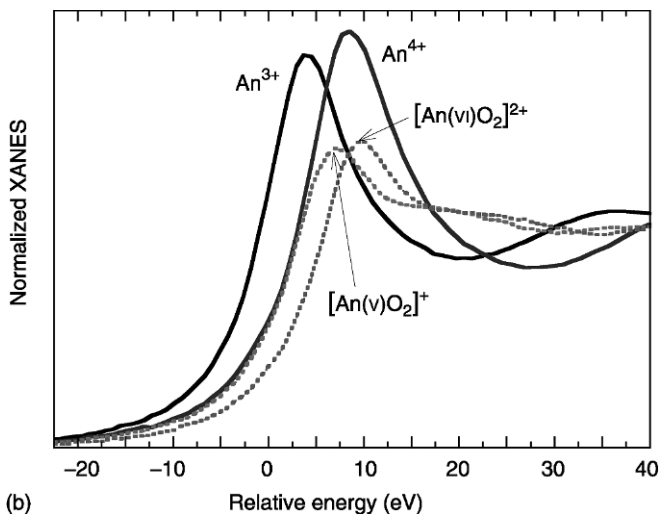


Fig. 28.2 (b) Representative XANES data as a function of oxidation state and coordination environment. The trivalent and tetravalent spectra show about a 4 eV difference in the edge energy, as do the pentavalent and hexavalent dioxo moieties. However, a comparison of tetravalent with pentavalent dioxo spectra show very small, sometimes negative shifts in the edge energies, as shown. In addition, the shapes of the spectra are different. The trivalent and tetravalent species tend to have a larger white-line feature whereas the dioxo coordination of the higher oxidation states produces multiple-scattering that results in the shoulder to higher energy of the edge peak itself (Hudson et al., 1995a).

Today EXAFS is widely used to determine the coordination environment of an actinide in a non-crystalline sample. All measurements of the EXAFS response, including the use of both primary (e.g. transmission, fluorescence, electron-yield) and secondary (e.g. optical luminescence, ion-yield, photoconductivity, photoacoustic) detection schemes, are made as a function of incident X-ray energy, E , in electron volts. Following a number of data reduction treatments, the EXAFS signal, χ , is plotted as a function of the photoelectron wave vector k (\AA^{-1}), which is obtained according to:

$$k = \frac{2\pi}{\lambda_e} = \sqrt{\frac{2m}{\hbar^2}(E - E_0)} = \sqrt{0.263(E - E_0)} \quad (28.1)$$

Here, E_0 is the experimental energy threshold chosen to define the energy origin of the EXAFS spectrum in k -space. That is, $k = 0 \text{ \AA}^{-1}$ when the X-ray energy E equals E_0 , and the photoelectron of wavelength λ_e has no kinetic energy. Examples of representative data, $\chi(k)$ vs k , and their corresponding FTs are shown in Fig. 28.3. Under favorable conditions, the number, distance, and identity of the coordinating ion can be determined and, together with XANES

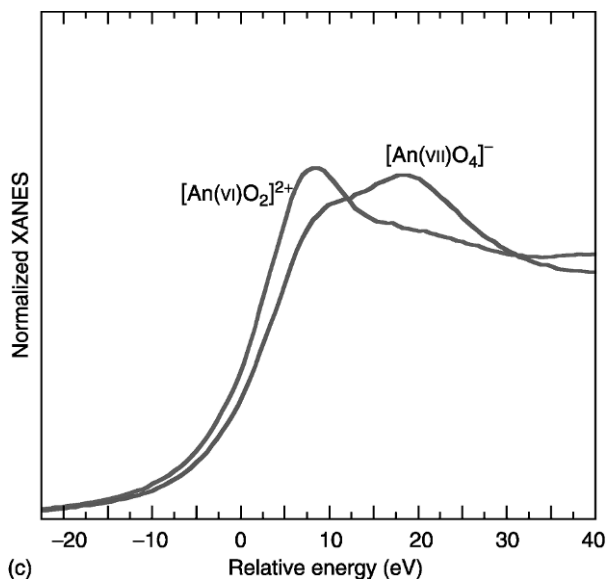


Fig. 28.2 (c) A comparison of XANES spectra from an An(VI) dioxo-coordinated ion with that of a tetraoxo An(VII)-coordinated ion. The increased shoulder intensity for the latter coordination is presumed to arise from an increased number of multiple-scattering pathways.

data, provide metrics on actinide-ion speciation. FEFF plays a very important role by providing element-specific phase and amplitude functions, thereby eliminating the need for obtaining these quantities from standard compounds. Until FEFF was in common use, the need for standard compounds to study actinides was a significant problem because of the very limited number of transuranic compounds with well-known structures and because of the radically different coordination environments, including dioxo coordination, which was difficult to resolve well enough experimentally to obtain adequate independent phase and amplitude functions.

In most cases, non-linear least squares minimization techniques are applied to fit the EXAFS or FT data with a semiempirical, phenomenological model of short-range, single-scattering according to (Teo, 1986):

$$\chi(k) = S_0^2 \sum_{i=1}^n \frac{N_i F_i(k, r_i)}{k r_i^2} \exp(-2k^2 \sigma_i^2) \exp\left(\frac{-2r_i}{\lambda_e(k)}\right) \sin(2kr_i + \varphi_i(k, r_i) + \varphi_c(k)) \quad (28.2)$$

The backscattering amplitude, $F_i(k, r_i)$, and phase, $\varphi_i(k, r_i)$, as well as the central atom phase, $\varphi_c(k)$, are typically obtained from the FEFF and used as input for the iterative refinement procedures. An overall amplitude reduction

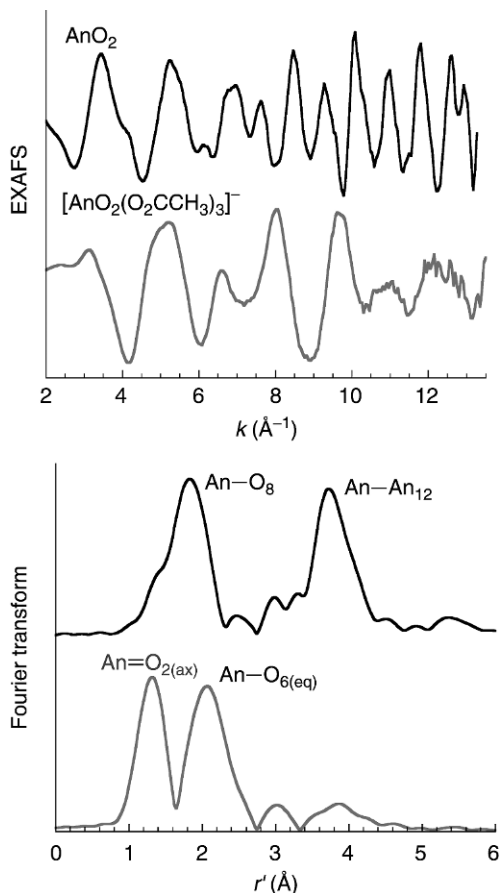


Fig. 28.3 Representative L_3 EXAFS data comparing tetravalent and dioxo-hexavalent absorbers. Data are plotted as $k^3\chi(k)$, and their corresponding Fourier transforms (FTs) for a tetravalent oxide, AnO_2 , and a hexavalent actinyl absorber with acetate ligation, $[AnO_2(O_2CCH_3)_3]^-$. The FT data for the dioxide shows a single peak at 1.83 Å (before phase shift correction) due to O backscattering, whereas the dioxo complex anion shows two strong peaks due to O at 1.32 and 2.07 Å (before phase shift correction) that are diagnostic of the axial (ax) and equatorial (eq) backscattering, beyond which there is little response. In contrast, the strong, distant peak at 3.73 Å (before phase shift correction) observed in the FT data for the dioxide is diagnostic of An–An backscattering.

factor, S_0^2 , is normally a fixed input parameter too. The exponential term that includes the photoelectron mean free path, $\lambda_e(k)$, is not explicitly used for a standard analysis. The three principal structure parameters obtained from the fitting include the coordination number, N_i , interatomic distance, r_i , and the Debye–Waller factor, σ_i , for each of the i -th scattering shells about the central absorbing ion out to about 4 Å. An energy scale (ΔE_0) parameter is also fitted to

account for differences between the experimental and theoretical values of E_0 . The distances and energy scale both depend on the period of EXAFS oscillations and are therefore correlated, as are the coordination number and Debye–Waller factor, which both depend on the amplitude of the oscillations. The number of parameters that can be determined from a data set, N_p depend on the k - and r -ranges over which the data are fit, and can be calculated according to: $N_p = 2\Delta k \Delta r / \pi$ (Teo, 1986). A rule-of-thumb error estimate is that the fitted distances are precise to about $\pm 1\%$ whereas the coordination numbers can be quoted to ± 1 .

It has been understood for some time that correlations exist between the bond distance, coordination number, and oxidation state for a metal species, M^{n+} . A quantitative, electrostatic model for coordination environments in complex ionic solids was proposed in 1929 (Pauling, 1929). Improvements in X-ray diffraction techniques have allowed significant refinement of this original model, and the development of an empirical correlation between valence and the length of a bond (Brown, 1981, 1987, 2002). This correlation, built up by examining the published X-ray structures now available, has been approximated by a simple, two-parameter expression for the experimental bond-valence, S_{ij} :

$$S_{ij} = \exp\left(\frac{R_0 - R_{ij}}{B}\right)$$

where R_{ij} is the distance between atoms i and j . R_0 is an empirically derived parameter, determined such that it represents the length of the bond of unit valence. Its value is dependent on the two ions involved in the bond, and has been tabulated for a variety of bond pairs (Brown, 1996, 2002). Unless otherwise noted, B is generally assumed to be very close to 37 pm. The valence sum rule:

$$V_i = \sum S_{ij}$$

states that the sum of the experimental bond-valences around i th atom is equal to the atomic valence (Brown, 2002). In this way, the bond distance, coordination number, and metal-ion valence can all be correlated.

This concept has been nicely realized for the hexavalent uranyl ion (Burns *et al.*, 1997), for which Brown's R_0 and B parameters have been established from a wide range of X-ray single-crystal structural refinements. A representative plot of bond-valence sum (BVS) versus bond distance is shown in Fig. 28.4, for which the BVS for hexavalent U has been optimized to six. These results can be used in several ways, including confirmation of a coordination number from EXAFS data when a bond distance has been determined. This concept is a useful added tool because the coordination numbers are often not adequately determined from EXAFS alone to answer a question in hand. Likewise, confirmation of oxidation state can come from correlations between bond distances

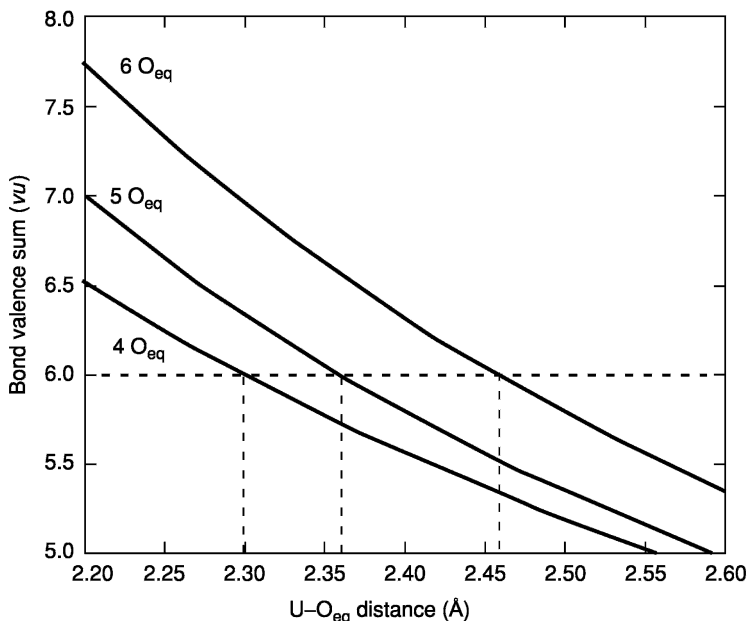


Fig. 28.4 Bond-valence sums (Brown, 2002) calculated for the uranyl(VI) ion with ligating oxygen ions. Parameters used in the calculation (Burns et al., 1997) were derived from an extensive analysis of available single-crystal structures. Whereas $O=U=O$ bonds are seen to be invariant to changes in coordination environment, the distances to the O_{eq} are seen to be dependent on the number of coordinating ions in the equatorial plane. For $U(VI)O_2^{2+}$ the average bond distances are 2.29(5), 2.37(9), and 2.47(12) Å for 4, 5, and 6 equatorial ligation. These distances can be compared with those obtained from fitting EXAFS data to support a determination of the equatorial coordination environment. Unfortunately, the good quality, single-crystal X-ray structural data necessary to determine a similar plot for transuranic ions is not currently available.

and XANES data. Interpretation of the XAS data can be further checked by comparison with a variety of published data on similar systems. Published compendia of XAS spectra and analyses for a variety of Th- and U-containing mineral and related phases facilitate these comparisons (Farges, 1991; Thompson *et al.*, 1997; Hanchar, 1999). Unfortunately, the use of well-established trends in bond distances and oxidation states or coordination numbers for transuranic studies is limited by the paucity of well-determined single-crystal structures for these ions.

XAS is a single-ion probe that can be tuned to an energy that selects the absorption edge of an ion of interest, an essential attribute when studying an ion's speciation in chemically complex samples. Unfortunately, the spectrum that is obtained is the sum of all the oxidation states and coordination

environments that occur in the sample. This can be particularly problematic for actinide-containing samples in which multiple redox states and coordination environments often occur within one sample. Although difficult to ascertain from simple data analysis, there are two recent developments that are proving to be powerful tools to assess and overcome this problem. The increased brightness afforded by the newer generation synchrotrons has made microsynchrotron-X-ray fluorescence (μ -SXRF) particularly valuable for examining inhomogeneous natural samples. The utility of this technique was clearly demonstrated in seminal experiments examining Pu speciation when adsorbed onto natural tuff samples (Duff *et al.*, 1999a). The results of the experiments demonstrated that Pu was preferentially associated with Mn phases, as opposed to Fe-bearing phases as had been hypothesized, and that some of the Pu had been oxidized. The observation of Pu in multiple oxidation states, and its association with Mn phases were made possible by the use of a very small, focused beam. The second development is the application of principal component analysis (PCA) to XAS data (Wasserman, 1997; Wasserman *et al.*, 1999). PCA can be used on a series of data to determine how many different independent species are required to account for all of the spectra. This mathematical approach provides an estimate of the number of species present in the samples, information that is not otherwise available. Together with model compound spectra, PCA can suggest which of a variety of chemically possible species are present in different samples.

This chapter presents an overview of synchrotron studies on actinide species in environmentally relevant samples. The discussion is organized into solution studies in aqueous acid and base media, sorption studies onto mineral, natural soil, and bacterial surfaces. With the exception of selected experiments on μ -SXRF, almost all of the work has involved XAS studies.

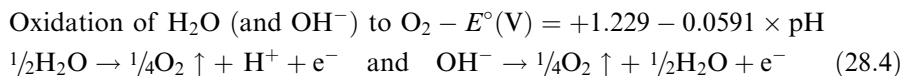
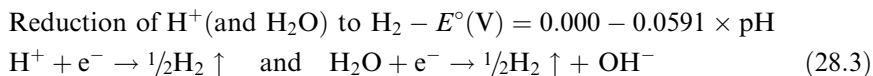
28.2 THE TERRESTRIAL AQUATIC ENVIRONMENT

Since the discovery of the anthropogenic transuranium elements in the 1940s to 1950s, massive efforts have been directed at preventing the despoliation of the environment, particularly the ground- and surface-water supplies, fresh and saline alike, with radionuclide ions. Because of the legacy of the Cold War, the fate and migration of actinide (An) ions presently in the geosphere is a subject of intense interest (Lieser, 1995; Silva and Nitsche, 1995; Nitsche, 1997; Sterne *et al.*, 1998). In terms of its sheer abundance and essentially isotropic distribution on Earth, water is viewed as the principal dispersant of radionuclide pollution. Moreover, because potable water is vital to humanity and all its activities, especially agriculture and aquaculture, fundamental research about An speciation in aqueous media is of historical and contemporary significance.

From a science perspective too, water is the single-most important system with dual benchmark properties of solvent and coordinating ligand. Insofar as both hydration and coordination influence reactivity as well as spectro- and electrochemical responses of 5f-ions in aquatic environments, information about An aquo ions is pivotal to a thorough and predictive understanding of basic chemical phenomena involving migration, absorption, solvation, complexation, exchange, electron transfer, and hydrolysis behaviors, just to name a few, pertinent to hydrologic and geochemical processes. By comparison with the extent of knowledge about An oxidation states and their well-known redox activity (Morss, 1994), metrical details about the coordination of water with the trans-uranium elements are generally sparse. Despite the availability of potential-pH (Pourbaix) equilibrium diagrams for Th, U, Np, Pu, and Am in aqueous solutions at 25°C (Pourbaix, 1974), these do not provide quantitative information about bond lengths and coordination numbers as a function of oxidation state, the so-called An redox speciation. Nor do these diagrams apply to ligands other than H_3O^+ , H_2O , and OH^- , and no diagrams are available to describe the redox equilibrium behavior of Ac, Pa, and the trans-Am elements in aqueous solution.

To build a foundation for a thorough understanding of An redox speciation in aqueous media containing environmentally relevant ligands that are known An complexants, e.g. HCO_3^- , CO_3^{2-} , Cl^- , NO_3^- , and SO_4^{2-} , it is first important to understand the structure of the pure molecular An aquo ions and the nature of the An-OH₂ interactions in each of their accessible oxidation states without other interference. In order to suppress and eliminate possible complicating effects of hydrolysis, disproportionation, oligomerization, precipitation, etc., experiments have been routinely performed at low pH in aqueous non-complexing mineral acids. Perchloric acid is the system of choice because the ClO_4^- anion does not participate in direct, inner-sphere interactions with An ions, thereby providing immediate access to the hydrated An species in the absence of competitive binding effects.

Within the domain of the thermodynamic stability of water, which consists of a small (1.229 V) polarization window (Bratsch, 1989), all An electrochemical equilibria are limited by the pH-dependent reduction and oxidation of water itself. Under standard conditions at 25°C that include no complexing ions and 1 atm partial pressures of H_2 and O_2 , the potential limits of water with respect to the standard hydrogen electrode (SHE) are imposed by the following reactions:



The linear and parallel potential, E° (V), dependencies for the reactions (28.3) and (28.4) as a function of pH are conveniently visualized in the Pourbaix diagrams for all elements from $Z=1$ to 95 (Am) such as is illustrated in Fig. 28.5 for Fe. As can be seen from Table 28.1, there are a number of solution-stable An species under both acid and alkaline conditions that exhibit redox activity within the electrochemical window afforded by water. In fact, some transuranium ions, notably Np and Pu, are known to have a remarkable variety of solution species as well as intricacies and ambiguities of valence with five accessible oxidation states – III, IV, V, VI, and VII. In this regard, electrochemical research has played a central role in the advancement of actinide science. And, in the field of equilibrium electrochemistry, the cornerstone of all practical, thermodynamic applications of electroanalytical techniques, e.g. potentiometry and polarography, is the Nernst equation (28.5). (Archer, 1989):

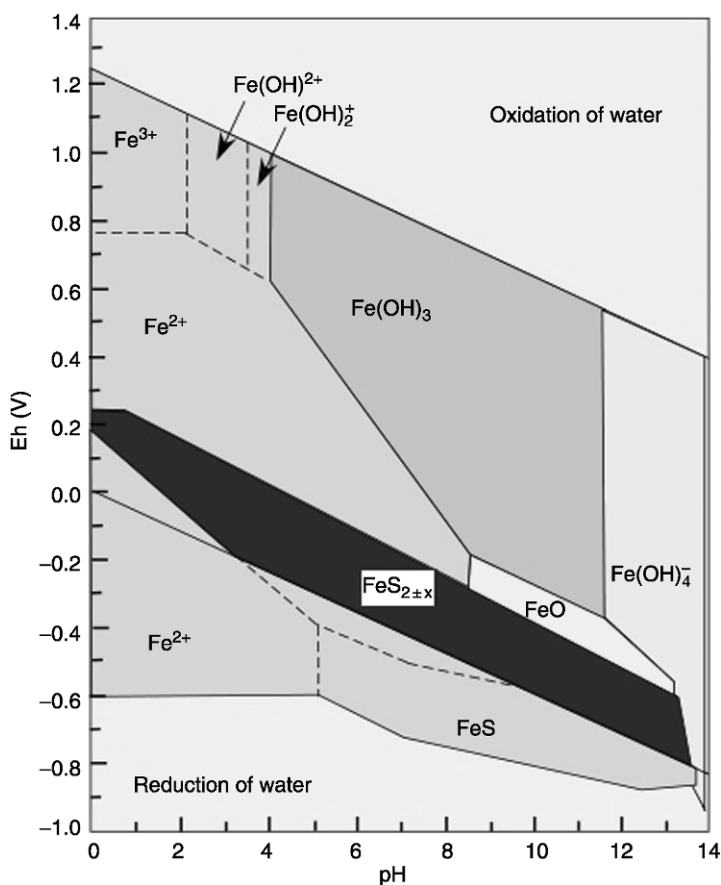


Fig. 28.5 The complex behavior of iron in an aqueous environment, showing both changes in oxidation state and ligation as a function of solution Eh and pH (Hem, 1985).

Table 28.1 The standard reduction potentials (E° , V vs SHE) for some one- and two-electron half-reactions of selected ions. The more positive the potential, the more favored the reaction as written. Except where noted, all values are from Bratsch (1989).

Reduction half-reaction couples	E°
acid solutions	
$\text{U}^{4+} + \text{e}^- \rightarrow \text{U}^{3+}$	-0.577
$\text{Eu}^{3+} + \text{e}^- \rightarrow \text{Eu}^{2+}$	-0.35
$\text{H}^+ + \text{e}^- \rightarrow \frac{1}{2}\text{H}_2\uparrow$	0.0000
$\text{Np}^{4+} + \text{e}^- \rightarrow \text{Np}^{3+}$	+0.157
$\text{CO}_2\uparrow + 8\text{H}^+ + 8\text{e}^- \rightarrow \text{CH}_4\uparrow + 2\text{H}_2\text{O}$	+0.1694
$[\text{UO}_2]^{2+} + 4\text{H}^+ + 2\text{e}^- \rightarrow \text{U}^{4+} + 2\text{H}_2\text{O}$	+0.273
$[\text{NpO}_2]^+ + 4\text{H}^+ + \text{e}^- \rightarrow \text{Np}^{4+} + 2\text{H}_2\text{O}$	+0.567
$\text{Fe}^{3+} + \text{e}^- \rightarrow \text{Fe}^{2+}$	+0.771
$\text{Hg}^{2+} + 2\text{e}^- \rightarrow \text{Hg}\downarrow$	+0.852
$[\text{PuO}_2]^{2+} + \text{e}^- \rightarrow [\text{PuO}_2]^+$	+0.966
$[\text{PuO}_2]^{2+} + 4\text{H}^+ + 2\text{e}^- \rightarrow \text{Pu}^{4+} + 2\text{H}_2\text{O}$	+1.000
$[\text{PuO}_2]^+ + 4\text{H}^+ + \text{e}^- \rightarrow \text{Pu}^{4+} + 2\text{H}_2\text{O}$	+1.035
$\frac{1}{4}\text{O}_2\uparrow + \text{H}^+ + \text{e}^- \rightarrow \frac{1}{2}\text{H}_2\text{O}$	+1.2291
$[\text{NpO}_2]^{2+} + \text{e}^- \rightarrow [\text{NpO}_2]^+$	+1.236
$\text{Bk}^{4+} + \text{e}^- \rightarrow \text{Bk}^{3+}$	+1.67
$\text{Ce}^{4+} + \text{e}^- \rightarrow \text{Ce}^{3+}$	+1.72
alkaline solutions	
$\text{H}_2\text{O} + \text{e}^- \rightarrow \frac{1}{2}\text{H}_2\uparrow + \text{OH}^-$	-0.8280
$[\text{SO}_4]^{2-} + 8\text{e}^- + 5\text{H}_2\text{O} \rightarrow \text{SH}^- + 9\text{OH}^-$	-0.683
$[\text{Fe}(\text{OH})_4]^- + \text{e}^- \rightarrow [\text{Fe}(\text{OH})_4]^{2-}$	-0.68
$[\text{NpO}_2(\text{OH})_4]^{2-} + \text{e}^- \rightarrow [\text{NpO}_2(\text{OH})_4]^{3-}$	+0.17 ^a
$[\text{PuO}_2(\text{OH})_4]^{2-} + \text{e}^- \rightarrow [\text{PuO}_2(\text{OH})_4]^{3-}$	+0.27 ^a
$\frac{1}{4}\text{O}_2\uparrow + \frac{1}{2}\text{H}_2\text{O} + \text{e}^- \rightarrow \text{OH}^-$	+0.4011
$[\text{NpO}_4(\text{OH})_2]^{3-} + 2\text{H}_2\text{O} + \text{e}^- \rightarrow [\text{NpO}_2(\text{OH})_4]^{2-} + 2\text{OH}^-$	+0.58
$[\text{PuO}_4(\text{OH})_2]^{3-} + 2\text{H}_2\text{O} + \text{e}^- \rightarrow [\text{PuO}_2(\text{OH})_4]^{2-} + 2\text{OH}^-$	+0.95

^a From (Shilov, 1998).

$$E_p = E^{\circ'} + \frac{RT}{nF} \ln \frac{[\mathfrak{R}_{\text{ox}}]}{[\mathfrak{R}_{\text{rd}}]} \quad (28.5)$$

Derived in 1888 by W. H. Nernst (1864–1941), his eponymous equation establishes the equality between an electrode potential, E_p , and the formal electrode potential, $E^{\circ'}$, which is a thermodynamic value, for a redox reaction, such as shown in Table 28.1, under any conditions of pH, electrolyte, ionic strength, etc. In general, for a reversible electrode couple involving n electrons, as illustrated by equation (28.6), the extent of the forward and reverse redox reactions can be manipulated by the application of an applied potential in the vicinity, typically ± 0.20 V, of $E^{\circ'}$:



Through measurement of the solution concentrations of both the oxidized and reduced ions, $[\mathcal{R}_{\text{ox}}]$ and $[\mathcal{R}_{\text{rd}}]$, respectively, at a series of selected potentials, a so-called Nernst plot can be prepared in the form of E_p vs $\ln([\mathcal{R}_{\text{ox}}]/[\mathcal{R}_{\text{rd}}])$. An example of a Nernst plot for the one-electron reaction of equation (28.7) for the neptunium redox couple is shown in Fig. 28.6:



For this so-called Nernstian process, meaning that the reaction (28.7) is thermodynamically reversible, wherein the reactant, Np^{4+} , and electrogenerated product, Np^{3+} , maintain equilibrium concentrations at the electrode surface with variation of E_p , a linear plot results. The x -axis intercept is obtained when $[\mathcal{R}_{\text{ox}}]=[\mathcal{R}_{\text{rd}}]$ and provides the formal potential, $E^{\circ'}$. The slope, RT/nF , of the plot provides the number of electrons, n , transferred in the redox reaction. For measurements at room temperature, $T=298.15$ K, it is a matter of convenience to simplify equation (28.5) with numerical substitutions for the constants, where R is the universal gas constant, 8.314570 J K⁻¹ mol⁻¹, and F is the Faraday constant, 96485 C mol⁻¹, and by conversion from the natural logarithm, \ln , to the common logarithm, \log , as shown in the following equation:

$$E_p = E^{\circ'} + \frac{0.05915}{n} \log \frac{[\mathcal{R}_{\text{ox}}]}{[\mathcal{R}_{\text{rd}}]} \quad (28.8)$$

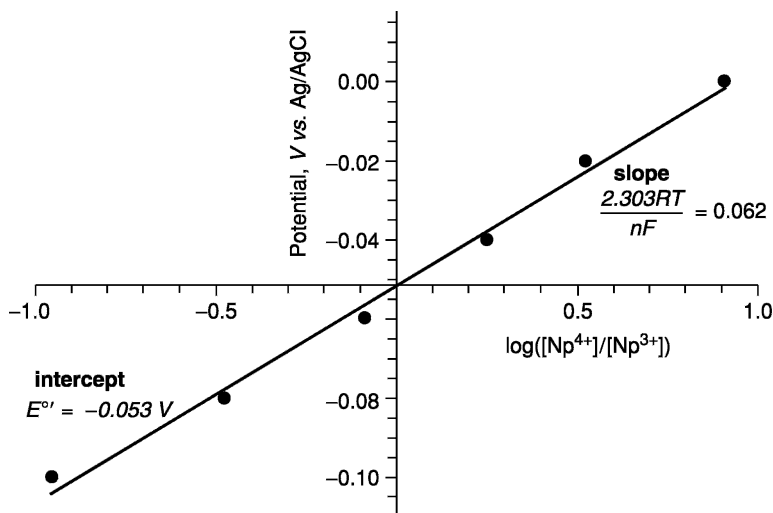


Fig. 28.6 Nernst plot for the $\text{Np}^{4+}/\text{Np}^{3+}$ redox reaction (28.7). The experimental data (circles) were obtained through use of XANES spectroelectrochemistry. (Soderholm et al., 1999) The linear least-squares fit shown as a line ($R^2 = 0.994$) provides a slope that corresponds to a 1 e^- couple, and an intercept of -0.053 V, which compares favorably with published values (Cohen and Hindman, 1952; Riglet et al., 1989; Li et al., 1993).

In the plot of Fig. 28.6, the relative concentrations of the oxidized and reduced Np species were determined by use of XANES spectroscopy (Soderholm *et al.*, 1999). Optical, vibrational, and nuclear magnetic resonance (NMR) probes of concentration are more typically employed in experimental combinations of spectroscopy and electrochemistry, shortened to spectroelectrochemistry in common usage, than are X-ray techniques (Gale, 1988). Regardless of the method, a range of controlled electrochemical potentials must be selected at which the forward and reverse reactions provide sufficient concentration variations of admixtures of \mathcal{R}_{ox} and \mathcal{R}_{rd} to perform a Nernst analysis. A typical abscissa range extends between log values of -1 and $+1$, corresponding to concentration ratios, $[\mathcal{R}_{\text{ox}}]/[\mathcal{R}_{\text{rd}}]$, of $1/10$ and $10/1$, respectively.

In 1980, XAS, consisting of the methods of XANES and EXAFS, was first brought to bear upon the issue of An speciation in aqueous solutions. This section contains a review of the results published since then for the An aquo species of Th and U–Cf, inclusive (there are no published reports for Ac, Pa, Es, and beyond) with particular emphasis on hydration numbers and inner-sphere An–O interatomic distances with the neutral water molecule. The results are discussed in Section 28.2.2. The interactions of An ions in solution and as solid-state complexes with anionic ligands of mono- and multidentate organic anions are treated separately in Section 28.3.4.

28.2.2 Acid redox speciation

Because of their high charge, small size, and oxophilicity, the 5f-elements are especially prone to hydrolysis reactions and precipitation in neutral and alkaline media. Their solubility and stability in aqueous acid media of $\text{pH} \leq 2$ facilitates spectroscopic research, especially the EXAFS work reviewed here whose origins can be attributed to the study of what is now considered to be a concentrated (0.2M) hexavalent U sample dissolved in 0.2M HNO_3 (Karim *et al.*, 1980). The L_3 -edge EXAFS was acquired with a rotating anode X-ray source and, despite the low signal-to-noise (S/N) quality, provided ‘striking’ information about the uranyl moiety, $[\text{UO}_2]^{2+}$, in solution. The two resolved peaks of the FT data, which are immediately recognized in modern EXAFS research, were attributed to a combination of backscattering from the O nearest atoms of the linear *trans*-dioxo cation, $[\text{O}=\text{U}^{6+}=\text{O}]^{2+}$, and the next-nearest O atoms of an equatorial arrangement of ligands typical of a hydrolysis complex or, alternatively, the H_2O molecules of a hydration shell. The comparison of the solution FT with that for crystalline UO_2F_2 (a known structure) confirmed the existence of the ‘ubiquitous’ uranyl group upon dissolution of the solid. At the time in 1980, the theoretical central atom phase function for U was not available. As a result, the functions of Teo and Lee (1979) were extrapolated to simulate the U L_3 $k\chi(k)$ EXAFS with two O atoms at 1.77 \AA and five O atoms at 2.38 \AA . As shown in Table 28.2, these distances, especially that for the close O atoms of the

Table 28.2 Uranium redox speciation for $U(III)$, $U(IV)$, $U(V)$, and $U(VI)$. For the spherical ions, the hydration numbers (n , n' , coordinated H_2O) and $U-OH_2$ interatomic distances are listed. For the uranyl ions, the axial (ax.) oxygen coordination numbers and $U=O$ distances precede the equatorial (eq.) hydration numbers (n'' , n''') and the $U-OH_2$ bond lengths. Estimated standard deviations, where available, are obtained from the primary sources and are given after the \pm sign or within parentheses.

Aquo ion	CN, O/ H_2O	Distance(s)	Technique/Conditions	References
$U(III) \cdot nH_2O$	8,7(9)	2.56(1)	EXAFS/1 M HCl	David <i>et al.</i> (1998)
$U(IV) \cdot n'H_2O$	8	nd ^a	Optical/ ≤ 6 M HNO_3 ; organic-1 M HNO_3 (aq.) mixtures	Rykov <i>et al.</i> (1973); Vasil'ev <i>et al.</i> (1974)
	5.9 – 10.1	2.419–2.519	X-ray scattering/1 M $HClO_4$	Pocev and Johansson (1973)
	9.4 \pm 1.1	2.42	EXAFS/pH = 2	Charpin <i>et al.</i> (1985)
	11.0 \pm 0.8	2.39	EXAFS/1.5 M $HClO_4$	Moll <i>et al.</i> (1998)
	10 \pm 1	2.42(1)	EXAFS/1.5 M $HClO_4$	Moll <i>et al.</i> (1999)
	2 ax. O + 4.5 eq. H_2O	nd	geometric modeling	Mauerhofer <i>et al.</i> (2004)
$[U(V)O_2]^{2+} \cdot n''H_2O$	2 ax. O + 5 eq. H_2O	1.77, 2.38	EXAFS/0.2 M HNO_3 ^c	Karim <i>et al.</i> (1980)
$[U(VI)O_2]^{2+} \cdot n'''H_2O$ ^b	2 ax. O + 5 eq. H_2O	nd	Optical MCD/ H_2O	Görller-Walrand and Colen (1982)
	2 ax. O + 5 eq. H_2O	1.702(5), 2.421(5)	X-ray scattering, 1H NMR/0.09 M $HClO_4$	Aberg <i>et al.</i> (1983)
	2 ax. O + 5 eq. H_2O	1.75–1.77, 2.42–2.48	EXAFS/pH = 2	Charpin <i>et al.</i> (1985)
	2 ax. O + 5–6 eq. H_2O	1.77(1), 2.40(2)	EXAFS/ HNO_3 , pH = 1.8 molecular dynamics	Dent <i>et al.</i> (1992)
	2 ax. O + 5 eq. H_2O	nd		Guilbaud and Wipff (1993)
	2 ax. O + 5 eq. H_2O	1.78(2), 2.46(2)	EXAFS/ HNO_3 , pH = 2	Chisholm-Brause <i>et al.</i> (1994)
	2 ax. O + 5 eq. H_2O	1.78, 2.41	EXAFS/0.5 M HCl	Hudson <i>et al.</i> (1995b)

Table 28.2 (Contd.)

<i>Aquo ion</i>	<i>CN, O/H₂O</i>	<i>Distance(s)</i>	<i>Technique/Conditions</i>	<i>References</i>
	2 ax. O + 4.8(3) eq. H ₂ O	1.77, 2.42	EXAFS/H ₃ CCO ₂ H, pH = 0.5	Reich <i>et al.</i> (1996a)
	2 ax. O + 5 eq. H ₂ O	1.77, 2.42	EXAFS/HNO ₃ pH < 1	Thompson <i>et al.</i> (1997)
	2 ax. O + 5 eq. H ₂ O	1.76(1), 2.41(1)	EXAFS/0 M HCl	Allen <i>et al.</i> (1997)
	2 ax. O + 4.5(4) eq. H ₂ O	1.78, 2.41	EXAFS/0.1 M HClO ₄	Moll <i>et al.</i> (1998)
	2 ax. O + 5 eq. H ₂ O	nd	¹ H NMR/HClO ₄	Bardin <i>et al.</i> (1998)
	2 ax. O + 5 eq. H ₂ O	1.77, 2.42	EXAFS/0.2, 1.0 M [NO ₃] ⁻ , 2.5–25.0°C	Schofield <i>et al.</i> (1999)
	2 ax. O + 5 eq. H ₂ O	1.7477, 2.502	density functional theory	Spencer <i>et al.</i> (1999)
	2 ax. O + 4.5(4) eq. H ₂ O	1.78, 2.41	EXAFS/0.1 M HClO ₄	Wahlgren <i>et al.</i> (1999)
	2 ax. O + 5 eq. H ₂ O	1.756, 2.516	density functional theory	Hay <i>et al.</i> (2000)
	2 ax. O + 5 eq. H ₂ O	1.76, 2.42	Hartree–Fock/MP2, B3LYP	Tsushima and Suzuki (2000); Tsushima <i>et al.</i> (2002)
	2 ax. O + 4.2–4.9 eq. H ₂ O	1.75–1.76, 2.40–2.43	EXAFS/0.1–11.5 M HClO ₄	Sémon <i>et al.</i> (2001)
	2 ax. O + 4.5–4.8 eq. H ₂ O	1.75–1.76, 2.41–2.42	EXAFS/5–10 M CF ₃ SO ₃ H	Sémon <i>et al.</i> (2001)
	2 ax. O + 5.2(4) eq. H ₂ O	1.77, 2.41	EXAFS/0.1 M HClO ₄	Vallet <i>et al.</i> (2001)
	1.8 ax. O + 5.5 eq. H ₂ O	1.77(1), 2.41(2)	EXAFS/0.1 M HClO ₄	Rao <i>et al.</i> (2002)
	2 ax. O + 5.0 eq. H ₂ O	1.76, 2.40(1)	EXAFS/1 M HClO ₄	Moll <i>et al.</i> (2003)
	2 ax. O + 5 eq. H ₂ O	1.76, 2.43	density functional theory	Bridgeman and Cavigliasso (2003)
	2 ax. O + 5.2 eq. H ₂ O	nd	geometric modeling	Mauerhofer <i>et al.</i> (2004)

^a Not determined.

^b Citations to literature published from 1980 only.

^c Rotating anode X-ray tube source.

^d Magnetic circular dichromism.

uranyl group, are precisely comparable with numerous subsequent synchrotron radiation measurements.

In the historic work of Karim *et al.* (1980), the exact extent of equatorial O coordination could not be determined because of S/N complications and the imprecise knowledge of Debye–Waller factors and electron mean-free-path terms. Now, decades later, and despite remarkable advances in the theory of EXAFS (Rehr and Albers, 2000), similar problems with scattering losses, amplitude reduction effects, etc. continue to plague aspects of the precision and accuracy of coordination numbers extracted from EXAFS data by curve-fitting methods (Allen *et al.*, 2000). This is especially true for distant, next-nearest neighbors in multi-shell systems wherein spectral congestion and phase cancellation effects can make analyses difficult. Uncertainties can also arise in the determination of the coordination numbers for the simple trivalent and tetravalent hydrated cations, $An^{3+} \cdot nH_2O$ and $An^{4+} \cdot n'H_2O$, where n and n' are the numbers of water molecules directly bound to the An ions in the immediate hydration sphere. The case in point is illustrated by the results of Table 28.3 for the Th^{4+} aquo ion in 1–1.5M $HClO_4$.

(a) The monatomic spherical An(III) and An(IV) ions

Under conditions that pertain to most ecological habitats, the low-valent 3+ oxidation states of the 5f-elements would not be stable until Am ($Z=95$) and beyond. This is one of the obvious contrasts with lanthanide coordination chemistry wherein stability is dominated by the spherical, monatomic, tripisitive ions. Actinide coordination chemistry in natural systems may, however, be influenced by the 4+ oxidation states that are stabilized in anoxic, subsurface aquifers and lacustrine and marine basins wherein redox processes are mediated by species other than O_2 , such as S-bearing entities. Under such reducing conditions, An(IV) interactions with H_2O are largely driven by classical, electrostatic forces. This facilitates various approaches in the modeling of thermodynamic properties for the aquo species of the two spherical, monatomic

Table 28.3 Thorium speciation with hydration numbers (n , coordinated H_2O) and $Th-OH_2$ interatomic distances obtained from literature sources. Estimated standard deviations, where available, are given after the \pm sign or within parentheses.

Aquo ion	CN, H_2O	Distance(s)	Technique/ Conditions	References
$Th(IV) \cdot nH_2O$	8.0 ± 0.5	2.485 ± 0.010	X-ray scattering/1 M $HClO_4$	Johansson <i>et al.</i> (1991)
	11.0 ± 0.7	2.43	EXAFS/1 M $HClO_4$	Moll <i>et al.</i> (1998)
	10 ± 1	2.45(1)	EXAFS/1.5 M $HClO_4$	Moll <i>et al.</i> (1999)
	12.7	2.45	EXAFS/1.5 M $HClO_4$	Rothe <i>et al.</i> (2002)
	12.7	2.45	EXAFS/1.5 M $HClO_4$	Neck <i>et al.</i> (2002)

An(III) and An(IV) cations (David and Vokhmin, 2003). These efforts incorporate or rely upon the significant body of metrical information obtained from the An EXAFS reviewed below.

(i) *Thorium(IV)*

The initial analysis of Th L₃ EXAFS for a 0.055 M solution of Th⁴⁺ in 1 M HClO₄ provided an O coordination number of 11.0 ± 0.7, which at the 95% confidence level means that hydration numbers of 10, 11, and 12 are statistically equivalent (Moll *et al.*, 1998). In a more rigorous follow-up study with two solutions – 0.03 and 0.05 M – of Th⁴⁺ in 1.5 M HClO₄, hydration numbers of 11.0 ± 0.9 and 11.2 ± 0.9 and corresponding distances of 2.43 and 2.45 Å, respectively, were obtained from curve-fitting analyses of the L₃-edge EXAFS with and without the use of cumulant methods, which account for an asymmetrical distribution of distances about Th⁴⁺ (Moll *et al.*, 1999). Despite the evidence for an asymmetric distribution of H₂O about Th⁴⁺, the effects of pair asymmetry on the Th–OH₂ interatomic distance were small, 0.01–0.02 Å, and of approximately the same magnitude as the experimental error itself.

Based upon a combination of results from the primary (Th EXAFS) data and a variety of other metrical comparisons, Moll *et al.* (1999) concluded that the EXAFS results were compatible with hydration numbers of 9–11, and they ultimately “...selected 10 ± 1 as the most likely coordination number” for the Th⁴⁺ (and U⁴⁺) aquo ion in perchloric acid. The addition of fluoride ion in the form of NaF at the same concentration (0.05 M) as that for Th⁴⁺ in the acid solution was shown to have a significant effect on the coordination environment, but not on the total coordination number. The EXAFS data were analyzed to reveal a pair distribution (Th–F and Th–O) asymmetry with 1 F⁻ at 2.14 Å and 10 H₂O at 2.48 Å. The subsequent Th L₃-edge results (Neck *et al.*, 2002; Rothe *et al.*, 2002) for a 0.055 M Th⁴⁺ solution in 1.5 M HClO₄ indicate that the aqueous speciation consists of 12.7 O atoms at an average distance of 2.45 Å about Th⁴⁺. Although the interstudy agreement of Th–O distances is better than 1%, there is an approximately 25% study-to-study variation of coordination number. Because of the experimental conditions employed and the interatomic distances obtained, the results of the four studies (Moll *et al.*, 1998, 1999; Neck *et al.*, 2002; Rothe *et al.*, 2002) are essentially the same. Thus the coordination number discrepancy may not arise from genuine variations of sample condition. Rather, it appears to stem from different approaches to the curve-fitting analyses including, in addition to a host of other factors, the choice of amplitude reduction factor, S_0^2 , which has direct impact on the absolute accuracy of EXAFS determinations of coordination numbers (Allen *et al.*, 2000).

A final comment about the nature of the Th⁴⁺ aquo ion in these different experiments is necessary. The EXAFS results in each of the three aforementioned studies (Moll *et al.*, 1999; Neck *et al.*, 2002; Rothe *et al.*, 2002) on the

dilute and similar Th^{4+} solutions as summarized in Table 28.3 are contrasted with those from large-angle X-ray scattering studies (Johansson *et al.*, 1991) that reveal a less populated hydration sphere of 8.5 ± 0.5 water molecules at an average distance of 2.485 ± 0.010 Å. In the extremely concentrated solutions, ≈ 1 M Th^{4+} , required for the scattering measurements, it is reasonable to expect that inter-ion aggregation phenomena can lead to a different form of the aquo ion from the significantly less concentrated (18–33 times less) solutions of the EXAFS studies (Moll *et al.*, 1999). At high concentration, the Th^{4+} cations may be partially dehydrated because of an insufficient number of H_2O molecules to satisfy their own solvation requirements as well as those for the (5M) $[\text{ClO}_4]^-$ anions. There is also the possibility for some degree of nucleation and contact through cation–anion and cation–cation interactions. Until one (or both) of the experiments can be repeated under identical conditions, comparisons are not reliable, and it certainly is not obvious that either one (or more) of the studies is in error. In the interim, results from DFT calculations indicate that the first hydration shell about Th^{4+} contains 9 H_2O molecules with Th–O bond lengths of 2.54–2.55 Å (Yang *et al.*, 2001).

(ii) *Uranium(IV)*

The first U L_3 -edge EXAFS results for a dilute, acidic (pH=2) solution of the U^{4+} aquo ion revealed a hydration number of nine with an average U–O interatomic distance of 2.42 Å (Charpin *et al.*, 1985). The earliest structure report using X-ray scattering was ultimately interpreted to show that the coordination number of U^{4+} in HClO_4 was “not significantly different from eight” (Pocev and Johansson, 1973). The indefinite nature of this phrase may reflect the variations in coordination number (between six and ten) obtained with different analysis procedures, especially data set length, and numerical modeling treatments of the data for the acid solution of concentrated (2.044M) U^{4+} in which about 2% (0.035M) was present as uranyl(VI). The low-limit value of the reported range of U–O distances, 2.42–2.52 Å (Pocev and Johansson, 1973) is the same as the EXAFS-determined distance (Charpin *et al.*, 1985). The initial work on a dilute (0.05M) solution of U^{4+} in 1.5 M HClO_4 revealed an O coordination number of 11 ± 1 and, moreover, that the hydration numbers of U^{4+} and Th^{4+} are the same (Moll *et al.*, 1998). In a subsequent and more extensive paper on the subject of the tetravalent aquo ion, including the effects of fluoride ion, an EXAFS-determined value of 10.8 ± 0.5 water molecules about U^{4+} at an average distance of 2.41–2.42 Å was reported (Moll *et al.*, 1999). The presence of F^- at concentrations equal to (0.055 M) and greater than that for $[\text{U}^{4+}]$ (0.09M) was shown to affect the speciation, wherein the immediate coordination environment was shown to consist of ca. one F^- at 2.10 Å and 8.2–8.7 H_2O at 2.45–2.46 Å.

Additional insights about the magnitude of the 10.8 ± 0.5 hydration number for the pure aquo ion were provided by comparison of the U–O interatomic

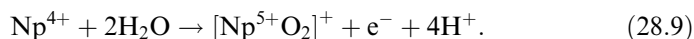
distance with the previously reported Er–O distance (2.36 Å) (Johansson and Wakita, 1985) for the Er³⁺ aquo ion, which has an exact hydration number of eight. The comparison is appropriate because the ionic radii of U⁴⁺ and Er³⁺ (1.00 and 1.004 Å, respectively, for CN 8) (Shannon, 1976) are essentially identical. Because An–OH₂ bond lengths are mainly influenced by electrostatic effects, the extent of such interatomic interactions is known to increase with increasing coordination number. It is argued that the 0.06 Å longer distance for the U⁴⁺ aquo species “...can only be explained by a coordination number larger than eight” (Moll *et al.*, 1999). Based upon this and other comparisons with available U–O distances in solid-state crystal structures, they suggested that coordination numbers of either nine or ten are possible and ultimately selected ten as the most likely one. The fact that the larger value (≈ 11) obtained from the actual analyses of the data can be so readily disregarded with sound arguments based upon EXAFS-determined distances further underscores the generally recognized problems with the accuracy of EXAFS coordination number determinations mentioned above. Similar selections of coordination numbers other than those obtained from analysis of the primary data are scattered throughout the literature reviewed here for aqueous An species.

(iii) *Neptunium(IV)*

Neptunium is considered to be the most problematic of the transuranium elements for waste storage because of its high solubility in groundwater (Viswanathan *et al.*, 1998; Kaszuba and Runde, 1999) and the projected dose commitments to the public that would arise from its breach of long-term containment (Hursthouse *et al.*, 1991). The aquo ion of tetravalent ²³⁷Np has been the subject of three independent EXAFS investigations (Allen *et al.*, 1997; Reich *et al.*, 2000; Antonio *et al.*, 2001). Well before these, optical data were interpreted to reveal a hydration number of eight (Rykov *et al.*, 1973). Neptunium L₃-edge measurements of dilute (0.005 M) Np⁴⁺ were originally obtained in various concentrations of HCl from 1–10 M (Allen *et al.*, 1997). No inner-sphere Cl[−] complexation was noted for the solution of Np⁴⁺ in 1 M HCl, and the EXAFS data for the aquo ion were analyzed to reveal 11.2 O neighbors at an average distance of 2.40 Å. Comparisons of this interatomic distance with a selection of related Np⁴⁺ and Pu⁴⁺ species suggested “...that the number of waters around the Np⁴⁺ ion lies in the range of 9–11.” On increasing HCl concentrations from 5 to 10 M, the data analysis revealed a systematic replacement of inner-sphere H₂O molecules by inner-sphere Cl[−] ions (reaching values of 7.7 and 2.0, respectively) that was accompanied by a 0.04 Å elongation of the Np–O bond length. The trends were interpreted to indicate the formation of a mixture of multi-aquo-chloro complexes of the general form [Np(OH₂)_xCl_y]^{4−y}, for $y \geq 2$.

In the second study (Reich *et al.*, 2000), a dilute (0.05 M) solution of Np⁴⁺ in 0.1 M HNO₃ was stabilized by the addition of 2 M H₂SO₄ to suppress the

spontaneous oxidation reaction,



Analysis of the L₃-edge EXAFS revealed an O coordination number of 11 with an average Np–O distance of 2.39(1) Å, both of which bear close resemblance to the initial results (Allen *et al.*, 1997). Upon further analysis of distant features in the FT data, evidence was found for the inner-sphere coordination that contains two [SO₄]²⁻ groups bound to Np⁴⁺ in a bidentate fashion (Reich *et al.*, 2000). So, the total O coordination number of 11 is the sum of four O from two sulfate groups and seven from H₂O molecules and, despite the agreement with the earlier work (Allen *et al.*, 1997), the mixed sulfate–hydrate of Np⁴⁺ species is not a pure aquo ion.

In order to avoid such troublesome effects of complexation as well as those from oxidation, hydrolysis, disproportionation, and precipitation reactions, a dilute (0.0047M) solution of Np in the non-complexing, supporting electrolyte of perchloric acid (1 M) was used for *in situ* L₂-edge EXAFS spectroelectrochemical measurements of all four –III, IV, V, and VI–aquo ion species (Antonio *et al.*, 2001). The *in situ* technique eliminates interferences from chemical reductants/oxidants that may be required to produce and maintain a specific Np oxidation state during the time required to perform a conventional *ex situ* experiment. Moreover, the use of the non-complexing, supporting electrolyte of perchloric acid further assures that all inner-sphere Np–O bonding is free of interferences from Np–[ClO₄]⁻, Np–[SO₄]²⁻, Np–[Cl]⁻, etc., interactions. The EXAFS analyses of the data for the Np⁴⁺ aquo ion revealed a coordination number of 9(1) O atoms at an average distance of 2.37(2) Å. Comparison of this solution Np⁴⁺–O distance with the corresponding distance for crystalline NpO₂, containing eight-coordinate Np⁴⁺, reveals that the average distance for the aquo ion is 0.02 Å longer. Insofar as interatomic distances can be used to estimate coordination numbers, it was concluded that “. . . hydration numbers of either 8 or 9 are more realistic than hydration numbers of either 10 or 11” for the Np⁴⁺ aquo ion (Antonio *et al.*, 2001). In support of this conclusion, a simple numerical model, based upon an adaptation of the original method of Egami and Aur (1987) used previously with success for metal-ions in glass matrices, was introduced for estimating An ion coordination numbers. The number calculated for Np⁴⁺ was eight.

The *in situ* X-ray absorption technique was further developed as a means to determine the formal electrode potential (*E*^{o'}) of Np redox reactions (Soderholm *et al.*, 1999), including the Np⁴⁺/Np³⁺ couple of equation (28.7). As discussed previously, for reversible reduction–oxidation reactions of An ions in general, the measurement of thermodynamic formal potentials is important from fundamental and practical perspectives concerning An mobility and reactivity in the geosphere. Whereas the equipment and methods of X-ray absorption spectroelectrochemistry have evolved since the first description of its use (Smith *et al.*, 1984), none of the myriad of multipurpose cell designs (Sharpe *et al.*, 1990;

Igo *et al.*, 1991; Farley *et al.*, 1999) were directly suitable to achieve the application-specific containment and safety standards necessary for *in situ* experiments with radionuclides. This led to the design of a purpose-built system (Antonio *et al.*, 1997), which by facilitating the simultaneous combination of electrochemistry and XANES, provides direct access to the formal electrode potentials of redox reactions of An ions. For example, by use of a series of controlled electrochemical potentials (E_p) at which the forward and reverse reactions of equation (28.7) provide concentration variations of Np^{4+} and Np^{3+} , sufficient XANES data were acquired (Soderholm *et al.*, 1999) to perform a Nernst analysis according to equation (28.8). The spectra for the admixtures of the two solution species were analyzed using standard linear regression analysis as well as PCA with the valence-pure Np^{4+} and Np^{3+} spectra to provide the relative partial concentrations used for the Nernst plot of potential, E_p , vs $\log[\text{Np}^{4+}]/[\text{Np}^{3+}]$ shown in Fig. 28.6. In this analysis, the slope (0.062 V) corresponds to $n = 1 e^-$. The x -axis intercept provides the formal potential, $E^{\circ'} = -0.053$ V. Besides the $\text{Np}^{4+}/\text{Np}^{3+}$ reaction of equation (28.7), the method was successfully applied to the $\text{Bk}^{4+}/\text{Bk}^{3+}$ (Antonio *et al.*, 2002) and $\text{Np}^{6+}/\text{Np}^{5+}$ (Soderholm *et al.*, 1999) aquo ion redox reactions as well as with the IV/III couples of Np and Pu in complexes with the electroactive, Wells–Dawson heteropolyoxoanion ligand, $[\text{P}_2\text{W}_{17}\text{O}_{61}]^{10-}$, which obscures the optical and electrochemical response of the An-ion itself (Chiang *et al.*, 2003). In this situation, the *in situ* XANES approach provides information about formal electrode potentials that is not obtainable from conventional spectrophotometric measurements, cyclic voltammetry, or potentiometric titrations alone.

(iv) *Plutonium(IV)*

Metrical aspects of the speciation of the $^{242}\text{Pu}^{4+}$ aquo ion came to light in three papers (Ankudinov *et al.*, 1998; Conradson, 1998; Conradson *et al.*, 1998). The experimental Pu XANES at the L_1 (Ankudinov *et al.*, 1998) and L_3 (Conradson *et al.*, 1998) edges for a 0.10M Pu^{4+} solution in 1M HClO_4 were compared with theoretical spectra obtained from multiple-scattering XANES calculations using the *ab initio* code known as FEFF (Rehr and Albers, 2000). Although these efforts provided no quantitative information about the Pu^{4+} coordination environment in terms of bond distances and hydration numbers, structural parameters for Pu^{4+} as well as for the three other Pu aquo ions were provided in an appendix (Ankudinov *et al.*, 1998). The primary source of the supplementary results was attributed to, at that time, an unpublished study. These structure details appear to be the same as those subsequently published in the review article (Conradson, 1998), which shows the FT data and the results from the curve-fitting analysis of the L_3 EXAFS. The Pu^{4+} aquo ion in 1M HClO_4 was shown to consist of eight or nine water molecules at an average distance of 2.39 Å. A similar hydration structure was found for the Np^{4+} aquo ion species that was also studied in 1M HClO_4 (Antonio *et al.*, 2001).

Independent EXAFS measurements of aqueous solutions of 0.05 M $^{239}\text{Pu}^{4+}$ in 3 and 8 M HNO_3 revealed an O coordination number of 11 with best fit Pu–O distances of 2.41 and 2.45 Å, respectively (Allen *et al.*, 1996b). Analysis of the distant peaks in the FT data revealed N backscattering that increased with the HNO_3 concentration. The N coordination numbers and Pu–N interatomic distances, in combination with results from ^{15}N NMR and optical spectroscopies (Veirs *et al.*, 1994), revealed the formation of di- and tetra-nitrato complexes with decreasing water content, $[\text{Pu}(\text{NO}_3)_2(\text{H}_2\text{O})_7]^{2+}$ and $[\text{Pu}(\text{NO}_3)_4(\text{H}_2\text{O})_3]$, respectively, wherein each $[\text{NO}_3]^-$ acts as a bidentate ligand. At 13 M HNO_3 , the Pu coordination sphere was fully dehydrated, consisting of a 12 O coordinate hexanitratro complex, $[\text{Pu}(\text{NO}_3)_6]^{2-}$, with an average Pu–O distance of 2.49 Å for the bidentate $[\text{NO}_3]^-$ bonds (Veirs *et al.*, 1994; Allen *et al.*, 1996b).

The discovery of significant oxygen hyperstoichiometry in the binary $\text{Pu}^{4+}\text{–O}$ system, e.g., PuO_{2+x} for $0.0 \leq x \leq 0.27$ (Haschke *et al.*, 2000), has sparked something of a revolution in the oxide chemistry of plutonium. Even though similar hyperstoichiometry is well-known and of considerable practical importance in the binary fluorite-type oxygen-excess uranium oxides, a similar situation was not recognized with plutonium oxides. It is only now clear that the fluorite lattice of PuO_2 (*Fm3m*) can accommodate excess O as well (Haschke *et al.*, 2001; Haschke and Allen, 2002; Haschke and Oversby, 2002). Considerable international interest in the PuO_{2+x} system has arisen vis-à-vis actinide environmental science because of the possibility that the oxidized Pu ions, either Pu^{5+} and/or Pu^{6+} required for charge compensation, might be easily leached out of the otherwise water-insoluble PuO_2 . Although the precise location of the excess O^{2-} in these materials is still open to question, the Pu L₃-edge X-ray absorption work (Conradson *et al.*, 2003, 2004) provides valuable insights about the Pu valence and speciation. Most important, and contrary to initial suggestions (Haschke *et al.*, 2000), the XANES and EXAFS “. . . results indicate that the excess O in PuO_2 occurs as localized Pu^{5+} –oxo moieties” with distances of 1.83–1.91 Å, and not as localized Pu^{6+} sites (Conradson *et al.*, 2003). Also contrary to initial concern, the unusual stability of the PuO_{2+x} system suggests that the Pu^{5+} ions in the bulk solid of PuO_{2+x} may not have any higher solubility than the Pu^{4+} ions (Conradson *et al.*, 2003). Still, many pieces of this new puzzle in plutonium chemistry remain, and until the time that additional definitive and conclusive evidence is reported, many of the issues opened up in the landmark publication (Haschke *et al.*, 2000) will continue to fuel contemporary research interests.

(v) *Berkelium(IV/III)*

Of the trans-plutonium elements, only Bk has a comparatively stable, tetravalent aquo ion. Because of their spontaneous reactivity with water ($E^\circ > +2.6$ V), (Bratsch, 1989) the tetravalent aquo ions of Am, Cm, and Cf have, as yet, to be

stabilized for detailed physical, spectroscopic, and structure characterization. In comparison to the extensive volume of results for the aquo ions of Th, U, Np, and Pu (see Tables 28.2–28.5), there are significantly fewer metrical details about the coordination of water with the trans-plutonium elements (cf. Tables 28.2 to 28.6). For example, despite significant research in the years since the discovery of Bk in 1949, no direct structural information about the aquo ion of Bk^{4+} as well as that of Bk^{3+} was available until 2002. At that time, the simultaneous combination of XAS and electrochemical methods was used to probe the redox speciation of ^{249}Bk (Antonio *et al.*, 2002). Through use of *in situ* L_3 -edge measurements of a dilute (0.47 M) Bk solution in a non-complexing aqueous mineral acid electrolyte (1 M HClO_4) the inner-sphere hydration environments were found to undergo reorganization, with regard to the average $\text{Bk}-\text{OH}_2$ interatomic distances and the number of coordinated H_2O molecules, corresponding to controlled variation of redox state. Bk^{4+} was found to be eight-coordinate with an average $\text{Bk}-\text{O}$ distance of 2.32(1) Å, whereas Bk^{3+} was found to be nine-coordinate with an average $\text{Bk}-\text{O}$ distance of 2.43(2) Å. The change in hydration was shown to have a number of parallels with the well-recognized change between the aquo ions of the large, light trivalent lanthanide ions, e.g. La–Pm, and the small heavy ones, e.g. Tb–Lu (Habenschuss and Spedding, 1980; Cossy *et al.*, 1995).

(vi) *Curium(III)*

The trivalent aquo ions of ^{248}Cm and ^{249}Cf , the elements adjacent to Bk, have been independently investigated in HCl media through use of L_3 -edge EXAFS. The spectrum for a 0.01 M solution of Cm^{3+} in 0.25 M HCl was fit to reveal 10.2 O at an average distance of 2.45 Å (Allen *et al.*, 2000). The single sinusoidal-like variation of the EXAFS data was interpreted to indicate an inner-sphere coordination of water molecules without interference from Cl^- complexation. No compelling evidence for inner-sphere $\text{Cm}-[\text{Cl}]^-$ interactions was obvious from the FT data and the curve-fitting results until surprisingly high LiCl concentrations, $\geq 8.7\text{M}$. Although the EXAFS data suggest that little chloride complexation occurs at low $[\text{Cl}^-]$ ($\sim 5\text{M}$ or less), this absence of evidence may reflect, in part, general problems with the method itself concerning resolution and detection limitations of Cl backscattering in a dilute admixture of one (or more) chloro complex(es) in an aquo ion system.

(vii) *Californium(III)*

In the highest Z (98) EXAFS yet reported, a multinational effort on a dilute (0.007 M) solution of $^{249}\text{Cf}^{3+}$ in 1 M HCl led to the publication of two reports (David *et al.*, 1998; Revel *et al.*, 1999). The initial one (David *et al.*, 1998) contained metrical results from EXAFS analyses that revealed 9.5(9) O around

Table 28.4 Neptunium redox speciation for $Np(III)$, $Np(IV)$, $Np(V)$, $Np(VI)$, and $Np(VII)$. For the spherical ions, the hydration numbers (n , n' , coordinated H_2O) and $Np-OH_2$ interatomic distances are listed. For the neptunyl ions, the axial (ax.) oxygen coordination numbers and $Np=O$ distances precede the equatorial (eq.) hydration numbers (n'' , n''') and the $Np-OH_2$ bond lengths. Estimated standard deviations, where available, are obtained from the primary sources and are given after the \pm sign or within parentheses.

Aquo ion	CN, O/ H_2O	Distance(s)	Technique/Conditions	References
$Np(III) \cdot nH_2O$	9.8(9) 8-9	2.52(1) 2.48(2)-2.51	EXAFS/1 M HCl EXAFS/1 M $HClO_4$, DFT	David <i>et al.</i> (1998) Antonio <i>et al.</i> (2001)
$Np(IV) \cdot n'H_2O$	8 11 11 \pm 1	nd ^a 2.40(1) 2.39(1)	Optical/ \leq 6 M HNO_3 EXAFS/1 M HCl EXAFS/0.1 M HNO_3 + 2 M H_2SO_4	Rykov <i>et al.</i> (1973) Allen <i>et al.</i> (1997) Reich <i>et al.</i> (2000)
$[Np(V)O_2]^{+} \cdot n''H_2O$	8-9 2 ax. O + 6 eq. H_2O 1.6 ax. O + 5.2 eq. H_2O 2 ax. O + 5 eq. H_2O	2.37(2) nd 1.83(2), 2.52(2) nd	EXAFS/1 M $HClO_4$, DFT NMR/0-8 M LiCl, NH_4NO_3 EXAFS/ $HClO_4$, pH = 2 optical/ H_2O -organic mixtures	Antonio <i>et al.</i> (2001) Glebov <i>et al.</i> (1977) Combes <i>et al.</i> (1992) Garnov <i>et al.</i> (1996)
	2 ax. O + 5 eq. H_2O 1.9(2) ax. O + 3.6(6) eq. H_2O 2 ax. O + 5 eq. H_2O 2 ax. O + 5 eq. H_2O	1.85(1), 2.50(2) 1.822(3), 2.488(9) 1.81, 2.61 1.81, 2.52	EXAFS/3 M LiCl EXAFS/0.1 M HNO_3 density functional theory Hartree-Fock/MP2	Allen <i>et al.</i> (1997) Reich <i>et al.</i> (2000) Hay <i>et al.</i> (2000) Tsushima and Suzuki (2000)
	2 ax. O + 5 eq. H_2O 2 ax. O + 4.8(10) eq. H_2O	1.80(2), 2.44(3) 1.82(2), 2.51(2)	EXAFS/1 M $HClO_4$ EXAFS/ $HClO_4$, pH = 1	Antonio <i>et al.</i> (2001) Den Auwer <i>et al.</i> (2003a)
$[Np(VI)O_2]^{2+} \cdot n'''H_2O$	2 ax. O + 3.9 eq. H_2O 2 ax. O + 6 eq. H_2O	nd nd	geometric modeling 1H , ^{17}O NMR/ H_2O -organic mixtures	Mauerhofer <i>et al.</i> (2004) Shcherbakov <i>et al.</i> (1974); Mashirov <i>et al.</i> (1975); Shcherbakov and Iorga (1975)

Table 28.4 (Contd.)

<i>Aquo ion</i>	<i>CN, O/H₂O</i>	<i>Distance(s)</i>	<i>Technique/Conditions</i>	<i>References</i>
	2 ax. O + 5 eq. H ₂ O	nd	optical/H ₂ O–organic mixtures	Garnov <i>et al.</i> (1996)
	2 ax. O + 5 eq. H ₂ O	nd	¹ H NMR/HClO ₄	Bardin <i>et al.</i> (1998)
	2.0(1) ax. O + 4.6(6) eq. H ₂ O	1.754(3), 2.414(6)	EXAFS/0.1 M HNO ₃	Reich <i>et al.</i> (2000)
	2 ax. O + 5 eq. H ₂ O	1.752, 2.50	density functional theory	Hay <i>et al.</i> (2000)
	2 ax. O + 5 eq. H ₂ O	1.67, 2.50	Hartree–Fock	Tsushima and Suzuki (2000)
	2 ax. O + 5 eq. H ₂ O	1.73(2), 2.36(3)	EXAFS/1 M HClO ₄	Antonio <i>et al.</i> (2001)
	2 ax. O + 5.3 eq. H ₂ O	nd	geometric modeling	Mauerhofer <i>et al.</i> (2004)
	2 ax. O + 4 eq. OH ⁻	1.85(2), 2.18(3)	EXAFS/2.5 M NaOH	Clark <i>et al.</i> (1997)
	4 eq. O + 2 ax. OH ⁻	1.86–1.87(1), 2.24(4)	EXAFS/1 M NaOH, DFT	Williams <i>et al.</i> (2001)
	4 eq. O + 2 ax. OH ⁻	1.89–1.90, 2.32–2.33	EXAFS/2.5 M NaOH, DFT	Bolvin <i>et al.</i> (2001)

^a Not determined.

Table 28.5 Plutonium redox speciation for Pu(III) , Pu(IV) , Pu(V) , and Pu(VI) . For the spherical ions, the hydration numbers (n , n' , coordinated H_2O) and Pu-OH_2 interatomic distances are listed. For the plutonyl ions, the axial (ax.) oxygen coordination numbers and Pu=O distances precede the equatorial (eq.) hydration numbers (n'' , n''') and the Pu-OH_2 bond lengths. Estimated standard deviations, where available, are obtained from the primary sources and are given after the \pm sign or within parentheses.

Aquo ion	CN, O/ H_2O	Distance(s)	Technique/Conditions	References
$\text{Pu(III)} \cdot n\text{H}_2\text{O}$	10,2 ^a	2.51(1)	EXAFS/0.01 M LiCl	Allen <i>et al.</i> (1997)
	9,9(9)	2.51(1)	EXAFS/1 M HCl	David <i>et al.</i> (1998)
	9	2.48	EXAFS/ns ^b	Ankudinov <i>et al.</i> (1998)
	8-9	2.49	EXAFS/ns ^b	Conradson (1998)
	8-9	2.51-2.55	density functional theory	Blaudeau <i>et al.</i> (1999)
$\text{Pu(IV)} \cdot n\text{H}_2\text{O}$	8	nd ^c	Optical/ ≤ 6 M HNO_3	Rykov <i>et al.</i> (1973)
	8	2.39	EXAFS/ns ^b	Ankudinov <i>et al.</i> (1998)
	8-9	2.39	EXAFS/ns ^b	Conradson (1998)
	nd	2.41	hydration free energy	Babu and Lim (1999)
		nd	Optical/ H_2O -organic mixtures	Garnov <i>et al.</i> (1996)
$[\text{Pu(V)}\text{O}_2]^+ \cdot n''\text{H}_2\text{O}$	2 ax. O + 5 eq. H_2O	1.84, 2.45	EXAFS/ns ^b	Ankudinov <i>et al.</i> (1998)
	2 ax. O + 4 eq. H_2O	1.81, 2.47	EXAFS/ns ^b	Conradson (1998)
	2 ax. O + 4 eq. H_2O	1.808, 2.61	density functional theory	Hay <i>et al.</i> (2000)
	2 ax. O + 5 eq. H_2O	1.65, 2.36	Hartree-Fock	Tsushima and Suzuki (2000)
	2 ax. O + 5 eq. H_2O	nd	geometric modeling	Mauerhofer <i>et al.</i> (2004)
$[\text{Pu(VI)}\text{O}_2]^{2+} \cdot n'''\text{H}_2\text{O}$	2 ax. O + 3.6 eq. H_2O	1.75, 2.45	optical/ H_2O -organic solutions	Garnov <i>et al.</i> (1996)
	2 ax. O + 5 eq. H_2O	1.74, 2.45	EXAFS/1 M HClO_4	Runde <i>et al.</i> (1997)
	2 ax. O + 6 eq. H_2O	1.74, 2.40	EXAFS/ns ^b	Ankudinov <i>et al.</i> (1998)
	2 ax. O + 6 eq. H_2O	1.7568, 2.523	EXAFS/ns ^b	Conradson (1998)
	2 ax. O + 5 eq. H_2O	1.742, 2.485	density functional theory	Spencer <i>et al.</i> (1999)
	2 ax. O + 5 eq. H_2O	1.59, 2.29	Hartree-Fock	Hay <i>et al.</i> (2000)
	2 ax. O + 5.5 eq. H_2O	nd	geometric modeling	Tsushima and Suzuki (2000)
				Mauerhofer <i>et al.</i> (2004)

^a Subsequently adjusted to 9.2 (Allen *et al.*, 2000).

^b Although the conditions were not specified in the primary sources cited here, it is likely that the conditions were the same as those of the XANES study of the Pu aquo ions in 1 M HClO_4 (Conradson *et al.*, 1998).

^c Not determined.

Table 28.6 Americium, curium, berkelium, and californium redox speciation with hydration numbers (n , n' , coordinated H_2O) and $An-OH_2$ interatomic distances obtained from literature sources. For the two americium ion entries, the axial (ax.) oxygen coordination numbers precede the equatorial (eq.) hydration numbers (n'' , n'''). Estimated standard deviations, where available, are given after the \pm sign or within parentheses.

Aquo ion	CN, O/ H_2O	Distance(s)	Technique/Conditions	References
Am(III)· nH_2O	9,5(9) 10,3	2.51(1) 2.48	EXAFS/1 M HCl EXAFS/0.25 M HCl	David <i>et al.</i> (1998) Allen <i>et al.</i> (2000)
[Am(V)O ₂] ⁺ · $n'H_2O$	8–9	2.47–2.49	EXAFS/HClO ₄ pH ≈ 0.5	Stumpf <i>et al.</i> (2004)
[Am(VI)O ₂] ²⁺ · $n''H_2O$	2 ax. O + 3.8 eq. H ₂ O	nd ^a	Geometric Modeling	Mauerhofer <i>et al.</i> (2004)
Cm(III)· nH_2O	2 ax. O + 5.9 eq. H ₂ O	nd	Geometric Modeling	Mauerhofer <i>et al.</i> (2004)
Bk(III)· nH_2O	10,2	2.45	EXAFS/0.25 M HCl	Allen <i>et al.</i> (2000)
	9	nd	Diffusion/HClO ₄ pH = 2.5	Latrous and Oliver (1999)
Bk(IV)· $n'H_2O$	9,0(6)	2.43(2)	EXAFS/1 M HClO ₄	Antonio <i>et al.</i> (2002)
Cf(III)· nH_2O	7,9(5)	2.32(1)	EXAFS/1 M HClO ₄	Antonio <i>et al.</i> (2002)
	9,5(9)	2.44(1)	EXAFS/1 M HCl	David <i>et al.</i> (1998)
	8,5 ± 1,5	2.42(2)	EXAFS/1 M HCl	Revel <i>et al.</i> (1999)

^a Not determined.

Cf^{3+} at an average distance of 2.44(1) Å. For ensuing calculations of the molecular radius of H_2O and comparison with that obtained from an ionic model, the authors selected 8.5 as the O coordination number, which is the value inferred from previous conductivity measurements (Fourest *et al.*, 1995) because the EXAFS-determined coordination number was “measured with insufficient accuracy.” The second note (Revel *et al.*, 1999) contains, in addition to the $L_{1,2,3}$ -edge Cf XANES data, the $k^3\chi(k)$ EXAFS curve-fitting results for a single shell of 8.5 ± 1.5 O atoms at 2.42(2) Å. It is not clear if the coordination number, which is described as an indicative value, was refined in the fitting procedure. Despite the concentration (1M) of the HCl solution, there was no evidence for the formation of an inner-sphere chloro complex of Cf^{3+} . This result is consistent with the aforementioned EXAFS conclusions (Allen *et al.*, 2000) for Cm^{3+} in chloride media of $< 5\text{M}$.

(viii) *Americium(III)*

The aquo ions of the trivalent actinides have been of particular interest for comparison with those of the trivalent lanthanides in order to address fundamental issues about the nature of An–O bonding, i.e. the comparative extent of 5f versus 4f orbital overlap with O orbitals. Because the ionic radius (IR) of Am^{3+} (1.09 Å for CN=8) (Shannon, 1976) is intermediate of those for Nd^{3+} (1.109 Å) and Sm^{3+} (1.079 Å), this similarity facilitates direct comparisons of the coordination environments of the Am^{3+} aquo ion and the nine-coordinate Nd^{3+} and Sm^{3+} aquo ions. Although no metrical details were reported, the FT data obtained from the EXAFS for an Am^{3+} solution of unspecified concentration in 1M HClO_4 indicate that the Am^{3+} – OH_2 bond distance for the pure aquo ion decreases slightly with the addition of Cl^- , suggesting a subtle reorganization of either of its inner- and/or outer-hydration sphere (Runde *et al.*, 1997). The results of the analysis of the EXAFS data for an Am^{3+} solution (also of unspecified concentration) in 1M HCl were reported to reveal 9.5(9) O atoms at 2.51(1) Å (David *et al.*, 1998). For subsequent modeling and calculations of the molecular radius of H_2O , the coordination number of nine was selected largely on the basis of other indirect measurements (Fourest *et al.*, 1995). The L_3 -edge EXAFS data of a 0.01M solution of ^{243}Am in 0.25M HCl were fit to show that the aquo ion has 10.2 O at 2.45 Å (Allen *et al.*, 2000). The O coordination number decreases to 8.9 and 6.4 at Cl^- concentrations of 8 and 12.5M, respectively, as the number of Am–Cl interactions simultaneously grow in, reaching a maximum of ca. 2. Remarkably, there is essentially no effect on the Am–O interatomic distances, which range from 2.48–2.51 Å in no particular order with $[\text{Cl}^-]$, which is qualitatively different from the preliminary observations of Am^{3+} (Runde *et al.*, 1997).

(ix) Uranium(III)

The significant amount of work on the tripositive aquo ions of Np and Pu (Tables 28.4 and 28.5) stands in obvious contrast with the sole study of the U^{3+} aquo ion in 1 M HCl (David *et al.*, 1998; see Table 28.2). Although the concentration is not specified and despite the notorious instability of U^{3+} to oxidation upon contact with air, EXAFS data were acquired and analyzed to provide a coordination number of 8.7(9) and an average U–O distance of 2.56(1) Å, which sets the benchmark as the longest one of the entire An^{3+} series for which data are available. This result is consistent with the effects of the contraction of 5f-element IR with increasing Z , where near the beginning of the series, i.e. U^{3+} , the interatomic distances are longer than for those ions near the end of the series, for example Cf^{3+} mentioned above, which has a distance of 2.42–2.44 Å (David *et al.*, 1998; Revel *et al.*, 1999) for its aquo ion. Curiously, the experimental An^{3+} –O bond length variation between U ($Z=91$) and Cf ($Z=98$) of 0.12–0.14 Å is nearly twice (1.6 to 1.9 times) the difference between their ionic radii, 0.075 Å, for CN=6.

Concurrent with the measurements of the U^{3+} aquo ion and in the same manner, EXAFS data were collected and analyzed for the aquo ions of Np^{3+} and Pu^{3+} , which were also of unspecified concentration in 1 M HCl and of considerable reactivity with respect to oxidation (David *et al.*, 1998). The metrical details were reported as, in order of Np^{3+} and Pu^{3+} , 9.8(9) O at 2.52(1) Å and 9.9(9) O at 2.51(1) Å. As expected, both interatomic distances are within the aforementioned scale and, moreover, are near to that for U^{3+} –O. The collective results of David *et al.* (1998) indicate that the trivalent aquo ions of U, Np, Pu, Am, and Cf are either nine or ten-coordinate with O atoms of water molecules. For the most part, the results of the comparable studies of Tables 28.2 and 28.4–28.6 as discussed separately in sections above and below bear this out.

(x) Neptunium(III)

The *in situ* L_3 EXAFS data for the aquo ion of Np^{3+} (0.0047 M in 1 M $HClO_4$), in which the oxidation state was precisely maintained by electrochemical methods, were best fit with 9(1) O atoms at 2.48(2) Å (Antonio *et al.*, 2001). The corresponding results from density functional theory (DFT) methods, including relativistic effects, indicate that coordination numbers of either eight or nine lead to the most stable conformations. In addition, the coordination number calculated from a simple geometric model was eight. The combination of the EXAFS, DFT, and modeling results led to the conclusion that Np^{3+} has a coordination number of eight or nine in aqueous perchloric acid. The same conclusion was obtained for Np^{4+} . The 0.04 Å difference in the experimental, average Np^{3+} –O distances of 2.48(2) Å (Antonio *et al.*, 2001) and 2.52 Å (David *et al.*, 1998) may reflect the influence of the (1 M) chloride ion on the hydration sphere in the solution of the latter experiment. The perchlorate anion is known

to be significantly less interacting, essentially non-complexing, with cations than is Cl^- and, moreover, $[\text{ClO}_4]^-$ - H_2O interactions are less well-defined than those for $[\text{Cl}]^-$ - H_2O (Neilson *et al.*, 1985).

(xi) *Plutonium(III)*

The speciation of the Pu^{3+} aquo ion and the surprising results about the effects of Cl^- on the Pu hydration sphere were addressed in two provocative reports (Allen *et al.*, 1997, 2000). In the first, for a solution of $0.02\text{ M }^{242}\text{Pu}^{3+}$ in dilute (0.01 M) LiCl at $\text{pH}=3$, the L_2 -edge EXAFS was best fit to show an environment that consisted of $10.2 \pm 1\text{ O}$ at 2.51 \AA . In the subsequent work, the value of the O coordination number was refined to 9.2 by use of a larger amplitude reduction factor than fixed previously. The independent investigation (David *et al.*, 1998) for an aqueous Pu^{3+} solution of unspecified concentration in 1 M HCl confirmed the original Pu–O distance exactly and, within the error of the measurement, the O coordination numbers too (see Table 28.5). A remarkable aspect of the results is that the Pu EXAFS "...showed no evidence for the formation of inner-sphere chloro complexes up to a Cl^- concentration of 12.3 M " (Allen *et al.*, 1997). Although the O coordination number was shown to decrease from 9.2 to 5.2 with increasing $[\text{Cl}^-]$, there was no systematic change in the Pu–O distance, which held constant at 2.50 – 2.51 \AA . The apparent dehydration of the Pu^{3+} aquo ion was not simultaneously compensated by the addition of Cl^- , thereby leading to the formation of some type of coordinately unsaturated Pu^{3+} aquo ion in the $12.3\text{ M }[\text{Cl}^-]$ medium. What seems odd about this behavior is the insensitivity of the Pu–O bond length to the significant change in O coordination number. The combination of this observation with the contradictory behavior noted for the effects of Cl^- on the aquo ions of Am^{3+} and Cm^{3+} presents something of a quandary. There is the possibility that the EXAFS method itself may be the source of inherently misleading information for this Pu^{3+} system, wherein, for example, the apparent absence of Pu–Cl backscattering and the reduction of the Pu–O backscattering arise from cancellation effects. The confluence of coincidental phase and amplitude differences relating to the O and Cl interatomic distances, their Debye–Waller factors, and their coordination numbers, may lead to a significant degree of destructive interference and, ultimately signal cancellation. Such problems with EXAFS have been noted beforehand with multi-shell systems (Antonio *et al.*, 1983; Goulon *et al.*, 1983; Martens *et al.*, 1985; Roehler, 1992; Zhang *et al.*, 1998). Whether it applies to the Pu^{3+} system described here is, of course, unknown and requires independent confirmation of the experimental results.

Two other associated EXAFS studies of the Pu^{3+} aquo ion provide experimental results, i.e. eight to nine O at 2.48 – 2.49 \AA (Ankudinov *et al.*, 1998; Conradson, 1998) that are in reasonable accord with the aforementioned ones (see Table 28.5) obtained in chloride media. Although details about the composition of the Pu^{3+} specimen were not included in either report, the EXAFS data

are likely to have been collected on the very same sample, 0.10 M Pu³⁺ in the non-complexing aqueous mineral acid solution of 1 M HClO₄, from which the XANES was acquired (Conradson *et al.*, 1998). If true, the shorter bond lengths (2.48–2.49 Å) for the Pu³⁺ aquo ion in the perchlorate solution compared with that (2.51 Å) for the chloride-containing solutions are consistent with subtle differences in the hydration of Pu³⁺. Additional studies would be beneficial in this regard. Nevertheless, all of the EXAFS metrical information (Allen *et al.*, 1997; Ankudinov *et al.*, 1998; Conradson, 1998; David *et al.*, 1998; Allen *et al.*, 2000) are in reasonable accord with the relativistic DFT investigation (Blaudeau *et al.*, 1999) showing that the first solvation shell of Pu³⁺ contains eight or possibly nine H₂O molecules with Pu–O bond lengths of 2.51–2.55 Å.

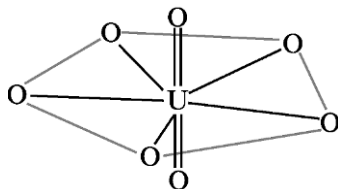
(b) The triatomic An(v) and An(vI) ions

Up to this point, the discussions have focused on the spherical, monatomic trivalent and tetravalent An ions involving only An–OH₂ bonding. We now turn attention to the penta- and hexavalent An ions, which in acidic aqueous solution invariably take the form of the linear, triatomic *trans*-dioxocations, [O=An⁵⁺=O]⁺ and [O=An⁶⁺=O]²⁺. In these so-called actinyl cations, the terminal O interactions with the An ions have double bond character as indicated and, moreover, the An ions are coordinately unsaturated. Their coordination spheres are completed by the complexation of H₂O molecules that encircle the An ions in an equatorial plane perpendicular to the axial O=An=O moiety. The exact degree of hydration of the actinyl cations [AnO₂]⁺ and [AnO₂]²⁺ has been the subject of decades-long study and debate. The extent that the results from An EXAFS experiments have provided insights into the structure of these hydrated ions is summarized below. Additional aspects of actinyl electronic properties and coordination in molecular complexes as probed by XAS have been reviewed elsewhere (Den Auwer *et al.*, 2003b).

(i) *Uranyl(vI)*

The aqueous uranyl ion, [UO₂]²⁺, with formally hexavalent U is the most studied system, whereas its pentavalent homolog, [UO₂]⁺ is the least studied because of its limited stability and susceptibility to disproportionation. Even before the first U EXAFS measurements were recorded with a laboratory spectrometer (Karim *et al.*, 1980), the consensus from a number of structural experiments was that, in the solid-state, the [UO₂]²⁺ ion exhibits a preference for five equatorial ligands thereby forming a pentagonal bipyramid (Evans, 1963). More contemporary compilations of structural data bear this out (Burns *et al.*, 1997). In the solid-state, the pentagonal bipyramidal polyhedron of [UO₂]²⁺ is more common than either of the square or hexagonal bipyramidal coordination polyhedra. From the survey of solution EXAFS results presented in Table 28.2, the consensus is clear. The *trans*-dioxo [UO₂]²⁺ cation exists in acidic aqueous

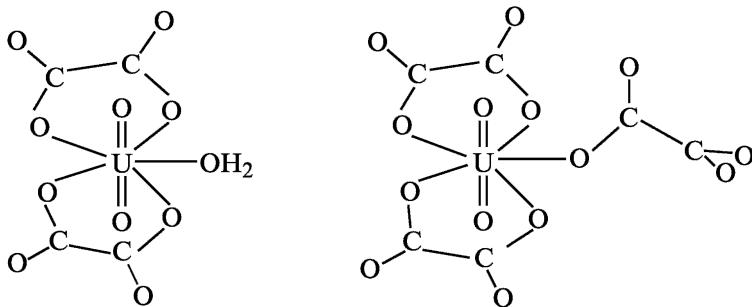
solution just as it does in the solid-state and that it has a hydration number of five. It is generally assumed that the U coordination geometry in dilute ($<0.25\text{M}$) solutions is the same as that in the solid-state with an equatorial arrangement of five H_2O molecules between the two axial O atoms, wherein U^{6+} is seven-coordinate in the form of a pentagonal bipyramid, which is illustrated below. The selection of results shown in Table 28.2 from a number of theoretical calculations and other spectroscopic measurements are in agreement about the structure of the $[\text{UO}_2]^{2+} \cdot 5\text{H}_2\text{O}$ aquo ion.



For the uranyl cation, the EXAFS-determined axial $\text{U}=\text{O}$ distances of Table 28.2, 1.75–1.78 Å, have a small (0.03 Å) dispersion, and are essentially independent of differences in experimental conditions. By comparison, the 1.702(5) Å $\text{U}=\text{O}$ bond length obtained for a concentrated (1 M) $[\text{UO}_2]^{2+}$ solution through use of X-ray scattering is anomalously short (Aberg *et al.*, 1983). The bond length dispersion is more than twice as large (0.08 Å) for the EXAFS-determined $\text{U}-\text{OH}_2$ distances, which for the synchrotron radiation studies exhibit a range of 2.40–2.48 Å. This suggests that the equatorial hydration of $[\text{UO}_2]^{2+}$ is sensitive to experimental variations, such as pH as well as the nature and concentration of the anion in the inorganic and organic acids.

To address aspects of these issues, an exhaustive series of U L_3 -edge EXAFS measurements have demonstrated that the perchlorate anion does not coordinate directly to the $[\text{UO}_2]^{2+} \cdot 5\text{H}_2\text{O}$ aquo cation even in 11.5 M HClO_4 (Sémon *et al.*, 2001). The average, equatorial $\text{U}-\text{OH}_2$ distances (2.40–2.43 Å) for the $[\text{UO}_2]^{2+}$ aquo ions in perchloric acid are independent of concentration, and are at the short end of the range of distances for the mineral acid aquo ion systems of Table 28.2. In contrast, the systematic U L_3 EXAFS studies of the $[\text{UO}_2]^{2+}$ ion in 0–10 M solution concentrations of HCl reveal inner-sphere Cl^- complexation at and above 4 M, which is accompanied by expansion of the $\text{U}-\text{OH}_2$ bond lengths (Allen *et al.*, 1997). The total equatorial coordination number remained constant at five, suggesting a simple replacement of H_2O with Cl^- as the concentration of HCl increased. Subsequent treatments of the ten EXAFS spectra in the $[\text{Cl}^-]$ series through principal component (factor) analysis revealed the presence of three distinct species (Wasserman *et al.*, 1999). Two of these reflect the inner-sphere replacement of H_2O by Cl^- at the equatorial position in the 1–10 M HCl solutions. The third species, significant only for the $[\text{UO}_2]^{2+}$ ion in 12 and 14 M solutions of LiCl, was attributed to a product resulting from the use of the Dowex anion-exchange resin for the preparative chemistry.

In acidic solutions (pH \approx 5) of 0.052 M $[\text{UO}_2]^{2+}$ with excess fluoride ion (0.21 and 0.45 M), the equatorial coordination number was also found to be five, consisting of a combination of U–F and U–OH₂ interactions that were not resolved in the FT data (Vallet *et al.*, 2001). The F[−] and H₂O coordination numbers were determined from the combined results of equilibrium measurements and the U L₃-edge EXAFS analysis to reveal tri- and tetrafluoride complexation, $[\text{UO}_2\text{F}_3(\text{H}_2\text{O})_2]^-$ and $[\text{UO}_2\text{F}_4(\text{H}_2\text{O})]^{2-}$, with average U–F and U–OH₂ distances of 2.25–2.26 and 2.47–2.48 Å, respectively. At 3 M [F[−]], water does not participate in the equatorial coordination, which was shown to consist of five F[−] anions at 2.26 Å, of the uranyl(vi) pentafluoride complex, $[\text{UO}_2\text{F}_5]^{3-}$ (Vallet *et al.*, 2001). Solution EXAFS and quantum chemical methods have been brought to bear upon the nature of aqueous uranyl(vi) complexes with fluoride and oxalate, $[\text{C}_2\text{O}_4]^{2-}$, ligands (Vallet *et al.*, 2003). At pH=4.2 in the absence of F[−], the equatorial bonding in the $[\text{UO}_2(\text{O}_2\text{C}_2\text{O}_2)_2\text{H}_2\text{O}]^{2-}$ complex was determined to consist of five O atoms of which four are attributable to the two symmetric oxalate ligands, wherein each carboxylate group chelates to U in a monodentate fashion with one O, and the fifth is from H₂O. In this molecular complex, whose structure is illustrated below (left), the average equatorial U–O distance is 2.38 Å. Upon the addition of F[−] at a concentration slightly in excess of that (0.06 M) for $[\text{UO}_2]^{2+}$, the fluoride ion displaces the water molecule without any effect on the nature of the oxalate chelation, thereby maintaining the five-coordinate equatorial ligation, $[\text{UO}_2(\text{O}_2\text{C}_2\text{O}_2)_2\text{F}]^{3-}$. With excess (1.68 M) oxalate at pH=6.5, a five-coordinate complex with three oxalate ligands, $[\text{UO}_2(\text{O}_2\text{C}_2\text{O}_2)_3]^{4-}$, is formed. In this structure (illustrated below, right) two of the oxalates are chelate-bonded exactly as in the aquo and fluoride complexes and the third is bound to U through a single carboxylate O.



The early EXAFS experiments indicated that the dissolution of solid uranyl nitrate, $\text{UO}_2(\text{NO}_3)_2 \cdot 6\text{H}_2\text{O}$, and sodium uranyl acetate, $\text{NaUO}_2(\text{CH}_3\text{CO}_2)_3$, at concentrations of 0.25 M and less in acidic media leads to their complete dissociation and formation of the pentahydrate aquo ion, $[\text{UO}_2]^{2+} \cdot 5\text{H}_2\text{O}$ (Charpin *et al.*, 1985). In subsequent concentration- and temperature-dependent U L₃-edge EXAFS measurements (Schofield *et al.*, 1999), no evidence was found for equatorial ligand replacement of H₂O with $[\text{NO}_3]^-$ in acidic solutions of 1 M nitrate and less at 150°C and below. In related *in situ*,

temperature-dependent U L₃-edge EXAFS studies of the uranyl ion speciation in acidic acetate solutions with different concentration ratios, [CH₃CO₂⁻]: [UO₂²⁺], (Mosselmans *et al.*, 2001), little direct evidence was apparent in the FT data for [CH₃CO₂]⁻ coordination to the pentahydrate [UO₂]²⁺ cation at low ratios. Whereas the equatorial coordination number was also found to be five at high ratios, the evidence for distant U–C backscattering suggests the coordination of at least two bidentate acetate ligands even at temperatures as high as 250°C. The presence of one H₂O molecule is presumed to complete the equatorial O coordination in a neutral aquo species, [UO₂(CH₃CO₂)₂H₂O].

For the binary, aqueous [UO₂]²⁺–[SO₄]²⁻ system in acidic solution pH ≤ 2, bidentate O coordination of the sulfate ligand to [UO₂]²⁺ was evident through observation of distant S backscattering in the U L₃-edge EXAFS data for each of two solution species identified as UO₂SO₄(aq) and [UO₂(SO₄)₂]²⁻ in the equilibrium distribution diagram (Moll *et al.*, 2000a). Both were shown to have an equatorial O coordination number of five, meaning that in addition to the two O atoms from the bidentate [SO₄]²⁻ groups, the former has three H₂O molecules, i.e. [UO₂SO₄(H₂O)₃], and the latter has one H₂O molecule, i.e. [UO₂(SO₄)₂H₂O]²⁻, in the inner-sphere equatorial coordination environment of [UO₂]²⁺. At the higher pH of 5.25, obtained by adjustment with NaOH, the EXAFS metrical results showing bidentate sulfate chelation in the [UO₂]²⁺–[SO₄]²⁻–[OH]⁻ system were used to verify the previously proposed structure models for the tri- and pentanuclear complex anions, [(UO₂)₃O(OH)₂(SO₄)₃(H₂O)₂]⁴⁻ and [(UO₂)₅O₃(OH)₂(SO₄)₄(H₂O)₂]⁶⁻, respectively. For a related sulfur-bearing oxoanion in acidic aqueous solutions, the triflate anion, [CF₃SO₃]⁻, was found to act as a monodentate ligand by inner-sphere coordination to U through one O atom at high (>8M) concentrations of the anion (Sémon *et al.*, 2001). The total equatorial O coordination number is approximately five, suggesting the displacement of one H₂O molecule from the pentahydrate aquo species and the formation of [UO₂(CF₃SO₃)₁(H₂O)₄]⁺.

(ii) Neptunyl(*ν*)

Although there are, as yet, no experimental structural details for the aqueous uranyl ion of U⁵⁺, [UO₂]⁺, the calculated structure (Hay *et al.*, 2000) using DFT methods is, not surprisingly, a pentagonal bipyramid with U=O and U–OH₂ bond lengths of 1.810 and 2.616 Å, respectively. Unlike U, the most stable form of Np in acidic aqueous solution is the pentavalent neptunyl ion, [NpO₂]⁺·*n*"H₂O. It can be conveniently and reversibly interconverted to the hexavalent form, [NpO₂]²⁺·*n*'''H₂O, by electrochemical means, suggesting that the one-electron redox reaction is either independent of possible differences in the hydration of Np or, alternatively, that the hydration numbers *n*" and *n*''' for [Np⁵⁺O₂]⁺ and [Np⁶⁺O₂]²⁺, respectively, are equivalent. This has been an issue of some controversy since the 1970s, when original work involving NMR

studies of perchlorate salt solutions of $[\text{NpO}_2]^{2+}$ was interpreted to provide a mean number of six-coordinated water molecules (Shcherbakov *et al.*, 1974; Mashirov *et al.*, 1975; Shcherbakov and Iorga, 1975). Similarly, based upon ^1H NMR experiments, a hydration number of six was proposed for $[\text{NpO}_2]^+$ (Glebov *et al.*, 1977). Recent interpretations of electronic absorption spectra suggest that the hydration number for both neptunyl species, $[\text{NpO}_2]^+$ and $[\text{NpO}_2]^{2+}$, is five and, furthermore, that their coordination polyhedra are pentagonal bipyramids (Garnov *et al.*, 1996). This interpretation is consistent with the accepted coordination of the pentahydrate, hexavalent uranyl ion, $[\text{UO}_2]^{2+} \cdot 5\text{H}_2\text{O}$.

As shown in Table 28.4, the first Np L_3 -edge EXAFS brought to bear upon the $[\text{NpO}_2]^+ \cdot n\text{H}_2\text{O}$ ion indicated that $^{237}\text{Np}^{5+}$ has an equatorial coordination of five H_2O molecules at 2.52(2) Å (Combes *et al.*, 1992). Two subsequent, independent EXAFS investigations (Allen *et al.*, 1997; Antonio *et al.*, 2001) as well as the results from two theoretical calculations (Hay *et al.*, 2000; Tsushima and Suzuki, 2000) confirmed the hydration number of five. A lower value of four H_2O molecules was extracted from the analysis of the EXAFS data for an aqueous solution of 0.05 M $[\text{NpO}_2]^+$ in 0.1 M HNO_3 , the sole exception (Reich *et al.*, 2000). Although the exact reasons for the variance are not known, the complex hydrolytic behavior of Np^{5+} , particularly at $\text{pH} \approx 1$, might have some bearing upon this as well as the unusually large (0.08 Å) range of average interatomic distances, 2.44–2.52 Å, involving the equatorial coordination of water molecules. Alternatively, it may suggest that the hydration sphere of $[\text{NpO}_2]^+$ has substantial sensitivity to experimental conditions, such as pH, counter-anion, ionic strength, etc., whereas the axial $\text{Np}=\text{O}$ interactions (1.80–1.85 Å) are less sensitive. In either case, complicating chemical behaviors, e.g. hydrolysis, disproportionation, complexation, oligomerization, precipitation, etc., are generally suppressed in a highly acidic ($\text{pH} \approx 0$) non-complexing perchloric acid medium. The EXAFS experimental conditions cover a range of pH values starting from effectively 0 in 1 M HClO_4 (Antonio *et al.*, 2001) to $\text{pH} \approx 1$ in 0.1 M HNO_3 (Reich *et al.*, 2000), to $\text{pH} \approx 2$ in perchloric acid (Combes *et al.*, 1992) and, finally, to $\text{pH} \approx 3$ in hydrochloric acid with excess (3 M) chloride as LiCl (Allen *et al.*, 1997). At Cl^- concentrations of ca. 6 M and above, the equatorial coordination number remains constant at five, but whereas one (or more) Cl^- ions displace and replace an equal number of H_2O molecules about $[\text{NpO}_2]^+$ (Allen *et al.*, 1997). This is accompanied by an elongation of the $\text{Np}-\text{OH}_2$ bond lengths.

(iii) *Neptunyl(vi)*

The two independent Np L_3 -edge EXAFS studies (Reich *et al.*, 2000; Antonio *et al.*, 2001) and the two independent theoretical studies (Hay *et al.*, 2000; Tsushima and Suzuki, 2000) of the hexavalent neptunyl ion are in consensus

about the hydration number (five). The EXAFS results reveal axial Np=O bond lengths (1.73–1.75 Å) and equatorial Np–OH₂ bond lengths (2.36–2.41 Å) that are consistently shorter (ca. 0.03–0.16 Å) than the corresponding interactions for the pentavalent neptunyl aquo ion [NpO₂]⁺·5H₂O. The shorter bond distances for the hexavalent species [NpO₂]²⁺·5H₂O are consistent with the expected decrease in the Np IR with increasing oxidation state. The well-known ionic radii (IR) tabulations of Shannon (1976) are limited to the comparison between Np⁵⁺ (0.75 Å) and Np⁶⁺ (0.72 Å) for CN = 6. The 0.03 Å difference is considerably smaller than the corresponding IR contraction of 0.14 Å between Np³⁺ (1.01 Å) and Np⁴⁺ (0.87 Å), which is clearly borne out in the Np–OH₂ distances of Table 28.4 for the Np³⁺·*n*H₂O and Np⁴⁺·*n*'H₂O systems. The absence of experimental detail for the pentavalent uranyl aquo ion prevents the analogous metrical comparisons between it and the hexavalent uranyl aquo ion. Because the Pu aquo system has stable pentavalent and hexavalent plutonyl ions, additional comparisons, both absolute and relative, can be drawn with regard to the data of Table 28.5.

(iv) *Plutonyl(vi/v)*

Two reports of Pu L₃-edge EXAFS measurements (Ankudinov *et al.*, 1998; Conradson, 1998) constitute the full extent of experimental investigation of the [Pu⁵⁺O₂]⁺·*n*"H₂O system and the majority of that for [Pu⁶⁺O₂]²⁺·*n*"H₂O. For plutonyl(v), the curve-fitting analysis furnished axial Pu=O bond lengths of 1.81–1.84 Å and an equatorial coordination number of four with Pu–OH₂ bond lengths of 2.45–2.47 Å. This hydration number (four) stands in contrast to that (five) obtained from the results of two different levels of calculation with DFT (Hay *et al.*, 2000) and Hartree–Fock (Tsushima and Suzuki, 2000) methods. The theoretical investigations of the hexavalent plutonyl aquo ion reach the same conclusion, namely that [PuO₂]²⁺ forms the most stable and strongly bound complexes with five H₂O molecules in the equatorial coordination (Spencer *et al.*, 1999; Hay *et al.*, 2000; Tsushima and Suzuki, 2000). Whereas the optical spectroscopy (Garnov *et al.*, 1996) and the early EXAFS experiments (Runde *et al.*, 1997) are in agreement, showing an O coordination number of five, the later EXAFS work (Ankudinov *et al.*, 1998; Conradson, 1998) provides an O coordination number of six. The fact that the average Pu–OH₂ distances of 2.45 Å (Runde *et al.*, 1997) for the pentahydrate plutonyl(vi) and 2.40–2.45 Å (Ankudinov *et al.*, 1998; Conradson, 1998) for the hexahydrate plutonyl(vi) species are overlapping despite the unit difference in hydration number remains something of a quandary. In strongly acidic (1 M HClO₄ and 1 M HCl) [PuO₂]²⁺ solutions with aqueous chloride concentrations of 5 M and above, Pu EXAFS data reveal the formation of plutonyl(vi) chloro complexes, wherein some number of inner-sphere H₂O are replaced by Cl[−] ions (Runde *et al.*, 1997). Although the exact extent of the

Cl⁻ substitution was not determined, the effects include a weakening and elongation (0.01 to 0.06 Å) of the remaining equatorial Pu–OH₂ interactions as well as the axial Pu=O bonds.

According to the data of Table 28.5, the axial Pu–O interatomic distance contraction between the plutonyl(v) and (vi) aquo ions amounts to 0.06–0.10 Å. This is more than twice that expected based upon the difference in the Pu⁵⁺ (0.74 Å) and Pu⁶⁺ (0.71 Å) IR for CN=6 (Shannon, 1976). As mentioned previously, the same phenomenon was observed for the neptunyl(v) and (vi) aquo ions. This behavior is to be contrasted with that between the aquo ions of Pu³⁺ and Pu⁴⁺, which exhibit a 0.09–0.12 Å Pu–OH₂ interatomic distance contraction that is consistent in magnitude with the 0.14 Å difference of IR for CN = 6. In view of the apparent difference in the equatorial coordination number between [PuO₂]⁺ and [PuO₂]²⁺, it is difficult to ascribe any significance to the 0.0–0.07 Å difference between the Pu–OH₂ distances of Table 28.5. Comparisons with corresponding Am species, [AmO₂]⁺ and [AmO₂]²⁺, would be informative but are not possible because of the present lack of metrical information for these two aquo ions.

28.2.3 Base redox speciation

The aqueous actinide chemistry of the four oxidation states – III, IV, V, and VI – described above for acidic solutions have been complemented by studies, albeit far fewer in number, of the same four states plus the heptavalent (VII) one in alkaline and carbonate solutions (Shilov and Yusov, 2002). In particular, the An⁷⁺ ions of Np, Pu, and Am are extremely unstable species under all but the most alkaline of conditions. Concentrated carbonate solutions too have been shown to facilitate studies of the otherwise unstable Am⁴⁺, Cf⁵⁺, and Cm⁶⁺ ions. Aspects of An redox speciation in hydroxide and carbonate media as obtained by use of EXAFS spectroscopy are surveyed in this section.

(a) Hydroxide solution systems

(i) Neptunium(vii/vi)

A longstanding problem in actinide science about the nature of the Np⁷⁺ species in aqueous, basic solutions was resolved through use of EXAFS and quantum chemistry. Since the first report of its preparation (Krot and Gelman, 1967), the coordination environment of Np⁷⁺ has remained controversial, in part because of the technical difficulties associated with the stabilization of the high-valent ion. The existence of an anionic species of Np⁷⁺ in alkaline solution was proposed early on (Spitsyn *et al.*, 1969), “. . .and its formula is believed by most researchers to be NpO₅³⁻” (Fahey, 1986). Still, equally probable trianionic

forms include $[\text{NpO}_4(\text{OH})_2]^{3-}$ (Burns *et al.*, 1973) and $[\text{NpO}_2(\text{OH})_6]^{3-}$, among others. In order to address this speciation issue, Np L_3 -edge EXAFS was brought to bear upon a 0.03 M solution of Np^{7+} in 2.5 M NaOH prepared by ozonation of the neptunyl(vi) hydroxide, $\text{NpO}_2(\text{OH})_2$ (Clark *et al.*, 1997). The analysis provided evidence for a linear, *trans*-dioxo species of Np^{7+} , which has an overall pentagonal bipyramidal coordination consisting of the two axial O atoms at 1.85(2) Å and five equatorial O atoms attributed to four OH^- at 2.18(3) Å and one H_2O at 2.43(3) Å. This environment is consistent with the formation of a monoanionic neptunyl(vii) species, $[\text{NpO}_2(\text{OH})_4(\text{H}_2\text{O})]^-$, whose coordination polyhedron is similar, albeit with different Np–O distances, to those for the *bona fide* dioxo species of $[\text{Np}^{5+}\text{O}_2]^+$ and $[\text{Np}^{6+}\text{O}_2]^{2+}$ that are ubiquitous in acid solution.

In contrast, two subsequent Np EXAFS and DFT studies (Bolvin *et al.*, 2001; Williams *et al.*, 2001) of the coordination geometry of Np^{7+} in alkaline solution came to the conclusion that Np^{7+} has a tetraoxo square planar coordination environment. The presence of two distant, axial O atoms, presumably hydroxide ligands, completes the coordination sphere, which has a square bipyramid structure. In one study (Williams *et al.*, 2001), bulk electrolysis techniques in simultaneous combination with ozonation were utilized to control the Np valence in a freshly prepared suspension of Np^{5+} (0.0065 M) in 1 M NaOH for *in situ* Np L_3 -edge EXAFS of the Np^{7+} and Np^{6+} ions, whose electrochemical interconversion is facile (Zielen and Cohen, 1970). The Np^{6+} EXAFS was fit to reveal a typical *trans*-dioxo species with two close, axial O atoms at 1.82(2) Å and an equatorial coordination of four distant O atoms at 2.21(3) Å, in what would likely be a square bipyramidal polyhedron, $[\text{NpO}_2(\text{OH})_4]^{2-}$. Geometry optimizations at the B3LYP level using a CPCM solvent model confirm this neptunyl(vi) structure and stoichiometry (Bolvin *et al.*, 2001). In contrast, the Np^{7+} EXAFS was fit to reveal four close O atoms at 1.87(1) Å and two distant ones at 2.24(4) Å, consistent with a polyhedron that could also be a square bipyramid. The accompanying DFT calculations predicted a slightly distorted square-planar geometry for the tetraoxo, $[\text{NpO}_4]^-$, anion (Williams *et al.*, 2001). The geometry was further elucidated at the DFT level using the hybrid functional B3LYP and a CPCM solvent model to reveal a six-coordinate Np^{7+} in the square bipyramid polyhedron, $[\text{NpO}_4(\text{OH})_2]^{3-}$ (Bolvin *et al.*, 2001). The associated Np L_3 -edge EXAFS acquisition and analysis for a solution of Np^{7+} (0.015 M) in 2.5 M NaOH revealed a coordination of 3.6 ± 0.3 O atoms at 1.89 Å and 3.3 ± 1.3 O atoms at 2.33 Å. The large error on the distant O coordination number was attributed to the low backscattering amplitude and the interference from the four close O atoms. From the combination of theoretical results and experimental data (including solid-state structural and solution electrochemical information) (Shilov, 1998), it was concluded "...that the predominant Np(vii) complex found in solutions with high concentration of OH^- is indeed $\text{NpO}_4(\text{OH})_2^{3-}$ " (Bolvin *et al.*, 2001).

(ii) *Plutonium(vii/vi)*

Although no EXAFS results have been published about the corresponding Pu⁷⁺/Pu⁶⁺ and Am⁷⁺/Am⁶⁺ redox speciation in alkaline solutions, the plutonium electrochemical behavior as a function of hydroxide ion activity is very much like that for neptunium, except for the more positive electrode potentials for Pu (Shilov, 1998). This suggests that the six O, tetragonal bipyramidal coordination environments for both Np⁷⁺ and Np⁶⁺ are likely to be obtained for the corresponding Pu species. In these, the absence of a substantial structural rearrangement between the hexa- and heptavalent species would explain the reversible and generally facile redox reaction:



The formulas shown in this equation are presently accepted by actinide electroanalytical chemists in general (for An \equiv Np, Pu, and Am) and this An⁷⁺/An⁶⁺ redox speciation appears, exactly as written, in contemporary compilations of standard electrode potentials (Bratsch, 1989). The estimated potential for the Pu⁸⁺/Pu⁷⁺ couple (> 3V) (Shilov and Yusov, 2002) is well beyond the polarization window of aqueous solutions. The existence of Pu⁸⁺ will have to be confirmed in other solvents, such as newly designed ionic liquids with immense (ca. 5V) polarization windows (Quinn *et al.*, 2002), or in the solid-state.

(iii) *Uranyl(vi)*

Because of practical and technological issues in nuclear waste storage and processing, the speciation and structure of U⁶⁺ complexes in strongly alkaline solutions has been investigated with U L₃-edge EXAFS, quantum chemical calculations, and other spectroscopic and physical methods (Moll *et al.*, 1998; Schreckenbach *et al.*, 1998; Clark *et al.*, 1999; Wahlgren *et al.*, 1999; Moll *et al.*, 2000b; Vallet *et al.*, 2001). Driven by implications of serious environmental concern, i.e. aging tanks of alkaline high-level waste, the original work (Clark *et al.*, 1999) on [UO₂]²⁺ (\approx 0.10 M) in a 3.5 M tetramethylammonium hydroxide, [(CH₃)₄N]OH, solution sparked interest of theoretical, applied, and fundamental importance. The FT data revealed a single asymmetric peak, which was shown to include backscattering contributions from axial and equatorial O coordination. The k³χ(k) EXAFS was fit to expose two nearest O atoms at 1.79(1) Å, attributed to axial U=O bonding, and 5.2(5) Å, attributed to equatorial U–OH bonding. This seven O pentagonal bipyramidal coordination of U⁶⁺ is not unusual on its own and, except for the relatively long and short axial and equatorial bonds, respectively, it is the prevalent structure in acid solution. Yet, comparison of the solution environment with that for the solid uranyl(vi) salt, [Co(NH₃)₆]₂[UO₂(OH)₄]₃·H₂O, crystallized from 3.5 M [(CH₃)₄N]OH revealed unexpected detail that has been the source of multinational debate. The single-crystal structure shows a six O pseudo-octahedral

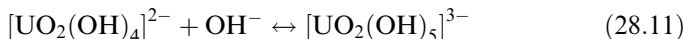
coordination of U^{6+} with two *trans*-oxo atoms at 1.82(1) Å and four OH⁻ ligands at 2.26(2) Å. The corresponding EXAFS data for the crystalline compound, collected and analyzed in the same manner as for the solution sample, are in agreement with the X-ray diffraction data. The $k^3\chi(k)$ EXAFS were best fit with two O atoms with an average U=O distance of 1.81(1) Å and 3.9(5) O atoms with an average U–O distance of 2.21(1) Å (Clark *et al.*, 1999). The pivotal difference between the solid and solution structures is the OH⁻ coordination number, which is four in the solid and five in solution.

Although such differences in coordination upon dissolution of a solid are not extraordinary, the remarkable aspect here is the observation of essentially identical, within experimental error, average U=O and U–OH distances despite the coordination number difference in the solution (7) and solid (6) uranyl hydroxide complexes. Based upon a comparison of the U^{6+} IR for CN=6 and 7 (0.73 and 0.81 Å, respectively) (Shannon, 1976), the U–O distances for the seven-coordinate solution sample are anticipated to be 0.08 Å longer than those for the corresponding six-coordinate solid sample. An expansion of this magnitude is not evident, suggesting that a simple ionic, electrostatic model of the U=O and U–OH interactions is inappropriate for these systems. Alternatively, it may be an indication of some degree of covalency and the participation of f-electrons in the U–O bonding, or that the solution coordination number is in error because of, for example, the effects of an equilibrium distribution of two monomeric uranyl(vi) species, a pentahydroxide, $[UO_2(OH)_5]^{3-}$, and a tetrahydroxide, $[UO_2(OH)_4]^{2-}$ (Clark *et al.*, 1999). These intriguing results, in particular, the equatorial coordination number (5) in highly alkaline solution conditions, have been experimentally confirmed through EXAFS (Moll *et al.*, 1998; Wahlgren *et al.*, 1999). Yet, remarkably, and as developed below, the EXAFS-determined value was set aside in favor of that (4) from bond length comparisons and theoretical and geometrical optimizations.

Uranium L₃-edge EXAFS was used to elucidate the coordination of $[UO_2]^{2+}$ (0.055 M) in solutions of $[(CH_3)_4N]OH$. The results obtained from the curve-fitting analyses are indistinguishable and reveal two axial O atoms at 1.82 Å as well as 5.0 ± 0.5 and 5.2 ± 0.5 equatorial O atoms at 2.24 Å in 1 and 3 M $[(CH_3)_4N]OH$, respectively (Moll *et al.*, 1998; Wahlgren *et al.*, 1999). This latter coordination number was subsequently reevaluated to be 4.6 ± 0.6 (Moll *et al.*, 2000b). A number of factors combine to cast doubt on the EXAFS result for the equatorial coordination number, including the general difficulty and large uncertainty associated with such determinations for uranyl complexes at ambient temperature. (Thompson *et al.*, 1995, 1997; Barnes *et al.*, 2000) Insofar as bond lengths generally increase with coordination number (Shannon, 1976), it is also peculiar that the average U–OH distance (2.24 Å) for a purportedly five-coordinate hydroxo anion of $[UO_2]^{2+}$ in solution is the same as that (2.26(2) Å) for the four OH⁻-coordinated $[UO_2]^{2+}$ complex anion, $[UO_2(OH)_4]^{2-}$, in a crystallographically characterized solid (Clark *et al.*, 1999). Despite the higher coordination number indicated by the EXAFS data, it was concluded "...that

the coordination number of uranyl(vi) ion in strongly alkaline solution is four, not five. . .” and that the mononuclear, tetrahydroxide species, $[\text{UO}_2(\text{OH})_4]^{2-}$, is the dominant complex in strongly alkaline solutions (Wahlgren *et al.*, 1999). This suggestion was corroborated by the results of geometry optimizations obtained through a number of *ab initio* quantum chemical calculations (Moll *et al.*, 1998; Schreckenbach *et al.*, 1998; Wahlgren *et al.*, 1999; Vallet *et al.*, 2001).

At the time of this publication, issues about the form of $[\text{UO}_2]^{2+}$ in alkaline solution were most recently revisited with regard, again, to its speciation in 0.5 and 3 M $[(\text{CH}_3)_4\text{N}]\text{OH}$ by use of U L_3 -edge EXAFS and ^{17}O NMR (Moll *et al.*, 2000b). The results serve to resolve, in part, the controversy generated by the watershed report (Clark *et al.*, 1999), whose experimental evidence indicated the formation of a pentahydroxide species, and the approximately coincident work (Wahlgren *et al.*, 1999), whose evidence was interpreted in favor of a tetrahydroxide species. The latest research has found evidence for the latter, $[\text{UO}_2(\text{OH})_4]^{2-}$, species from the primary EXAFS analysis of data obtained in a dilute (0.05 M) solution of $[\text{UO}_2]^{2+}$ in 0.5 M $[(\text{CH}_3)_4\text{N}]\text{OH}$ at $\text{pH}=13.7$ (Moll *et al.*, 2000b). The pseudo-octahedral environment of U^{6+} was shown to consist of 1.8 ± 0.3 O atoms at 1.83 Å and 4.2 ± 0.6 O atoms at 2.26 Å. In the concentrated, 3 M solution of $[(\text{CH}_3)_4\text{N}]\text{OH}$ of the original studies (Clark *et al.*, 1999), the presence of a fifth OH^- ligand in association with $[\text{UO}_2(\text{OH})_4]^{2-}$ was unambiguously established by use of ^{17}O NMR (Wahlgren *et al.*, 1999). A $[\text{UO}_2(\text{OH})_5]^{3-}/[\text{UO}_2(\text{OH})_4]^{2-}$ ratio of ≈ 0.3 in a 3 M solution of $[(\text{CH}_3)_4\text{N}]\text{OH}$ was calculated based upon an estimation of the equilibrium constant for the aqueous reaction,



The EXAFS results for this mixture of solution species provide a site-averaged coordination environment of 1.8 ± 0.3 O at 1.83 Å and 4.6 ± 0.6 O at 2.25 Å (Wahlgren *et al.*, 1999).

Since the publication of the results from the pioneering X-ray scattering experimentation (Aberg, 1970; Musikas and Narten, 1978), metrical details about the solution structures of polynuclear hydrolysis products of uranyl(vi) have been few and far between. At least, there is a dearth of EXAFS research, other than the investigation of an acidic solution ($\text{pH}=4.1$) of dilute (0.05 M) $[\text{UO}_2]^{2+}$ in 0.05 M $[(\text{CH}_3)_4\text{N}]\text{OH}$ (Moll *et al.*, 2000b). In these conditions, the formation of the triangular, trinuclear complex, $[(\text{UO}_2)_3(\text{OH})_5]^+$, was confirmed on the basis of the 3.80 Å U–U interatomic distance. The U coordination number for a pure specimen of this trinuclear hydrolysis complex is two. The lower, EXAFS-determined values of $1.3\text{--}1.4\pm 0.4$ are consistent with an admixture of the trinuclear complex and the binuclear one, $[(\text{UO}_2)_2(\text{OH})_2]^{2+}$, whose structure has been optimized at several levels of theory (Tsushima and Reich, 2001) and which is presumed to have the core structure of the solid-state hydroxo compound $[(\text{UO}_2)_2(\text{OH})_2\text{Cl}_2(\text{H}_2\text{O})_4]$, with a U coordination number of one and a U–U interatomic distance of 3.94 Å (Aberg, 1970).

The EXAFS-measured distribution of equatorial U–O interactions, which involve a combination of bridging as well as terminal oxo and hydroxide ligation and bond lengths, are also consistent with a mixed speciation of polynuclear complexes. The site- and species-averaged, axial U=O bond length of the uranyl ion was 1.79 Å (Moll *et al.*, 2000b).

(iv) *Thorium(IV)*

The hydrolysis of the tetravalent actinides leads to a complicated distribution of species with different degrees of aggregation, the exact extent of which hinges upon the solution conditions (Neck and Kim, 2001). For example, even below the onset of oligomerization, in the narrow (2 unit) pH range of 3–5, the calculated Th⁴⁺ speciation already indicates appreciable amounts of bi- and tetranuclear species, such as [Th₂(OH)₂]⁶⁺ and [Th₄(OH)₈]⁸⁺, in addition to the mononuclear ones, e.g. [Th(OH)]³⁺, [Th(OH)₂]²⁺, [Th(OH)₃]⁺ (Neck *et al.*, 2002). In view of the complexity for such an assortment of multi-site, polynuclear complexation, the use of EXAFS for studies of the aqueous speciation of suspended colloids above the onset of hydrolysis has been limited. The available studies concern the use of Th L₃-edge EXAFS for coulometrically titrated solutions (pH=1.38–3.67) of 0.0043–0.028 M Th⁴⁺ in 0.5 M NaCl (Neck *et al.*, 2002; Rothe *et al.*, 2002). The FT data for the aqueous solutions of pH ≤ 3 (below the onset of colloid formation) exhibit a strong, nearly symmetric peak due to O backscattering, fit as 11.6–12.7 O at 2.45–2.46 Å, that is typical of the Th⁴⁺ aquo ion. In contrast, the FT data for the aqueous suspension of colloidal species at pH=3.50 and 3.62 exhibit a weak, highly asymmetric peak due to O backscattering, fit as 10.5–10.6 O at 2.51 Å, that is expected for a broad distribution of Th–O interactions arising from the presence of a mixture of ultrafine (i.e. nanosize), polynuclear species and amorphous Th⁴⁺ colloids. The EXAFS data for the aqueous suspension at pH=3.67 also reveals a weak, distant peak attributed to Th–Th interactions. The structural parameters and Th⁴⁺ coordination environment for this specimen are similar to those for the carefully prepared amorphous hydrated oxyhydroxide solid, ThO_n(OH)_{4–2n}·xH₂O (Neck *et al.*, 2002; Rothe *et al.*, 2002).

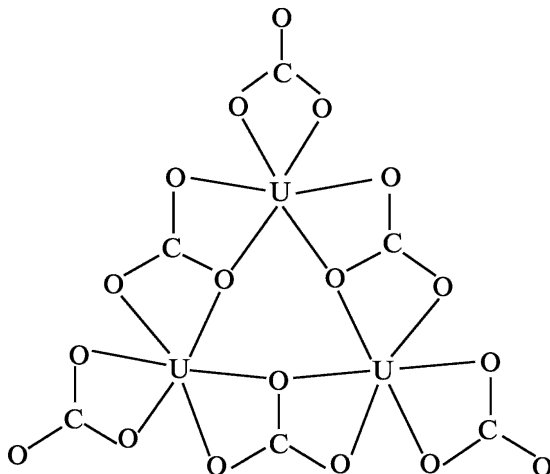
(b) **Carbonate solution systems**

A large part of the interest and activity in environmental and molecular sciences of the actinide elements concerns their interactions with carbonate, [CO₃]²⁻, and bicarbonate, [HCO₃]⁻, anions in hydrologic and geochemical processes. Besides H₂O (including hydroxide) itself, these are the predominant ligands for An-ion complexation found in fresh and saline waters alike. Of the Earth's estimated total water volume, approximately 97% or 317 × 10⁶ mi³ is attributed to seawater alone (Nace, 1967), which is known to contain an essentially uniform, worldwide distribution of uranium at 3.35 ± 0.2 × 10⁻⁹ g/cm³ (Ku *et al.*, 1977).

An estimate of the total amount of dissolved U in the oceans (4.43×10^{12} kg) provides a glimpse of the enormity of scale and the correspondingly keen interest in its aqueous speciation. From decades of experimental study, it is generally accepted that U takes the form of the mononuclear anionic, uranyl(vi) tris(carbonato) complex, $[\text{UO}_2(\text{CO}_3)_3]^{4-}$, in the slightly alkaline ($\text{pH} \approx 8$) ocean waters (Djogic and Branica, 1991). Despite comprehensive studies of actinide carbonate chemistry, which are very well reviewed elsewhere (Clark *et al.*, 1995), the field of synchrotron radiation research of An carbonate complexes was late to break open with the report on uranyl carbonate complexes in near-neutral aqueous solution (Allen *et al.*, 1995). In this section, we describe the results obtained from EXAFS studies of the carbonate solution chemistry of the trivalent and tetravalent An ions as well as for the actinyl, $[\text{AnO}_2]^{n+}$, carbonates of the pentavalent ($n=1$) and hexavalent ($n=2$) An ions.

(i) *Uranyl(vi)*

The apparent simplicity of the $[\text{CO}_3]^{2-}$ anion belies its flexibility in the formation of coordination compounds with $[\text{UO}_2]^{2+}$ in various degrees of polynuclear association. In addition to serving conventional mono- and symmetrical bidentate structural roles, it may serve to bridge and link metal-ions. Although some 14 modes of carbonate ligation with two, three, four, and six metal-ions are known (Cotton *et al.*, 1999), its service as a molecular bridge between uranyl cations is relatively rare (Allen *et al.*, 1995; Clark *et al.*, 1995). To elucidate aspects of such aggregation behavior, a multipronged approach was taken to unravel the solution species distribution of the monomeric tris(carbonato) complex, $[\text{UO}_2(\text{CO}_3)_3]^{4-}$, and the trimeric complex, $[(\text{UO}_2)_3(\text{CO}_3)_6]^{6-}$. The unusual structure of the trimer, schematically illustrated below without the axial O atoms, is built up of three bis(carbonato) monomers of empirical formula



$[\text{UO}_2(\text{CO}_3)_2]^{2-}$ with three bridging carbonate ligands linking three U^{6+} ions in a fashion (i.e. six-bond $-(\text{U}-\text{O})_3-$ ring) not depicted in Cotton *et al.* (1999).

A 0.2 M aqueous solution (pH = 5.7) of this crystallographically characterized triangular, trinuclear uranyl(vi) carbonate, $[(\text{UO}_2)_3(\text{CO}_3)_6]^{6-}$ as the guanidinium salt $[\text{C}(\text{NH}_2)_3]^+$, was studied by U L_3 -edge EXAFS (Allen *et al.*, 1995). The data analysis provided O, C, and U coordination numbers and interatomic distances consistent with the trimeric structure of the solid salt, $[\text{C}(\text{NH}_2)_3]_6[(\text{UO}_2)_3(\text{CO}_3)_6] \cdot 6.5\text{H}_2\text{O}$, suggesting that the oligomeric anionic unit is maintained upon dissolution of the solid under the selected conditions. The analysis was confirmed by the presence of a distant, 4.92 Å U–U interaction that was not evident in the EXAFS data for the corresponding monomeric species, $[\text{UO}_2(\text{CO}_3)_3]^{4-}$, which has an otherwise identical, eight O coordination of U^{6+} in a hexagonal bipyramid polygon (Reeder *et al.*, 2000). The two closest, axial O atoms are bonded at 1.79 Å in both the monomeric and trimeric anions. The six equatorial O atoms arise from the symmetrical bidentate coordination of three carbonate groups, with an average U–O distance of 2.42 Å for the monomer and 2.45–2.46 Å for the trimer. The EXAFS data for the trimer and the monomer alike provide evidence for distant backscattering that was fit to reveal three C at 2.89–2.90 Å as well as three O at 4.12 Å (monomer) and at 4.16–4.17 Å (trimer), which are attributed to the terminal O atoms of the three carbonate ligands.

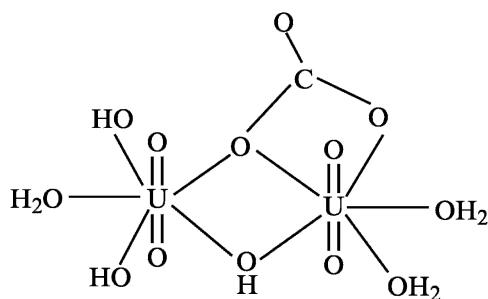
The recent discovery and characterization of the aqueous, neutral dicalcium uranyl(vi) tris(carbonato) complex, $[\text{Ca}_2\text{UO}_2(\text{CO}_3)_3]$, in natural, mining-related waters (Bernhard *et al.*, 1996) reinvigorates interest with the ages-old anionic species, $[\text{UO}_2(\text{CO}_3)_3]^{4-}$, particularly with regard to issues of ion-pairing. The combination of experimental (Bernhard *et al.*, 2001) and theoretical (Tsushima *et al.*, 2002) results reveal that counter-cations can play a significant role in the aqueous speciation and structure of the otherwise ordinary $[\text{UO}_2(\text{CO}_3)_3]^{4-}$ complex anion. The solution (pH = 8) U L_2 - and L_3 -edge EXAFS for $[\text{Ca}_2\text{UO}_2(\text{CO}_3)_3]$ (0.0005 M) and $[\text{UO}_2(\text{CO}_3)_3]^{4-}$ (0.001 M) do not differ significantly and, moreover, the carbonate coordination of uranyl(vi) in both is the same as that for the natural mineral liebigite, $\text{Ca}_2\text{UO}_2(\text{CO}_3)_3 \cdot 10\text{H}_2\text{O}$, which has two axial O at 1.78 Å, six equatorial O at 2.43 Å, three C at 2.86, and three O at 4.12 Å. In addition, the crystallographic structure of liebigite reveals a 4.07 Å U–Ca interaction arising from two Ca–O polyhedra in the equatorial plane. These distant Ca interactions are difficult to identify in the U EXAFS data of the $[\text{Ca}_2\text{UO}_2(\text{CO}_3)_3]$ aqueous species and solid mineral specimens at ambient temperature because of spectral congestion and overlap with the nearly equidistant interactions of the terminal O atoms (3) of the symmetrical, bidentate carbonate ligands. Nevertheless, based upon a rigorous analysis of the available EXAFS and in combination with other physical and spectroscopic evidence, Bernhard *et al.* (2001) concluded “. . .that the calcium atoms are likely to be in the same positions both in the solution complex and in the solid.” Structure optimizations of the neutral $[\text{Ca}_2\text{UO}_2(\text{CO}_3)_3]$ aquo species were subsequently

calculated at different levels (HF, MP2, and B3LYP) of theory with and without Ca^{2+} , i.e., $[\text{UO}_2(\text{CO}_3)_3]^{4+}$, and with and without hydration (Tsushima *et al.*, 2002). The calculated structure that included two Ca^{2+} and ten H_2O molecules is in good agreement with that deduced by EXAFS measurement and, thereby, demonstrates the need to explicitly incorporate counter-cations and water molecules to obtain accurate geometrical structures from theory.

Uranium L_3 -edge EXAFS was used to probe the coordination environment of the uranyl(VI) tris(carbonato) complex, $[\text{UO}_2(\text{CO}_3)_3]^{4+}$, before and after a stoichiometric, one-electron electrochemical reduction (Docrat *et al.*, 1999). In aqueous electrolytes of 1 M Na_2CO_3 at $\text{pH}=11.95$ (Docrat *et al.*, 1999) and 0.1 M $\text{Na}_2\text{CO}_3/0.1$ M NaNO_3 at $\text{pH}=11.3$ (Morris, 2002), the cyclic voltammetry data for $[\text{UO}_2(\text{CO}_3)_3]^{4+}$ (0.0022–0.010 M) show one electrochemically irreversible couple attributed to $\text{U}^{6+}/\text{U}^{5+}$ redox activity. The metastable reduced species formed by controlled potential coulometry was ascribed to the uranyl(V) tris(carbonato) complex, $[\text{UO}_2(\text{CO}_3)_3]^{5-}$. The U L_3 -edge position for the reduced species was 2.4 eV lower than that for the oxidized form, consistent with the reduction of $[\text{U}^{6+}\text{O}_2]^{2+}$ to $[\text{U}^{5+}\text{O}_2]^+$. The EXAFS analysis revealed that the basic geometry of the U coordination environment is essentially the same for both solution complexes, except for the expected variation of interatomic distances with change of U oxidation state. The average axial dioxo distance increases by 0.10 Å from 1.80(2) to 1.90(2) Å upon reduction. Elongations of similar magnitude (0.05–0.10 Å) are found for the six equatorial O bonds, the three C, and the three terminal O interactions with the carbonate ligands. These three distances increase, in order, from 2.43(2), 2.89(4), and 4.13(4) Å in the oxidized form to 2.50(2), 2.94(4), and 4.23(4) Å, respectively, in the reduced form. The absence of significant conformational variation between $[\text{UO}_2(\text{CO}_3)_3]^{4+}$ and $[\text{UO}_2(\text{CO}_3)_3]^{5-}$ makes it difficult to rationalize the less than ideal electrochemical response and the relative instability of the reduced species (Docrat *et al.*, 1999).

Four different isomers have been proposed for the binuclear complex anion, $[(\text{UO}_2)_2(\text{CO}_3)(\text{OH})_3(\text{H}_2\text{O})_n]^-$, in solution (Szabo *et al.*, 2000). This variety of bridge isomers is largely attributable to the assortment of different carbonate bonding modes (Cotton *et al.*, 1999) that can be envisioned to link the two $[\text{UO}_2]^{2+}$ groups in this ternary species. Although the use of U EXAFS alone is not sufficient to provide an unambiguous identification of the predominant isomer, the EXAFS results in combination with multinuclear (^{13}C and ^{17}O) NMR measurements have provided conclusive insight about the speciation. The U L_3 -edge EXAFS of a 0.05 M solution of $[(\text{UO}_2)_2(\text{CO}_3)(\text{OH})_3(\text{H}_2\text{O})_n]^-$ ($\text{pH} \approx 7-8$) was analyzed with multi-shell models of axial and equatorial O, U–C, and U–U interactions (Szabo *et al.*, 2000). The pivotal aspect of the analyses was the identification of terminal, equatorial OH⁻ bonding (1.3 ± 0.3 at 2.26 Å) and distant U interactions (0.5 ± 0.1 at 3.90 Å). The equatorial coordination sphere is completed by 3.9 ± 0.6 O atoms at 2.47 Å. This is consistent with a pentagonal bipyramidal uranyl(VI) environment, wherein the two axial O atoms are bonded

at 1.81 Å. The isomer structure consistent with the combined EXAFS and NMR data is suggested to consist of two $[\text{UO}_2]^{2+}$ groups that are bridged by two O atoms, one from hydroxide and one from the lone carbonate ligand that is in bidentate coordination with one uranyl unit. The terminal equatorial coordination is completed by a combination of the two remaining hydroxide ligands and three water molecules, $[(\text{H}_2\text{O})(\text{OH})_2\text{UO}_2(\text{OH})(\text{CO}_3)\text{UO}_2(\text{H}_2\text{O})_2]^-$, as illustrated below.



(ii) *Neptunyl(v)*

The study of neptunium in aqueous carbonate solutions provides fundamental information that can be applied to intricate environmental problems and to solving difficult issues with regard to the treatment of alkaline, high-level tank waste. Concerns about pentavalent neptunyl carbonate complexation, particularly the aqueous speciation, solubility, redox, and sorption behaviors, also relate to its fate and transport in subsurface geologic repositories (Efurd *et al.*, 1998; Kaszuba and Runde, 1999).

Three environmentally relevant neptunyl(v) carbonato complexes of general composition $[\text{NpO}_2(\text{CO}_3)_n]^{(2n-1)-}$ for $n=1$ $[\text{NpO}_2(\text{CO}_3)]^-$, $n=2$ $[\text{NpO}_2(\text{CO}_3)_2]^{3-}$, and $n=3$ $[\text{NpO}_2(\text{CO}_3)_3]^{5-}$, have long been of interest. Information about their molecular structures and the extent of hydration became available through Np L₃-edge EXAFS and complementary spectroscopic work on single-component solutions of the anions with unprecedented solubilities (0.001 M) achieved by use of the large, bulky tetra-*n*-butylammonium, $[(n\text{-Bu})_4\text{N}]^+$, counter-cations in place of alkali-metal cations (Clark *et al.*, 1996a,b). For the tris(carbonato) complex ($n=3$) in a Na_2CO_3 solution (of unspecified concentration), the EXAFS spectra show "...unequivocally that the carbonate ligands must be coordinated in a bidentate fashion due to the combination of six Np–O and three Np–C distances of 2.52 and 2.98 Å", (Clark *et al.*, 1996a) respectively. The overall eight-coordinate geometry of Np^{5+} is hexagonal bipyramidal, in which the two *trans*-neptunyl O atoms at 1.86(2) Å occupy the usual axial positions with respect to the six equatorial O atoms. Much less definitive information about the equatorial coordination was provided for the mono- and bis

(carbonato) species, $n=1$, and 2, respectively, in $[(n\text{-Bu})_4\text{N}]_2\text{CO}_3$ solutions (unspecified concentrations) because of curve-fitting difficulties and metrical uncertainties. What seems clear "... is a distinct change in coordination geometry about the neptunyl ion, from six O atoms in the tris- and bis-carbonato complexes, to five O atoms in the mono(carbonato) complex" (Clark *et al.*, 1996b). The five O atoms of the equatorial ligation for the mono(carbonato) complex are attributed to the coordination of three H_2O molecules and two O atoms from the $[\text{CO}_3]^{2-}$ anion in a symmetrical bidentate mode. The overall stereochemistry of Np^{5+} is expected to be a pentagonal bipyramid that has an average Np-O equatorial distance of 2.49(3) Å. This bond length is shorter than that (2.53(3) Å) for the 6-O equatorial coordination of the tris(carbonato) species, a detail that is consistent with the 5-O equatorial coordination of $[\text{NpO}_2]^+$ in $[\text{NpO}_2(\text{CO}_3)(\text{H}_2\text{O})_3]$. Similarly, the six O atoms of the equatorial ligation for the bis(carbonato) complex are attributed to the coordination of two H_2O molecules and four O atoms from the two bidentate $[\text{CO}_3]^{2-}$ anions, as $[\text{NpO}_2(\text{CO}_3)_2(\text{H}_2\text{O})_2]^{3-}$, with an average distance of 2.48(3) Å. It seems counter-intuitive that the higher coordination number for the bis(carbonato) complex does not correlate with a larger average equatorial Np-O distance, e.g. like that for the unequivocally characterized tris(carbonato) neptunyl(v) complex with six O atoms in the equatorial plane.

(iii) *Plutonyl(vI)*

The aqueous speciation of the plutonyl and americyl cations, $[\text{AnO}_2]^{n+}$ for $n=1$ and 2, in carbonate media has not been examined through XAS. Solid-state EXAFS studies of actinyl carbonates are similarly absent, except for the sole work in which $^{239}\text{Pu}^{6+}$ was precipitated from an acid solution of $\text{pH}=4$ with CO_2 over the course of 3–5 days (Runde *et al.*, 1999). The washed solids, identified as PuO_2CO_3 from powder X-ray diffraction measurements, were examined by Pu EXAFS to reveal the typical FT data with contributions from axial (1.74 Å) and equatorial O atoms (2.45 Å) as well as a distant, 4.2 Å Pu–Pu interaction. No coordination numbers were reported for this monocarbonate phase.

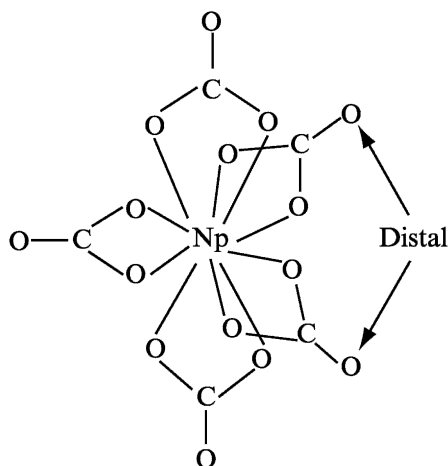
(iv) *Tetravalent An*

The tetravalent An carbonate series, $[\text{An}(\text{CO}_3)_n]^{4-2n}$ for $\text{An} \equiv \text{Th}, \text{U}, \text{Np},$ and Pu , has been the subject of systematic and comprehensive EXAFS investigations. In this collection of results, the predominant aqueous species is, by far, the pentacarbonato ($n=5$) complex, $[\text{An}(\text{CO}_3)_5]^{6-}$. For example, the extensive L_{3-} edge EXAFS measurements of U^{4+} , Np^{4+} , and Pu^{4+} in the aqueous $\text{K}^+ - \text{HCO}_3^- - \text{CO}_3^{2-} - \text{OH}^- - \text{H}_2\text{O}$ system (Rai *et al.*, 1998, 1999a,b) can be succinctly summarized as follows: The aqueous An^{4+} complexes in carbonate (5.4–6.0 M K_2CO_3) and bicarbonate (0.9–1.0 M) solutions were found to be

$[\text{An}(\text{CO}_3)_5]^{6-}$. Despite the excess concentrations of $[\text{HCO}_3^-]$, with respect to $[\text{An}^{4+}]$, no evidence was ever found for its complexation. This may reflect an inherent limitation of the technique, wherein the effects of protonation on the average An–O and An–C distances would be insignificant in comparison with the measurement error, and therefore extremely difficult to determine. In this regard, the detection of appreciably more coarse and substantial structural variations, especially the equatorial O coordination number, can be problematic and fraught with uncertainty. This, in turn, can make it difficult to determine the exact number of bicarbonate and carbonate groups, as well as their identity, involved in the complexation of tetravalent An ions.

(v) *Neptunium(IV)*

A case that illustrates this complicated issue as regards An^{4+} EXAFS in general concerns the investigation of the pure Np^{4+} ion (of unspecified milli-molar concentration) in 0.93 M KHCO_3 (Rai *et al.*, 1999a). In the FT data, the Np–O and Np–C interactions are not resolved, and correlation effects in the curve-fitting leads to metrical parameters that are not diagnostic of a unique structure. For example, from the nearest O and C coordination numbers, 11.0 ± 2.8 and 5.8 ± 1.8 , respectively, alone, it is difficult to establish the presence of tetra-, penta-, hexa-, or heptacarbonato complexation. In this situation, fortunately, the magnitude of the average Np–O and Np–C interatomic distances, 2.43(2) and 2.84(2) Å, respectively, is known to be diagnostic of bidentate carbonate coordination (Denecke *et al.*, 1997b). To provide added quantitative insights about the Np carbonate species, a distant and well-resolved peak in the FT data attributed to the distal O atoms of the bidentate $[\text{CO}_3]^{2-}$ groups was subjected to analysis. The coordination number obtained, 5.4 ± 1.6 O atoms, is a conclusive indicator "...that five carbonate groups were involved, and the complexed Np^{4+} species therefore is $\text{Np}(\text{CO}_3)_5^{6-}$ " in 0.93 M KHCO_3 (Rai *et al.*, 1999a).



The structure is illustrated above in which two of the five distal O atoms at 4.16 (2) Å are identified. For the corresponding 5.4 M K_2CO_3 solution, the unintended, partial oxidation of Np^{4+} leads to neptunyl(v) contamination and additional uncertainties with the EXAFS analyses. Nevertheless, the data are consistent with the suggestion that $[\text{Np}(\text{CO}_3)_5]^{6-}$ is the dominant species in carbonate solution.

(vi) *Uranium(IV) and plutonium(IV)*

From EXAFS acquisition and analyses (Rai *et al.*, 1998, 1999b), the speciation of U^{4+} and Pu^{4+} (of unspecified milli-molar concentrations) in 0.9 and 1.0 M KHCO_3 solutions, respectively, was shown to be like that for Np^{4+} . Namely, the three An^{4+} solution species are the anionic (6-) penta(carbonato) complexes, wherein the five carbonate groups are in bidentate coordination consisting of 9.5 O at 2.46 Å and 5.2 C at 2.90 Å for U (Rai *et al.*, 1998) and 9.8 ± 2.5 O at 2.41(2) Å and 5.5 ± 1.7 C at 2.88 Å for Pu (Rai *et al.*, 1999b). The corresponding distal O interactions consist of 4.1 O at 4.18 Å for U and 5.0 ± 1.5 O at 4.14(2) Å for Pu. Because of the presence of oxidation state impurities, e.g. uranyl(vi) and plutonyl(v), and the low S/N ratio of the primary data due to minuscule solubility, the EXAFS spectra for the U^{4+} and Pu^{4+} carbonate species in 5.4–6.0 M solutions of K_2CO_3 were not adequate for detailed analysis. Despite the uncertainties with the available EXAFS, it was concluded largely based upon other comparisons that $[\text{An}(\text{CO}_3)_5]^{6-}$ is the dominant An^{4+} species in concentrated carbonate solutions. Other complementary research (Clark *et al.*, 1998) provides thorough and convincing evidence in this regard. The Pu L_3 -edge EXAFS of the limiting $^{242}\text{Pu}^{4+}$ (ca. 0.1 M) ion in an aqueous solution of 2.5 M Na_2CO_3 was fit to reveal 10.0 ± 1.2 O atoms at 2.42(1) Å; 5.0 ± 0.6 C atoms at 2.88(2) Å; 5.0 ± 0.6 O atoms at 4.16(2) Å. These values are consistent with the formation of a monomeric penta(carbonato) anion, $[\text{Pu}(\text{CO}_3)_5]^{6-}$, that is essentially identical to the one found in the solid-state, single-crystal X-ray structure of $[\text{Na}_6\text{Pu}(\text{CO}_3)_5]_2 \cdot \text{Na}_2\text{CO}_3 \cdot 33\text{H}_2\text{O}$ (Clark *et al.*, 1998). In this anion, each of the five $[\text{CO}_3]^{2-}$ groups has bidentate coordination in a pseudo-hexagonal bipyramid polygon about Pu^{4+} with three in equatorial positions and two in axial ones. This definitive structure sets to rest a decade-long debate about the molecular structure of the limiting complex in the Pu^{4+} carbonate system under high $[\text{CO}_3^{2-}]$ in both solution- and solid-states.

(vii) *Thorium(IV)*

EXAFS investigations of the Th^{4+} carbonate system show that a penta(carbonato) $[\text{Th}(\text{CO}_3)_5]^{6-}$ solution species is obtained at high concentrations of carbonate (1–2 M Na_2CO_3 with 0.1–1.0 M NaOH) and bicarbonate (0.17–1.0 M NaHCO_3) (Felmy *et al.*, 1997; Hess *et al.*, 1997). Curve-fitting analysis of Th

L₃-edge EXAFS data for solutions of 0.001–0.009 M Th⁴⁺ reveals ten O atoms at 2.49–2.50 Å, a distance that is consistent with bidentate coordination of [CO₃]²⁻. Because the C backscattering is weaker than that for the nearer O and because the Th–C peak cannot be resolved from the Th–O peak in the FT data, the Th–C metrical parameters are subject to large uncertainties. For example, coordination numbers of 3.1–5.2 and distances of 2.97–3.01 Å make it difficult to be specific about the character of the carbonate complexation. The number of coordinated carbonate groups was determined through the analysis of the signal for the well-resolved distal O peak in the FT data to reveal 5 ± 1 O atoms at 4.21–4.26 Å, as expected for the [Th(CO₃)₅]⁶⁻ anion. In contrast, for solutions with a bicarbonate concentration of 0.1 M and less, “. . .the thorium speciation changes dramatically” (Felmy *et al.*, 1997; Hess *et al.*, 1997). The specific and exact nature of this change was not conclusively established from the EXAFS analysis because of data quality limitations, i.e. low S/N ratio, of the primary spectra for the dilute (≤0.0001 M) Th⁴⁺ solutions at pH=9.39–9.43. Although the issue is open to question, the initial EXAFS results suggest a contraction of the Th–O bond length (from ca. 2.50 Å for [Th(CO₃)₅]⁶⁻ to 2.46 Å) accompanied by a decrease in the number of nearest O atoms (from 10 for [Th(CO₃)₅]⁶⁻ to 8). Based upon this information, a mixed carbonate hydroxide species was proposed (Felmy *et al.*, 1997), wherein three [CO₃]²⁻ groups are in bidentate coordination around Th⁴⁺ along with two OH⁻ groups (Hess *et al.*, 1997).

28.2.4 Organic acids

EXAFS analyses provide an average structure of all the element-selected An ions in solution, regardless of their state of speciation – monomer, dimer, trimer, . . . , polymer – and their possible combined and simultaneous presence as hydrolysis products, intermediates, non-complexed aquo ions, etc. As such, the short-range metrical results for An materials containing an assortment of bonding sites and mixtures of phases are difficult to use for definitive comparisons with individual structures proposed in speciation diagrams. In these cases, additional spectroscopic information, such as from, for example, NMR, optical, vibrational, fluorescence, etc., experiments is necessary to confirm the available EXAFS results. For example, the use of EXAFS alone to study the coordination and binding stoichiometry of An ions in natural materials like organic macromolecules known as humic substances, which contain multiple coordination sites, different functional groups (i.e. carboxyl, carbonyl, hydroxyl, thiol, amido, etc.), and bonding modes, can be a difficult and intricately complicated problem. Fortunately, the carboxylate anions, –COO⁻, of organic acids are the most important and widespread functional group for An complexation in the surface-waters and in the subsurface geologic fluids of the terrestrial aquatic environment (Pittman and Lewan, 1994). Moreover, the use of EXAFS has been developed for such challenging environmental research thorough analysis and understanding of the spectra for smaller, molecularly characterized

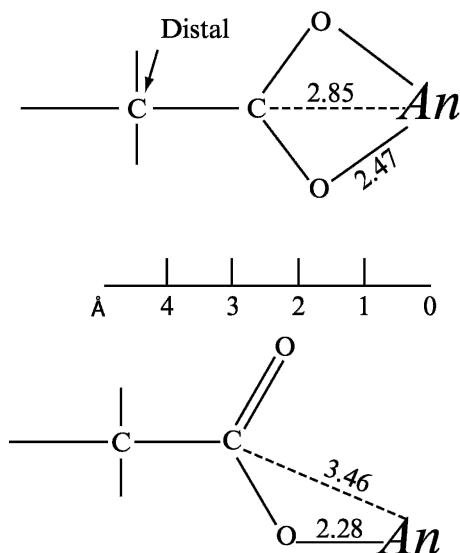
An carboxylate complexes of common organic, carboxylic acids both aliphatic (R-COOH) and aromatic (Ar-COOH), including the di- and tricarboxylic acids.

Tables 28.7 and 28.8 contain the structures of the mono-, di-, and tricarboxylate ligands as well as several phenolate ligands that are relevant with regard to their presence in natural waters and materials. Except for two publications, one about Th⁴⁺ (Denecke *et al.*, 1999) and the other on Np⁴⁺ (Denecke *et al.*, 2002), the EXAFS research available in time for this publication is exclusively focused on the uranyl(vi) ion, [UO₂]²⁺, complexes of these organic anions. Though large, the extent of the EXAFS structure investigations is dwarfed by the number of crystal and molecular structures studies that have been completely reviewed and discussed in the light of the complexation of radionuclides with humic substances, particularly the humic and fulvic acids, elsewhere (Leciejewicz *et al.*, 1995; Denecke *et al.*, 1997a).

(a) Model systems

Despite early success at probing the bonding of [UO₂]²⁺ with the aliphatic, monobasic acetate ligand through use of U L₃-edge EXAFS (Charpin *et al.*, 1985), research on An complexes of organic acids was not immediately impacted by the method. More than a decade later, three EXAFS studies were reported (Allen *et al.*, 1996a; Pompe *et al.*, 1996; Reich *et al.*, 1996a) with results for uranyl(vi) solutions and solids containing organic carboxylate ligands that set the groundwork for EXAFS measurements that continue today. A pivotal development was realized when the results from EXAFS were demonstrated to be diagnostic of carboxylate coordination (Denecke *et al.*, 1997a,b, 1998a,b). In particular, the distinction between mono- and bidentate O coordination is plainly reflected in the U–O interatomic distance, wherein long U–O distances of ca. 2.5 Å are indicative of bidentate coordination and shorter ones of ca. 2.3 Å suggest monodentate coordination. Oftentimes, the bidentate mode of coordination is corroborated by the appearance of either one or two U–C interactions. The first one with a U–C interaction of ca. 2.85 Å arises from the nearest C atom that is bonded to the two O atoms and the second oftentimes weak one at ca. 4.4 Å arises from the next nearest, the so-called distal C atom that is collinear with the nearest C and absorbing An atoms. Because these two U–C interactions occur at significantly longer distances for the monodentate-bonding mode, e.g. the first and closest U–C distance is ca. 3.5 Å, they are rarely observed in the FT data of An EXAFS. A schematic representation of these two binding forms is shown below. Similar schemes and interatomic distances apply for the bidentate and monodentate coordination of the carbonate ligand discussed above.

Despite the extensive research with the model ligands (L) of Tables 28.7 and 28.8, the results from EXAFS are not sufficient on their own to provide conclusive speciation information about the equatorial coordination of [UO₂]²⁺ and other An moieties. The An:L complexation ratio, e.g. 1:1, 1:2,



1:3, and 2:2, 2:3, etc., is especially difficult to determine from one-dimensional metrical information largely because of spectral congestion. For example, the identification of typically weak and distant U–U interactions that are expected for the 2:2 complexes is oftentimes complicated. Peaks that are purported to arise from U–U interactions can be essentially identical to the O–O peak (i.e. the U–O–U–O–U backscattering pathway) that arises from multiple-scattering within a single uranyl group, which is a common structural feature of the monomeric (1:1, 1:2, ...) and dimeric (2:2, 2:3, ...) complexes. Fortunately, in this regard, the U–U assignment can be convincingly made by use of low-temperature EXAFS (Thompson *et al.*, 1995, 1997; Barnes *et al.*, 2000; Hennig *et al.*, 2001b). Another difficulty arises in the identification of all of the equatorial O ligands in the molecular complexes of $[\text{UO}_2]^{2+}$ that contribute to the total coordination number of which five is the most common one of all the entries of Tables 28.7 and 28.8. For example, the O equatorial responses from carboxylate, phenolate, water, and hydroxide are difficult, oftentimes impossible, to distinguish from EXAFS alone. The use of vibrational spectroscopies, particularly FT-infrared, is especially useful with regard to information about the coordination of R–COO[−] and Ar–COO[−] moieties.

(b) Natural systems

Both humic and fulvic acids play key roles that are not very well understood in the biological and environmental sciences. Humic acid is, in large part, responsible for the immobilization of An ions and heavy metals in soils. The complexation of metals with reactive functional groups is an important regulatory

process of the solubility and fate of soil contaminants. As such, the identity of potential binding sites of 'hard' and 'soft' functional groups, including ligands of N (e.g. amino), O (e.g. hydroxyl, carboxyl, carbonyl), and S (e.g. thiol, sulfide, thiol-ether, sulfonyl) on the outer and inner surfaces of humic acid that would accommodate An ions with different charge/IR ratios has been a subject of practical concern. The difficulties in this area of research stem from uncertainties about the nature of humic acid itself. The diversity of the chemical building blocks that combine in their assembly to form humic acid is well-known and remains a matter of significant interest (Giordano, 1994; Silva and Nitsche, 1995; Nitsche, 1997; Paciolla *et al.*, 1999). In particular, the primary and secondary molecular and crystal structures of humic acid and its conformers, which are believed to vary with ancestry, are not known. Yet, despite the existing gap in knowledge about the specific formula and stereochemistry of humic acid, in general, and about the metal-binding sites of humic acid, in particular, the obvious strength of the EXAFS work is that it provides direct insight about the An coordination. The results of exhaustive U L₃-edge EXAFS data acquisition and analysis of humic and fulvic acids of both natural and synthetic origin, and under the neutral to slightly acidic conditions of pH and Eh that are of environmental relevance, are in consensus (Denecke *et al.*, 1997a, 1998a,b; Reich *et al.*, 1998a; Nitsche *et al.*, 1999; Schmeide *et al.*, 2003). The bonding of the uranyl ion is predominantly associated with carboxylate functional groups. Moreover, the U–O interatomic distances are consistent with the monodentate coordination structure shown above. Under alkaline conditions, the bonding appears to involve some degree of interaction with phenolic –OH groups (Reich *et al.*, 1996a), which are deprotonated at $8 \leq \text{pH} \leq 10$. The pH-dependent bonding of $[\text{UO}_2]^{2+}$ to carboxylate and phenolate functionalities has been demonstrated in several model systems (Rossberg *et al.*, 2000, 2003; Moll *et al.*, 2003). Additional work has been proposed to clarify this possibility with natural humic acids (Reich *et al.*, 1996a; Schmeide *et al.*, 2003).

28.3 SORPTION STUDIES

Chemical reactions that take place at the particle–water interface play a large role in controlling environmental speciation, bioavailability, and transport of ions. For example, adsorption/desorption equilibria and redox reactions can be significantly influenced by the nature of the surfaces seen by the solution. Simple solution solubilities may be altered in the presence of a mineral surface that can preferentially adsorb, and thereby concentrate and precipitate metal-ions at solution concentrations well below their solubility limits. In addition, surface redox reactions can also reduce metal solubility and result in mineral incorporation or crystallization reactions that would not occur in the absence of the active surface (Breit, 1995). In this manner, the mobility of radionuclides through the environment is strongly influenced by their interactions at water–mineral

Table 28.7 Uranyl(vi) complexes of low-molecular weight aliphatic carboxylate ligands (L) with axial (ax.) oxygen coordination numbers and U=O distances as well as equatorial (eq.) coordination numbers and U–O bond lengths. The L stick structures do not represent the true stereochemistry. Estimated standard deviations, where available, are obtained from the primary sources and are given after the ± sign or within parentheses.

Ligand (L) structure	Name/Formula	An	Coordination	Phase An:L speciation	References
	acetate	U ⁶⁺	2 ax. O ²⁻ , 1.75–1.76 Å	solids and solutions	Charpin <i>et al.</i> (1985)
	CH ₃ COO ⁻	U ⁶⁺	6 eq. O, 2.46–2.48 Å 2 ax. O ²⁻ , 1.77 Å 4.8(4) eq. O, 2.41 Å 2 ax. O ²⁻ , 1.78 Å 4.7(5) eq. O, 2.46 Å	Na[UO ₂ (L) ₃] and [P(C ₆ H ₅) ₄][UO ₂ (L) ₃] solid UO ₂ (L) ₂ ·2H ₂ O aqueous solution	Reich <i>et al.</i> (1996a)
		U ⁶⁺	4 ax. O ²⁻ , 1.787(1) Å 2.5 eq. O, 2.331(5) Å ⊥ 1 ax. O ²⁻ , 1.717(4) Å 6 eq. O, 2.378(3) Å 2 ax. O ²⁻ , 1.768(1) Å 5 eq. O, 2.384(2) Å	pH = 3.7, [UO ₂ (L) ₃] ⁻ oriented single-crystal UO ₂ (L) ₂ ·2H ₂ O parallel () and perpendicular (⊥) to [O=U=O] ²⁺ . polycrystalline solid	Hudson <i>et al.</i> (1996); Reich <i>et al.</i> (1998a)

Table 28.7 (Contd.)

Ligand (L) structure	Name/Formula	An	Coordination	Phase An:L speciation	References
		U ⁶⁺	2 ax. O ²⁻ , 1.78 Å	solid	Denecke <i>et al.</i> (1997b)
			4.3(6) eq. O, 2.49 Å	Na[UO ₂ (L) ₃]	
		U ⁶⁺	2 ax. O ²⁻ , 1.78 Å	solid	Denecke <i>et al.</i> (1998a,b)
			5.2 eq. O, 2.48 Å	Na[UO ₂ (L) ₃]	
		U ⁶⁺	2 ax. O ²⁻ , 1.78 ± 0.02 Å	aqueous solution	Reich <i>et al.</i> (1998a); Nitsche <i>et al.</i> (1999)
			6 eq. O, 2.44 ± 0.02 Å	pH = 3.7, [UO ₂ (L) ₃] ⁻	Mosselmans <i>et al.</i> (2001)
		U ⁶⁺	2 ax. O ²⁻ , 1.76–1.79 Å	aqueous solutions	
			3.9–5.2 eq. O, 2.36–2.44 Å	pH = 1.8–2.6 T = 25–250°C [UO ₂] ²⁺ :L = 0.01–2.0	
		U ⁶⁺	2 ax. O ²⁻ , 1.78(1) Å	solids	Jiang <i>et al.</i> (2002)
			2.8 eq. O, 2.36(2) Å	UO ₂ (L) ₂ ·2H ₂ O	
			1.8 eq. O, 2.49(2) Å		
			1.7 ax. O ²⁻ , 1.78(1) Å	Na[UO ₂ (L) ₃]	
			6.4 eq. O, 2.48(2) Å		

U ⁶⁺	2 ax. O ²⁻ , 1.78(1) Å 4 eq. O, 2.38(2) Å 2 eq. O, 2.50(2) Å 2 ax. O ²⁻ , 1.78(1) Å 5.9 eq. O, 2.42(2) Å 2 ax. O ²⁻ , 1.78(1) Å 1.9 eq. O, 2.34(2) Å 4.1 eq. O, 2.48(2) Å 2 ax. O ²⁻ , 1.81 Å 6 eq. O, 2.50 Å	aqueous solutions [UO ₂ (L) ₁] ⁺ , pH = 2.84 UO ₂ (L) ₂ , pH = 3.46 [UO ₂ (L) ₃] ⁺ , pH = 3.85, 4.5	Jiang <i>et al.</i> (2002); Rao <i>et al.</i> (2002)
U ⁶⁺	2 ax. O ²⁻ , 1.77–1.80 Å 3.3–5.4 eq. O, 2.39–2.46 Å	DFT, COSMO solvation model	Vazquez <i>et al.</i> (2003)
U ⁶⁺	2 ax. O ²⁻ , 1.77–1.80 Å 4.8–5.5 eq. O, 2.37–2.40 Å	aqueous solutions pH = 1.8–3.8 <i>T</i> = 25–250°C [UO ₂] ²⁺ ; <i>L</i> = 0.01–2.0	Bailey <i>et al.</i> (2004)
U ⁶⁺	2 ax. O ²⁻ , 1.77–1.80 Å 4.4–5.4 eq. O, 2.36–2.43 Å	aqueous solutions pH = 2–8 aqueous solution, pH = 2–8	Moll <i>et al.</i> (2003) Moll <i>et al.</i> (2003)

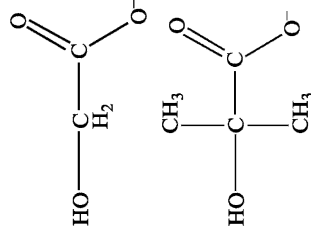
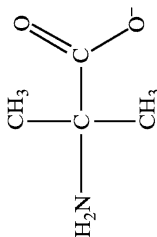
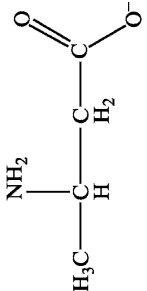
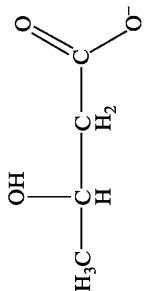
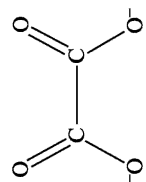
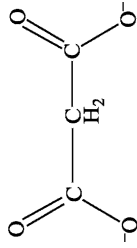


Table 28.7 (Contd.)

Ligand (L) structure	Name/Formula	An	Coordination	Phase An:L speciation	References
	α -aminoisobutyrate $\text{H}_2\text{NC}(\text{CH}_3)_2\text{COO}^-$	U^{6+}	2 ax. O^{2-} , 1.77 Å 5.1–5.6 eq. O, 2.39–2.40 Å	aqueous solutions pH = 3, 4	Moll <i>et al.</i> (2003)
	β -aminobutyrate $\text{H}_3\text{CCHNH}_2\text{CH}_2\text{COO}^-$	U^{6+}	2 ax. O^{2-} , 1.77 Å 5.5 eq. O, 2.43 Å	aqueous solution pH = 4	Moll <i>et al.</i> (2003)
	β -hydroxybutyrate $\text{H}_3\text{CCHOHCH}_2\text{COO}^-$	U^{6+}	2 ax. O^{2-} , 1.78 Å 5.4–5.5 eq. O, 2.41–2.453 Å	aqueous solutions pH = 2.5, 6	Moll <i>et al.</i> (2003)
	oxalate $^- \text{OOC} \text{COO}^-$	U^{6+}	2 ax. O^{2-} , 1.78–1.79 Å 5.1 ± 0.7 eq. O, 2.37–2.38 Å	aqueous solutions pH = 4.4, 6.5 $[\text{UO}_2(\text{L})_2]_2^{2-}$, $[\text{UO}_2(\text{L})_3]_4^{4-}$	Vallet <i>et al.</i> (2003)



malonate
 $\text{^-OOCCH}_2\text{COO}^-$

U^{6+}

2 ax. O^{2-} ,
 1.79 Å
 4.6(3) eq. O,
 2.37 Å

aqueous solution

Reich *et al.*
 (1996a)

U^{6+}

2 ax. O^{2-} ,
 1.78 ± 0.02 Å
 5 eq. O,
 2.36 ± 0.02 Å

aqueous solution

Reich *et al.*
 (1998a);
 Nitsche *et al.*
 (1999)
 Rao *et al.*
 (2002)

U^{6+}

2 ax. O^{2-} ,
 1.78(1) Å
 3.9 eq. O,
 2.34(2) Å
 1.9 eq. O,
 2.40(2) Å
 2.3 ax. O^{2-} ,
 1.79(1) Å
 5.2 eq. O,
 2.39(2) Å

aqueous solutions

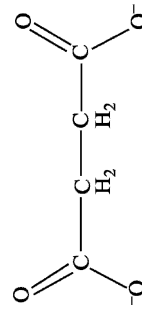
pH = 3.9,
 $[\text{UO}_2(\text{L})_2]^{2-}$
 $[\text{UO}_2(\text{L})_2]^{2-}$,
 pH = 3.5
 $[\text{UO}_2(\text{L})_2]^{2-}$,
 pH = 3.5
 $[\text{UO}_2(\text{L})_1]$,
 pH = 5.2

U^{6+}

2 ax. O^{2-} ,
 1.79–1.82 Å
 5–6 eq. O,
 2.41–2.52 Å

DFT, COSMO
 solvation model

Vazquez *et al.*
 (2003)



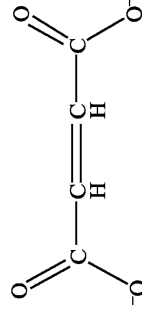
succinate
 $\text{^-OOC}(\text{CH}_2)_2\text{COO}^-$

U^{6+}

2 ax. O^{2-} ,
 1.78 ± 0.02 Å
 5 eq. O,
 2.48 ± 0.02 Å

aqueous
 solution

Reich *et al.*
 (1998a)



maleate
 $\text{^-OOC}(\text{CH})_2\text{COO}^-$

U^{6+}

2 ax. O^{2-} ,
 1.78 ± 0.02 Å
 6 eq. O,
 2.37 ± 0.02 Å

aqueous solution

Reich *et al.*
 (1998a);
 Nitsche *et al.*
 (1999)

Table 28.7 (Contd.)

Ligand (L) structure	Name/Formula	An	Coordination	Phase An:L speciation	References
	malate $^- \text{OOCCH}_2\text{CHOHCOO}^-$	U^{6+}	2 ax. O^{2-} , 1.78 ± 0.02 Å 2.7 eq. O, 2.33 ± 0.02 Å 2.7 eq. O, 2.45 ± 0.02 Å	aqueous solution pH = 2.0, (UO_2) ₂ (L) ₂	Allen <i>et al.</i> (1996a)
	tartrate $^- \text{OOCCHOHCHOHCOO}^-$	U^{6+}	2 ax. O^{2-} , 1.78 ± 0.02 Å 5 eq. O, 2.37 ± 0.02 Å 2.3 eq. O, 2.35 ± 0.02 Å 2.3 eq. O, 2.47 ± 0.02 Å	aqueous solution pH = 3.2, (UO_2) ₂ (L) ₂ aqueous solution pH = 2.2, (UO_2) ₂ (L) ₂	Reich <i>et al.</i> (1998a) Allen <i>et al.</i> (1996a)
	citrate $^- \text{OOCCH}_2\text{COHCO}_2^-$ CH_2COO^-	U^{6+}	2 ax. O^{2-} , 1.78 ± 0.02 Å 4 eq. O, 2.36 ± 0.02 Å 2 ax. O^{2-} , 1.78 ± 0.02 Å 5 eq. O, 2.38 ± 0.02 Å 2 ax. O^{2-} , 1.77 Å 5.0–5.3 eq. O, 2.36–2.37 Å	aqueous solution pH = 3.2, (UO_2) ₂ (L) ₂ aqueous solution pH = 3.8–3.9, [(UO_2) ₂ (L) ₂] ²⁻ solid and aqueous solution, pH = 6 2[(UO_2) ₂] ²⁺ :2Fe ³⁺ :4L [Na(UO_2) ₂] Fe ₂ (L) ₄ O(OH) ₂ (OH ₂) ₃ ⁻	Reich <i>et al.</i> (1998a) Allen <i>et al.</i> (1996a); Reich <i>et al.</i> (1998a) Dodge and Francis (1997, 2003)

Table 28.8 Uranyl(VI), thorium(IV), and neptunium(IV) complexes of low-molecular weight, aromatic carboxylate ligands (L) and high-molecular weight fulvates and humates of both natural and synthetic origin, including axial (ax.) oxygen coordination numbers and U=O distances as well as equatorial (eq.) coordination numbers and U–O bond lengths. The L stick structures do not represent the true stereochemistry. Estimated standard deviations, where available, are obtained from the primary sources and are given after the ± sign or within parentheses.

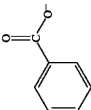
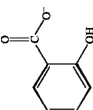
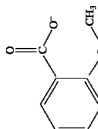
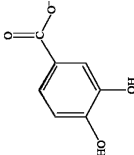
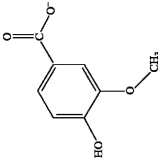
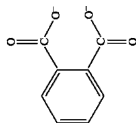
Ligand (L)	Structure	Name	An	Coordination	Phase An:L Speciation	References
		benzoate	U ⁶⁺	2 ax. O ²⁻ , 1.76 Å 4.1–4.5 eq. O, 2.29 Å	solid UO ₂ (L) ₂	Denecke <i>et al.</i> , 1997b, 1998a,b)
		salicylate	U ⁶⁺	2 ax. O ²⁻ , 1.78 Å 3.6(2) eq. O, 2.32 Å 2 ax. O ²⁻ , 1.77 Å	solid UO ₂ (L) ₂	Reich <i>et al.</i> (1996a)
		<i>o</i> -HOC ₆ H ₄ COO ⁻	U ⁶⁺	5.6(6) eq. O, 2.42 Å 2 ax. O ²⁻ , 1.78 Å	solid UO ₂ (L) ₂	Denecke <i>et al.</i> (1998a)
		<i>o</i> -methoxybenzoate	U ⁶⁺	4.3(5) eq. O, 2.44 Å 2 ax. O ²⁻ , 1.77 Å	solid UO ₂ (L) ₂	Reich <i>et al.</i> (1996a)
		<i>o</i> -CH ₃ OC ₆ H ₄ COO ⁻	U ⁶⁺	4.4(2) eq. O, 2.29 Å 2 ax. O ²⁻ , 1.79–1.81 Å 4.6–6.3 eq. O, 2.366–2.460 Å	solid UO ₂ (L) ₂	Denecke <i>et al.</i> (1998a)
		protocatechuate	U ⁶⁺		aqueous solutions pH = 4.3, 5.5, 10.0	Rossberg <i>et al.</i> (2000)
		3,4-dihydroxybenzoate				

Table 28.8 (Contd.)

Ligand (L)	Name	An	Coordination	Phase An:L	References
	vanillate	U ⁶⁺	2 ax. O ²⁻ , 1.784–1.805 Å 5.0–6.7 eq. O, 2.357–2.457 Å	see original article for [UO ₂] ²⁺ speciation aqueous solutions pH = 4.0–6.8. see original article for [UO ₂] ²⁺ speciation aqueous solution, pH = 4.1. see original article for [UO ₂] ²⁺ speciation aqueous solution, pH = 4.6. UO ₂ (L) ₁	Rossberg <i>et al.</i> (2003)
	3-methoxy,4-hydroxybenzoate	U ⁶⁺	2 ax. O ²⁻ , 1.78 ± 0.02 Å 4.7(8) eq. O, 2.437(8) Å		Rossberg <i>et al.</i> (2000)
	phthalate	U ⁶⁺	2 ax. O ²⁻ , 1.78 ± 0.02 Å 6 eq. O, 2.37 ± 0.02 Å		Reich <i>et al.</i> (1998a)
	<i>o</i> -carboxybenzoate				

	catechol <i>o</i> -hydroxyphenol	U ⁶⁺	2 ax. O ²⁻ , 1.78–1.82 Å 5.9–6.1 eq. O, 2.374–2.391 Å	aqueous solutions pH = 5.0, 10.0. see original article for [UO ₂] ²⁺ speciation.	Rossberg <i>et al.</i> (2000)
	pyrogallol <i>o,o'</i> -dihydroxyphenol	U ⁶⁺	2 ax. O ²⁻ , 1.80–1.81 Å 4.8–5.1 eq. O, 2.383–2.396 Å	aqueous solutions pH = 4.8, 8.0 see original article for [UO ₂] ²⁺ speciation.	Rossberg <i>et al.</i> (2000)
fulvate		Np ⁴⁺	2–4 OH ⁻ , 2.24–2.27 Å 5–7 O, 2.41–2.44 Å 9–10 O, 2.44 ± 0.01 Å	wet pastes, Gortleben, boom clay	Denecke <i>et al.</i> (2002)
humate ^{a,b}		Th ⁴⁺ U ⁶⁺	2 ax. O ²⁻ , 1.78 ± 0.02 Å 5 eq. O, 2.38 ± 0.02 Å	dry solid and wet paste dry solids and wet pastes. [UO ₂] ²⁺ sorbed on solid HA and precipitated out of HA solution at pH ≤ 5.4.	Denecke <i>et al.</i> (1999) Reich <i>et al.</i> (1996a)
			2 ax. O ²⁻ , 1.83 ± 0.02 Å 5 eq. O, 2.30 ± 0.02 Å	[UO ₂] ²⁺ precipitated out of HA solution at pH = 8–10.	

Table 28.8 (Contd.)

<i>Ligand (L)</i>	<i>Name</i>	<i>An</i>	<i>Coordination</i>	<i>Phase An:L Speciation</i>	<i>References</i>
<i>Structure</i>	<i>U⁶⁺</i>	<i>U⁶⁺</i>	2 ax. O ²⁻ , 1.78 ± 0.02 Å	wet pastes, [UO ₂] ²⁺ on	Pompe <i>et al.</i> (1996)
			4-5 eq. O, 2.38 ± 0.02 Å	natural and synthetic humics dry solids and	
<i>U⁶⁺</i>	<i>U⁶⁺</i>	<i>U⁶⁺</i>	2 ax. O ²⁻ , 1.77-1.78 Å	wet pastes with [UO ₂] ²⁺ ,	Denecke <i>et al.</i> (1997a)
			5 eq. O, 2.37-2.39 Å	see original article.	
<i>U⁶⁺</i>	<i>U⁶⁺</i>	<i>U⁶⁺</i>	2 ax. O ²⁻ , 1.78 ± 0.02 Å	solution	Reich <i>et al.</i> (1998a);
			4-5 eq. O, 2.38 ± 0.02 Å	[UO ₂] ²⁺ HA	Nitsche <i>et al.</i> (1999)
<i>U⁶⁺</i>	<i>U⁶⁺</i>	<i>U⁶⁺</i>	2 ax. O ²⁻ , 1.78 Å	dry solid	Denecke <i>et al.</i> (1998a)
			5.3(5) eq. O, 2.39 Å	[UO ₂] ²⁺ HA	
<i>U⁶⁺</i>	<i>U⁶⁺</i>	<i>U⁶⁺</i>	2 ax. O ²⁻ , 1.77-1.78 Å	solutions and aqueous solid	Denecke <i>et al.</i> (1998b)
			5 ± 0.7 eq. O, 2.37-2.39 Å	suspensions with [UO ₂] ²⁺ .	
<i>U⁶⁺</i>	<i>U⁶⁺</i>	<i>U⁶⁺</i>	2 ax. O ²⁻ , 1.78 ± 0.02 Å	see original article. dry solids	Schmeide <i>et al.</i> (2003)
			5 eq. O, 2.39 ± 0.02 Å	[UO ₂] ²⁺ HA	

^a HA = humic acid.

^b Partial building block structure of humic acid adapted from (Sonnenberg *et al.*, 1989; Giordano, 1994; Stevenson, 1994; Paciollo *et al.*, 1999).

interfaces. For example, uranium mobility in oxic groundwater is dominated by adsorption of U(VI) onto mineral surfaces. The sorption of uranyl on to organic and inorganic surfaces plays a major role in preconcentrating low-temperature sedimentary uranium and the formation of uranium-bearing minerals, such as uraninite, through reduction following adsorption from groundwater. To predict mobility, it is necessary to have a fundamental understanding of interaction processes including surface complexation and precipitation as well as radionuclide incorporation into mineral phases. Among physical factors that influence partitioning between solution and metal surface are the specific actinide involved, its concentration, coordinating ligands such as dissolved carbonate, phosphate, and other complexing ions, solution pH, and mineral surface contamination.

Published synchrotron studies examining actinide interactions on mineral surfaces focus on valence and structural details of binding. Questions to be answered have centered on the valence state of the actinide and its coordination environment, including the presence of mineral-phase atoms visible in the coordination sphere that may help to distinguish inner- from outer-sphere interactions. The presence of actinide-actinide interactions may indicate clustering or the formation of oligomers on the mineral surface. Such oligomers may represent precursors to mineral-phase formation.

Synchrotron work to date has focused on XAS and microprobe studies of U, Np, or Pu adsorption onto silicate, phosphate or iron-based mineral phases and onto more complex soil samples. Work has also been published that looks at sorption onto bacterial surfaces as well as incorporation into mineral phases. These topics will be reviewed in the following subsections.

28.3.1 Silicates

Silicates are the largest and most complicated class of minerals, with estimates that as much as 90% of the Earth's crust is composed of silicates. These complicated structures can form as single units, double units, chains, sheets, rings, and frameworks. Phyllosilicates are a silicate subclass in which rings of tetrahedra are linked by shared oxygens to other rings in a two-dimensional plane that produces a sheet-like structure. The silicon to oxygen ratio is generally 2:5, with the sheets typically connected to each other by cation layers. The cation layers are weakly bound and often have water and other moieties trapped between the sheets. Clays are a group of phyllosilicates that contain large percentages of water trapped between the silicate sheets. Most clays are chemically and structurally analogous to other phyllosilicates but contain varying amounts of water and allow facile ion-exchange of interlayer ions. It is the physical characteristics of clays, more so than their chemical and structural characteristics, which defines this group.

Clay minerals are further divided into four groups, one of which is the montmorillonite/smectite group. Montmorillonites differ mostly in chemical

content. The general formula is $(\text{Ca,Na,H})(\text{Al,Mg,Fe,Zn})_2(\text{Si,Al})_4\text{O}_{10}(\text{OH})_2 \cdot n\text{H}_2\text{O}$. The water content is variable, and in fact when water is absorbed, the crystals tend to swell to several times their original volume. The effect of montmorillonite is to slow the progress of water through soil or rocks.

There have been several studies of the adsorption of actinide ions onto silicate surfaces, as summarized in Table 28.9. These studies are driven by the realization that the surfaces of these mineral phases have a discernable influence on the migration of ions in natural environments. Silicates have been proposed to have two surface sites onto which an adsorbed ion can bind. Numerous experiments explore specific models which address these two broad classes of binding sites: external amphoteric 'edge' sites whose properties are pH-dependent, and fixed-charge, basal-plane 'exchange' sites whose reactivity is independent of pH (Sposito, 1984, 1990; Weiland *et al.*, 1994). Unlike many transition-metal mineral phases, the silicate surface itself shows no redox chemistry. This simplifies the types of interactions that can be expected on the surface to complexation,

Table 28.9 *Published studies of thorium and uranium surface sorption onto silicate phases.*

Common name	Formula	Sorbed ion	References
silica gels	$\text{SiO}_2 \cdot n\text{H}_2\text{O}$ amorphous	Th(IV)	Oesthols <i>et al.</i> (1997)
		U(VI)	Dent <i>et al.</i> (1992); Michard <i>et al.</i> (1996); Reich <i>et al.</i> (1996b, 1998b); Allard <i>et al.</i> (1999); Sylwester <i>et al.</i> (2000)
montmorillonite	$(\text{Ca,Na,H})(\text{Al},\text{Mg,Fe,Zn})_2(\text{Si,Al})_4\text{O}_{10}(\text{OH})_{2-x}\text{H}_2\text{O}$	Th(IV)	Giaquinta <i>et al.</i> (1997a); Daehn <i>et al.</i> (2002)
		U(VI)	Dent <i>et al.</i> (1992); Chisholm-Brause <i>et al.</i> (1992); Chisholm-Brause <i>et al.</i> (1994); Thompson <i>et al.</i> (1997); Sylwester <i>et al.</i> (2000); Hennig <i>et al.</i> (2002)
mica	bentonite vermiculite: $\text{Mg}_{0.7}(\text{Mg,Fe,Al})_6(\text{Si,Al})_8\text{O}_{22}(\text{OH})_2 \cdot 8\text{H}_2\text{O}$ hydrobiotite: $\text{K}(\text{Mg,Fe})_6(\text{Si,Al})_8\text{O}_{20}(\text{OH})_4 \cdot x\text{H}_2\text{O}$	U(VI), U(IV)	Giaquinta <i>et al.</i> (1997a,b)
		U(VI)	Hudson <i>et al.</i> (1999)
kaolinite	$\text{Al}_2\text{Si}_2\text{O}_5(\text{OH})_4$	U(VI)	Thompson <i>et al.</i> (1998)

precipitation, and incorporation, and thereby providing simple model for study. The main question that has been addressed to date is the mechanism by which the ion binds to a silicate surface. As demonstrated in Fig. 28.7 for an actinyl ion, surface binding can include mononuclear or polynuclear inner- or outer-sphere complexation. Inner-sphere complexes can bind with either monodentate or bidentate ligation with surface sites.

The simplest of the silica phases to be studied are silica gels, amorphous $\text{SiO}_2 \cdot n\text{H}_2\text{O}$. Non-porous pyrogenic silica samples, consisting of spherical particles amorphous by X-ray diffraction, were used in a study of Th adsorption in order to determine the molecular details of the adsorption (Oesthols *et al.*, 1997). Wet samples of Th sorbed onto amorphous silica were studied using Th L_3 -edge EXAFS. Solution pH values in the study were in the range of 2.8–4.0, which corresponded to the adsorption edge in the pH region of 2–3 that had previously been determined potentiometrically (Oesthols, 1995). Th surface coverages were

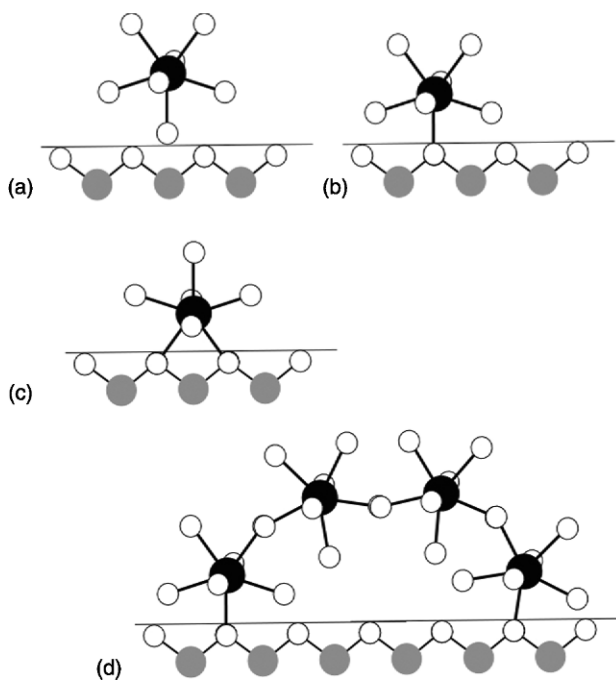


Fig. 28.7 Binding modes for a metal-ion to a mineral surface. The binding can be (a) outer sphere, in which the metal ion's first coordination sphere is not a bulk-surface ion; (b) a mononuclear, monodentate, inner-sphere complex, in which the metal-ion's first coordination sphere includes an ion from the bulk-surface; (c) mononuclear, bidentate coordination, in which the complexing metal-ion shares two ligands with the surface; and (d) polynuclear, bidentate coordination, in which the metal-ion has coordination to other metal-ions as well as the surface.

determined to be 3.8–230%. The spectra showed a decrease in structural order with increasing surface coverage. For lower surface coverage, 3.8–75.5%, two oxygen coordination shells were seen at approximately 2.28 and 2.54 Å with coordination numbers of about 2–2.7 and 5, respectively. These samples also showed about 2(1) Th–Si interactions at 3.85 Å. Samples with higher Th surface coverage, that is 92.7 and 230%, also showed two oxygen shells, with about two O at 2.33 Å and 4.5 O at 2.54 Å and 2.3 and 1.3 Th–Si interactions at 3.84 and 3.79 Å, respectively. None of the samples showed evidence of any Th–Th interactions, even the sample reported to have 230% surface coverage, suggesting that the surface layer resembles amorphous thorium hydroxide, which also shows no significant Th–Th correlations. The absence of Th–Th correlations, even in amorphous Th(OH)₄ was attributed to a high degree of disorder (Oesthols *et al.*, 1997). The EXAFS data were consistent with Th adsorption onto the amorphous silica surface via bidentate inner-sphere complexation, in which Th has a double corner-sharing bond with two different SiO₄ surface tetrahedra. Four to eight oxygen atoms are shared with coordinated solution–water molecules, which account for the longer Th–O correlations at 2.55 Å.

Uranium sorption by silica gels has also been shown to be pH sensitive (Michard *et al.*, 1996), increasing with increasing pH over the range of about 3–5. This pH interval corresponds approximately to that over which there are hydrolyzed uranyl species present in solution. A two-phase process has been proposed that involves an external mass transfer and an intra-particle mass transfer, of which only the former is strongly pH-dependent. Earlier, Raman studies had suggested that uranyl sorbs as an inner-sphere surface complex (Maya, 1982). This suggestion has been confirmed by EXAFS studies of UO₂²⁺ sorption products for samples prepared at pH 3 and 5 (Dent *et al.*, 1992), which were noted to be indistinguishable, but no detailed analysis was provided. Coordination information of uranyl sorbed to silicic acid and silica gel samples prepared at pH 4 was determined by EXAFS (Reich *et al.*, 1996b). The two materials are distinguished by different surface areas, 80 vs 470 mg/g for silicic acid and silica gel respectively, as determined by BET measurements. An analysis of EXAFS data showed the expected dioxo coordination with a U–O_{ax} distance of 1.78 Å for both samples. Two silicic acid samples, prepared with different solution uranyl concentrations, were examined. The sample, obtained from a 0.01 M UO₂²⁺ solution, has two resolvable O coordination shells in the equatorial plane with 2.6(4) O at a distance of 2.27 Å and 1.8 O at a distance of 2.50 Å. The sample obtained from a more concentrated uranyl solution, 0.05 M, has 2.1(4) equatorial O at a distance of 2.27 Å and 2.25 O at a distance of 2.48 Å. Both samples show a total equatorial O coordination of slightly less than 5. These results compare to those determined for silica gel samples obtained from a 0.05 M uranyl solution, which also have two equatorial O shells, one with 4(1) O at 2.29 Å and the other with 1.6(7) O at a distance of 2.50 Å, for a total O coordination greater than five. Similar results were determined for a sample prepared at pH 3.4 (Sylwester *et al.*, 2000).

The observation of two O coordination shells separated by about 0.2 Å, coupled by the absence of an EXAFS feature attributable to U–U interactions, is strong evidence that, at pH values 3.4 and 4, uranyl undergoes inner-sphere, mononuclear, bidentate surface complexation (Reich *et al.*, 1996b; Sylwester *et al.*, 2000). In contrast, samples prepared at higher pH values show additional U–Si and U–U coordination shells (Allard *et al.*, 1999; Sylwester *et al.*, 2000). For example, at pH 6.24 additional coordination shells are observable in the data, with one Si at 3.1 Å and about two U at 4 Å (Sylwester *et al.*, 2000). This result indicates some form of oligomeric uranyl phase, either a surface complex or a precipitate. The U–Si atomic distance and coordination number would imply a surface adsorption via bidentate complexation to two surface O associated with the same Si. Monodentate complexation with surface O would be expected to result in a longer U–Si distance of about 3.8 Å (Burns *et al.*, 1997).

EXAFS spectra of uranyl-loaded montmorillonite, which contains aluminol as well as silanol sites, are clearly different from that of the metal adsorbed onto silica (Chisholm-Brause *et al.*, 1992, 1994; Thompson *et al.*, 1997; Sylwester *et al.*, 2000; Hennig *et al.*, 2002). The degree of complexation at the edge aluminol or silanol sites should rise with increasing pH because these sites become increasingly deprotonated and therefore available for cation complexation. In studies with pH values in the range of about 3 (Chisholm-Brause *et al.*, 1994) to 5 (Dent *et al.*, 1992; Sylwester *et al.*, 2000), the data contain an unresolvable single-shell structure similar to those seen in aqueous solution and consistent with outer-sphere coordination. The observed U–O_{eq} bond distances of 2.41–2.43 Å support this finding. In contrast, studies at higher pH (5–7) indicate that an inner-sphere complexation process dominates the sorption. Although the short data range (3.1–11.4 Å⁻¹) prohibited the observation of a splitting in the shell attributed to equatorial ligation, large Debye–Waller factors (0.013–0.017 Å²) together with much shorter bond distances observed at higher pH, 2.34–2.38 Å, were used to support models for binding to amphoteric surface hydroxyl sites (Hennig *et al.*, 2002).

Another interesting study was published concerning the role of montmorillonite surface coverage on the local structure about the uranyl (Chisholm-Brause *et al.*, 1994). There were three samples studied whose final pH values decreased with increasing surface coverage, from 5.6 to 4.4 and finally to 3.4. At low surface coverage, 0.0103 mmol/g, the ratio of the integrated EXAFS amplitude from the equatorially bound O to that found in solution is only 0.58. The bond distance is also short at 2.391 Å. As the solution concentration was increased, the surface coverage also increased from 0.044 to 0.208 mmol/g, there was a higher ratio of uranyl ligation in the equatorial plane (0.65 and 0.77) and these O occurred at longer distances, specifically 2.414 and 2.444 Å, respectively. This same observation has been previously quantified in terms of significant differences in equatorial O coordination as a function of solution U concentration (Chisholm-Brause *et al.*, 1992; Dent *et al.*, 1992). The authors argue that these data suggest that uranyl forms at least three distinct sorption

complexes on montmorillonite, a result that is consistent with previously published modeling (Zachara and McKinley, 1993). Using simple bond-length to coordination-number correlations, it was also argued that the observed increase in amplitude of the EXAFS spectra with increasing surface coverage must be due, at least in part, to decreasing disorder, and not just an increase in the number of coordinating ligands (Chisholm-Brause *et al.*, 1994). An independent study (Hennig *et al.*, 2002) on samples with uranium loading of 1751–2473 ppm did not support this finding. These EXAFS data show no evidence of U–U interactions, even at pH values >5.4, where thermodynamic modeling predicts the formation of solid-hydrated uranyl oxides, indicating that surface complexation may be kinetically favored relative to precipitation under the conditions employed. It should be noted that molecular dynamics simulations of uranyl sorption onto a quartz surface find that water oxygen atoms and surface oxygen atoms are equidistant to the metal-ion. Equatorial splitting of the bond distances is caused not by inner-sphere coordination, but instead by the presence of other ligands in the first coordination sphere of the UO_2^{2+} , such as the carbonate anion (Greathouse *et al.*, 2002).

Uranyl sorption complexes on two related phyllosilicates, vermiculite, which is a montmorillonite, and hydrobiotite, which is a mica, were studied to gain further information on binding to different surface sites (Hudson *et al.*, 1999). Samples were prepared that favored fixed-charge, ion-exchange sites, or amphoteric surface hydroxyl sites. Samples made under conditions that significantly favored the ion-exchange sites had EXAFS spectra with one resolvable equatorial O distance, consistent with outer-sphere uranyl complexation. Upon dehydration, the EXAFS data are consistent with inner-sphere uranyl coordination. In addition to the standard EXAFS experiments, the local structure about the uranyl ion in the hydrated sample was also studied using polarized L_{1-} and L_{3-} edge XANES. Polarized X-ray absorption data have been demonstrated to yield information about the spatial orientation of the linear dioxo group (Hudson *et al.*, 1996). Polarization data were used to probe the orientation of the linear dioxo-groups with respect to the silicate surface in the vermiculite sample (Hudson *et al.*, 1999). The ion-exchanged sites, with outer-sphere coordination, showed a preferred orientation of the dioxo moiety parallel to the silicate layers. Samples that significantly favored the hydroxy sites have EXAFS spectra that show the uranyl ion in a highly distorted equatorial shell with the detection of a U–U interaction, which suggests the formation of surface precipitates and/or oligomeric complexes.

The reports on sorption onto montmorillonite have been extended by experiments on uptake at initial Th concentrations representing undersaturation (pH 2 and 3) and oversaturation (pH 5) with respect to amorphous ThO_2 (Daehn *et al.*, 2002). The sorption experiments were conducted with Th concentrations in the range of 2.7×10^{-6} to 4×10^{-4} M and under an N_2 atmosphere. At low and intermediate surface coverage, 1–34 and 157 $\mu\text{mol/g}$, two coordinating oxygen shells were observed, with about three O at 2.24 Å, six to

eight O at 2.45–2.48 Å, and one Si shell at 3.81–3.88 Å. Any attempt to include Th–Th interactions into the fit failed. The same coordination environment was observed for both pH values. The pH=5 samples had Th–O coordination similar to those observed at the lower pH. For the samples with lower Th loading (14 and 40 µmol/g), data analyses suggested a reduced number of Th–Si pairs, 1.4–1.7 at a distance of 3.87 Å, compared to the sorption samples prepared at pH=3, which had 2.5–2.9 Si at 3.83 Å. The reduced Th–Si coordination number at the higher pH could be explained by assuming that a fraction of Th is no longer directly bonded to the montmorillonite surface, but instead forms an outer-sphere complex. It could also indicate destructive interference with the EXAFS generated by the Th–Si pairs at 3.9 Å (Daehn *et al.*, 2002). This latter hypothesis is supported by the data from the pH=5 sample with the highest Th loading (166 µmol/g), which was satisfactorily fit with neither a Th–Si nor a Th–Th interaction. However, the similarity of EXAFS data from this sample with those obtained from a Th amorphous precipitate suggests the surface formation of similar precipitates at high Th concentrations and high pH.

Polarized EXAFS measurements were also obtained from Th-treated oriented films, prepared at pH values of 2 and 3, to investigate whether the sorbed Th was oriented with respect to the octahedral sheets of the clay (Daehn *et al.*, 2002). The spectra were recorded with an electric field vector at 10°, 35°, 55°, and 80° with respect to the clay-film plane. No significant polarization effects were observed in the spectra obtained from the pH=2 or 3 samples. It was postulated that Th adsorbs to the montmorillonite at its edge sites, by sharing double corners with Si tetrahedra, and that these sites are saturated when the concentration of Th is greater than 32 µmol/g. This hypothesis is supported by the observed difference in EXAFS spectra of the lower concentration samples compared with the higher surface-coverage samples, which look more similar to solution Th spectra. This result may indicate that Th is sorbed as an outer-sphere complex after the clay edge sites are saturated.

Studies on Th- (Giaquinta *et al.*, 1997a) and uranyl-exchanged bentonite (Giaquinta *et al.*, 1997a,b), a smectite clay, and zeolite (Wasserman *et al.*, 2000) samples extended previous work on two aspects: (1) the exchanged clays were coated with hydrophobic silanes in order to inhibit interlayer-water exchange and (2) uranyl-exchanged samples were subjected to hydrothermal conditions. The uranyl-ion-exchanged samples were thoroughly washed in an effort to produce samples with single-interlayer binding sites. The EXAFS from the simple, untreated samples were analyzed, assuming only one site. The results from Th L₃-edge EXAFS (Giaquinta *et al.*, 1997a) showed that Th had a single hydration sphere with approximately 11 O at a distance of 2.49 Å and 2.7(6) O at 3.66 Å. In contrast, EXAFS spectra from the hydrothermally treated samples were similar to that obtained from ThO₂. The first O shell shifted to a slightly shorter distance, 2.39 Å and there were two additional peaks present. The peak at 3.93 Å, present only in the treated sample, was attributed to a Th–Th

interaction and consistent with the formation of a thoria-like hydrous polymer (Baes and Mesmer, 1976). The EXAFS from the UO_2^{2+} exchanged sample, before treatment, was analyzed with 2.2 O at 1.77 Å, 5 O at 2.43 Å, and 2.6 O at 3.45 Å (Giaquinta *et al.*, 1997b). This result is consistent with outer-sphere uranyl complexation as seen for other montmorillonite samples.

In contrast to the Th samples, the uranyl-loaded clays from hydrothermally treated samples produced EXAFS spectra that were different from those obtained before treatment. The silane-treated uranyl samples also showed no change to the uranyl environment compared to those obtained before hydrothermal treatment, except that the spectra showed that the coordination shells were at longer distances. The methoxysilane data revealed dramatic changes in the uranium environment. The dioxo coordination environment disappeared and was replaced by a single oxygen shell at 2.33 Å. There was also an additional peak observed at 3.36 Å and another at 3.92 Å, determined to be a U–U interaction. This coordination is suggestive of small particle uraninite formation, which implies the reduction of U(VI) to tetravalent U. This suggestion was confirmed by U L_3 XANES experiments. The observation of uranyl reduction in the presence of an organic and under elevated temperature and pressure is important in terms of uranium migration under geological conditions.

Dissolved CO_2 is also believed to significantly influence uranium adsorption on mineral surfaces with a maximum at near-neutral pH, and decreasing sharply toward more acidic (pH < 6) and more alkaline (pH > 7) conditions. The mechanism behind this influence was studied using EXAFS to probe uranyl sorption onto the clay-mineral kaolinite (Thompson *et al.*, 1998). The combination of uranium concentrations and pH values used in these experiments were such that complex uranyl oxyhydroxides would be expected. Indeed U–U interactions were observed.

In addition to the work on the aluminosilicate clays, there have been limited EXAFS studies of actinide sorption onto aluminates, specifically uranyl onto $\gamma\text{-Al}_2\text{O}_3$ and $\alpha\text{-Al}_2\text{O}_3$. The former study was done on two samples with contact solution pH values of 3.48 and 6.50 (Sylwester *et al.*, 2000). EXAFS data from both samples demonstrated the standard dioxo uranium(VI) coordination at 1.78 Å. There were also two equatorial shells, the first with about 2.8 O at 2.37 Å and about 2.0 O at 2.53 Å, whereas the second had about 2.6 O at 2.34 Å and 3.1 O at 2.50 Å. The splitting of the equatorial coordination shell is again used as evidence for inner-sphere coordination to the alumina surface. The sample at near-neutral pH also showed a U–U interaction at 4.10 Å corresponding to about 0.5 U near-neighbors, which indicated the coordination of a mixture of mononuclear and polynuclear surface complexes. The study of uranyl sorption on $\alpha\text{-Al}_2\text{O}_3$ (Denecke *et al.*, 2003) examined the polarization dependence of uranyl ions sorbed onto a single-crystal (110) surface under different loading conditions. Although the authors indicate the potential of polarization experiments, no definitive information about uranyl coordination to the $\alpha\text{-Al}_2\text{O}_3$ surface was provided.

28.3.2 Carbonate incorporation

Carbonate minerals are among the most common secondary phases that form in near-surface environments. There are three main sedimentary carbonate minerals: calcite, aragonite, and dolomite, as listed in Table 28.10. Of these mineral phases, calcite is one of the most abundant of the non-silicate minerals, comprising about 4% by weight of the Earth's crust. Aragonite is a less common polymorph of calcite and is a major constituent of invertebrate skeletons that, in most environments, eventually converts to calcite. Carbonate minerals are known to incorporate trace amounts of uranium, an attribute that has been utilized for the U-series age determinations of ancient calcites and as marine paleoenvironmental (Brannon *et al.*, 1996) and diagenetic indicators (Russell *et al.*, 1994). In addition, the carbonate mineral class itself includes a variety of stable uranyl carbonates (Reeder, 1983). The studies of actinide interactions with carbonate phases have focused on incorporation studies.

It is important to develop a molecular level understanding of the speciation of actinides sequestered in carbonate phases in order to assist in the assessment of these ubiquitous minerals in actinide mobility and sequestration. The mechanism(s) of actinide incorporation into carbonates, particularly calcium carbonates, for which the actinide can substitute for Ca^{2+} , has been the source of significant recent study when the substituting ion is uranium (Shen and Dunbar, 1995). The structural work published to date has focused on uranium substitution and has not directly addressed the issue of transuranic substitution into a calcium carbonate lattice. U^{4+} is approximately the right size to substitute for Ca^{2+} in the calcite lattice, but there are two problems to this simple ion replacement. First, the substitution of a tetravalent ion for a divalent one requires some stable charge-balance mechanism available in the lattice. Second, U^{4+} has a low groundwater solubility because of the precipitation of insoluble uranous phases and as a result U is present in most natural waters as the dioxo uranium(vi) ion. Although $\text{U}(\text{vi})\text{O}_2^{2+}$ is divalent, its configuration and size would be expected to cause significant local structural disruption if it were to substitute directly for Ca^{2+} (Langmuir, 1978; Reeder, 1983).

Table 28.10 Carbonate mineralogy. The common carbonate mineral phases studied for actinide incorporation using synchrotron radiation.

Mineral	Formula	Crystallographic group	References
calcite	CaCO_3	trigonal ($\text{R}\bar{3}\text{c}$)	Effenberger <i>et al.</i> (1981)
aragonite	CaCO_3	orthorhombic (Pmcn)	Dal Negro and Ungaretti (1971); de Villiers (1971)
dolomite	$\text{CaMg}(\text{CO}_3)_2$	trigonal ($\text{R}\bar{3}$)	Effenberger <i>et al.</i> (1981)
strontianite	SrCO_3	orthorhombic (Pmcn)	de Villiers (1971)
siderite	FeCO_3	trigonal ($\text{R}\bar{3}\text{c}$)	Effenberger <i>et al.</i> (1981)

The structural details of uranium incorporation into calcite and dolomite were first probed by performing EXAFS experiments on powdered samples exposed to a uranyl perchlorate solution (Geipel *et al.*, 1997). The adsorption experiments were done with no external pH control and under atmospheric conditions, that is, without excluding CO₂. The final solution pH values, after equilibration, were measured to be between 8 and 9 and the final samples had loadings of about 12.8 to 66.3 mg U/g. XPS studies on the samples indicated that the uranyl ions displace Ca at the mineral surface. There was no chlorine-containing surface species detected, indicating that the perchlorate anion did not participate in the surface reaction. The U EXAFS of all the samples studied were indistinguishable and consistent with uranyl coordination. The uranyl equatorial shell was characterized by a broad distribution of U–O distances, with an average of 2.34(2) Å. These results support conclusions of earlier studies that uranyl carbonates and hydroxides form at the grain surfaces of calcite (Carroll and Bruno, 1991; Carroll *et al.*, 1992).

More recent studies have focused on the incorporation of uranyl into synthetic aragonite (Reeder *et al.*, 2000) and calcite (Reeder *et al.*, 2000, 2001). Several previous studies have shown uranyl to be preferentially taken up by aragonite relative to calcite (Kitano and Oomori, 1971; Meece and Benninger, 1993), which points to underlying important mechanistic or structural differences for its incorporation into these two polymorphs. This issue was directly examined by comparing synthetic samples of the two phases (Reeder *et al.*, 2000) that were formed under similar conditions, that is U concentrations were held in the range 10–82 mM, the pH values were maintained at about 8.2–8.3, and air was bubbled through the solutions. Because of the deleterious effects of Sr incorporation on XAS data collection, efforts were made to ensure its exclusion during sample preparation. The final aragonite samples had 985 and 10810 ppm U whereas the calcite samples had 700 and 1890 ppm U in agreement with previous findings that uranyl is preferentially taken up by the orthorhombic phase. U L₃ XANES data indicate the presence of uranyl(VI) in the samples. Fits to the EXAFS data for all uranyl-containing aragonite and calcite samples showed the typical dioxo-coordination environment.

The results of a detailed analysis of the EXAFS data are given in Table 28.11. The most significant differences between U in the two mineral phases were evident in the first equatorial shell. For the aragonite sample, a fit to the data determined that the uranyl ion in aragonite has the same coordination environment as the uranyl triscarbonato solution complex, which was also measured during the same experiment (Reeder *et al.*, 2000, 2001). The O_{eq} distances from aragonite compare to the U–O average distance of 2.47 Å determined for the uranyl coordination by six equatorial oxygens (Burns *et al.*, 1997). In addition to oxygen scattering, a correlation attributed to U–C₃, from carbonate at 2.89 Å is in the range characteristic of bidentate coordination by three carbonate groups (Allen *et al.*, 1995). A further correlation attributed to distal oxygens of carbonate groups at 4.1 Å was also observed, as was a linear

Table 28.11 Comparisons of coordination numbers (CN), distance from uranium (R), and Debye-Waller factor (σ^2) determined for the best fits of U L₃ EXAFS data from synthetic aragonite and calcite that were precipitated from solutions containing the uranyl ion (Reeder *et al.*, 2000). Multiple values for one parameter indicate fits from different samples. Underlined values indicate that the parameter was fixed during fitting.

	Aragonite			Calcite		
Shell	CN	R (Å)	σ^2 (Å ²)	CN	R (Å)	σ^2 (Å ²)
O_{ax}	<u>2</u>	1.80, 1.81	.003, .002	<u>2</u>	1.80	.002, .003
O_{eq}	5.9, 6.0	2.44, 2.42	.004, .005	<u>5</u> , 5.3	2.33	.009, .010
C	3.2	2.90, 2.89	.002, .003	2.1, 1.9	2.91, 2.81	.003, .005
C				1.6, 1.3	3.22	.005
Ca	2.8, 1.7	3.82, 3.78	.004			
Ca	2.9, 3.2	4.03, 3.96	.007, .006			
Ca	0.9, 1.0	4.75	.003, .004			
O_{dist}	3.9, 5.3	4.22, 4.10	.004			

Estimated errors are CN ($\pm 20\%$), R (± 0.01 Å, first 2 shells; ± 0.02 – 0.03 Å).

three-legged multiple-scattering path (O_{dist}–C–U) at essentially the same distance. The observation of bidentate coordination of U by three carbonate ions was supported by Raman and luminescence spectroscopies. There was no unambiguous evidence of any U–U interactions that would indicate clustering or co-precipitation of a uranyl mineral phase. In addition, evidence of U–Ca correlation was observed that was dependent on U concentration.

The same basic structural unit was determined for the uranyl incorporation into aragonite as was observed in the growth solution, which was also measured and analyzed (Reeder *et al.*, 2000). The EXAFS results, supported by Raman data, were used to postulate an incorporation mechanism for uranyl into aragonite. EXAFS show that the predominant aqueous uranyl species is $\text{UO}_2(\text{CO}_3)_3^{4-}$ and that this configuration is preserved in aragonite. The authors suggest that the entire solution species is incorporated into the mineral phase essentially intact (Reeder *et al.*, 2000).

In contrast to the well-defined coordination environment observed for uranyl in aragonite, the coordination environment of uranyl in calcite appears significantly more disordered (Reeder *et al.*, 2000, 2001). The second FT peak from the U EXAFS data, attributable to U–O_{eq}, is significantly less intense and at a smaller U–O distance, relative to the dioxo peak, in the calcite sample. This observation is manifested in the fit, which has fewer, about five, equatorial O with significantly larger Debye–Waller factors (0.009–0.010 Å²). Weak peaks in the FT suggest that there are carbon atoms coordinated at 2.9 and 3.2 Å with more than one type of U coordination by carbonate, indicating both mono and bidentate interactions. The luminescence data are also different for calcite, indicating the possibility of uranyl hydroxide formation on mineral surfaces, a postulate previously made from an independent study (Geipel *et al.*, 1997).

The work on powder-samples of calcite has been augmented by further work, on single-crystals, designed to address the issue of whether incorporation occurs at structurally distinct surface sites (Reeder *et al.*, 2001). The single crystals were grown at slightly lower pH values (7.5–7.6) than were the powder samples. Luminescence lifetime measurements indicated that more than one solution species was present in the growth solution. The average U concentrations in the crystals were rather low, about 15 and 225 ppm. Micro synchrotron X-ray fluorescence (μ -SXRF) and micro X-ray absorption near-edge structure (μ -XANES) data were obtained from the single-crystals using a monochromatic beam with spot size $15 \times 15 \mu\text{m}^2$ or $5 \times 6 \mu\text{m}^2$. The as-grown (10 $\bar{1}$ 4) face was examined, and had a single, polygonized growth hillock composed of four uniform vicinal faces that differed by the orientation of their growth steps and the direction of their advancement during growth. The presence of this hillock is significant because uranyl species can become incorporated into structurally distinct steps of the non-equivalent vicinal faces during crystal growth processes. The μ -SXRF data reveal a striking difference in the distribution of uranium corresponding precisely to the non-equivalent vicinal faces. The $[4\bar{4}1]_+$ and $[4\bar{4}1]_-$ surfaces were highly enriched in uranium relative to the $[48\bar{1}]_+$ and $[48\bar{1}]_-$ surfaces. The magnitude of differential uptake was approximately a factor of 6 to 10. The implications of these findings are that surface controls are significant and therefore that the relative proportions of crystal surface morphologies can strongly influence uranyl incorporation. Polarized μ -XANES revealed neither a discernible difference between the spectra obtained from the non-equivalent vicinals nor any orientational dependence. Fits to the EXAFS data were similar to those from the powder samples, listed in Table 28.11, with two axial O at 1.80 Å, 5.7 O at 2.36 Å, and 3.2 C at 2.92 Å. Weak features observed at higher r could be fit with minor contributions from a distal oxygen and a multiple-scattering path at 4.15 and 4.18 Å, respectively. The results indicate that there is no preferred orientation of the uranyl moiety within the single-crystal, and would be consistent with multiple uranium species, as suggested by luminescence and supported by the apparent disorder seen by EXAFS beyond the first coordination shell.

The uranyl concentrations in the synthetic calcite and aragonite samples far exceed that normally found in natural samples, raising the possibility that the obtained coordination environments do not reflect the environments seen in natural samples, which equilibrate over long time frames, and may undergo repeated dissolution/precipitation or structural transformations. Unfortunately, the low concentrations of U typically found in natural calcium carbonate mineral samples, combined with the presence of large amounts of Sr^{2+} , either substituting directly for Ca^{2+} ion in the lattice or as partially segregated into strontianite (Greeger *et al.*, 1997) complicate the acquisition of EXAFS data with adequate statistics for useful analyses. One study looked at U incorporation into natural coral skeletal aragonite (Pingitore *et al.*, 2002). Two live coral samples, collected from the Galapagos Islands, and one dead sample,

obtained from an exposed reef terrace on Guadeloupe were used in the study. Radiocarbon dating from nearby reefs yielded the age of the Guadeloupe sample as about 25000–30000 years old. The U content, determined from inductively coupled plasma-mass spectrometry (ICP-MS) was low, approximately 3 ppm. In contrast, the Sr concentrations were approximately 7000 ppm in all three samples, requiring XAS data acquisition at the U L₂-edge. XANES edge energies and shapes were used to infer that the U in the two live samples was present as uranyl(VI) whereas that in the dead sample from the exposed reef on Guadeloupe was predominately U⁴⁺. Unfortunately, the EXAFS data were not of sufficient quality to confirm this observation and furthermore it should be noted that XANES data can sometimes be misleading when distinguishing between tetra- and hexavalent U (Eller *et al.*, 1985; Calas *et al.*, 1987; Greaves *et al.*, 1989; Biber *et al.*, 1997; Hess *et al.*, 1998; Sturchio *et al.*, 1998).

There have been two reports published on natural calcite samples that contain uranium. The first looked at a natural sample of spar calcite from a Mississippi Valley-type zinc ore deposit (Sturchio *et al.*, 1998). This sample has a relatively high U concentration (5–35 ppm). The sample also included a high concentration of Sr, necessitating data collection at the U L₂-edge. The XANES data are inconclusive with respect to the U oxidation state. In contrast, the EXAFS data fit well with a single coordination environment. The missing peak at 1.8 Å in the FT confirms the absence of a uranyl ion and the overall coordination environment confirms the incorporation of tetravalent U into the calcite lattice. Although the EXAFS results show an important difference for the U coordination over that of Ca²⁺, it is clear that the U does directly substitute for Ca²⁺ in the lattice. In calcite, the Ca²⁺ has a first coordination shell of octahedral O about Ca²⁺ at a distance of 2.36 Å (Effenberger *et al.*, 1981). In contrast the incorporated U is best fit with two shells: one at 2.21 and one at 2.78 Å. More distant shells were also observed, including six C at 3.26 Å, six Ca²⁺ at 4.02 Å, and six Ca²⁺ at 4.98 Å. These distances are indistinguishable from those observed in calcite itself. An X-ray synchrotron microprobe analysis of the same sample confirms the substitution of U into the calcite structure and is inconsistent with inclusions of distinct U-rich phases. The simultaneous presence of sulfide minerals and hydrocarbon inclusions indicates that this calcite sample was formed in a reducing environment. This may explain the high concentration of U in this sample, and indicates that U⁴⁺ is preferentially incorporated into calcite in such environments. In contrast, U⁶⁺ is generally excluded from calcite. These results provide insight into the geochemical cycle of U in deep groundwater aquifers and anoxic lacustrine and marine basins. The incorporation of U into calcite gives a potentially stable host for dispersed U⁴⁺ over geological time scales.

The second report of an XAS study of uranium in natural calcite (Kelly *et al.*, 2003) involved the use of XAS and X-ray microprobe to look at a sample relatively rich in U (about 360 µg/g) from a 13700-year-old speleothem deposit

in northern Italy (Spoetl *et al.*, 2002). X-ray fluorescence (XRF) mapping was done with a monochromatic beam (17.3 keV) focused to $5 \times 5 \mu\text{m}^2$. Fluorescence emission from U, Sr, and Ca were monitored. XRF mapping indicated that uranium concentrations vary between 80 and 500 ppm that were homogeneous on the 100- μm scale. The data were considered consistent with a dilute solid solution. It is interesting to note that there is petrographic evidence that this natural sample of calcite formed by recrystallization of a U-rich aragonite sample, which may explain the high uranium substitution. In contrast to the previous data on the natural calcite sample from the Mississippi valley, the XANES data from the northern Italy calcite sample indicated uranium is predominately hexavalent. The EXAFS data confirmed a hexavalent, dioxo-uranyl coordination that is monodentate to four carboxylates with U–O distances from the EXAFS fit of 2.41 Å. These results are similar, although more detailed, than those previously reported for synthetic calcite samples (Reeder *et al.*, 2000, 2001) but the interpretation is different. The authors of the paper, reporting uranyl incorporation into natural calcite (Kelly *et al.*, 2003), propose a direct substitution into the calcite lattice that involves the replacement by UO_2^{2+} of one Ca and two carbonate anions. Charge balance then requires the non-local substitution of excess Na^+ , which is observed in the chemical analysis. Overall, the reported EXAFS analyses are not inconsistent with their proposed model, although the complexity of the uranyl site requires eight scattering contributions with 19 variable parameters to adequately fit the data. Considering the reported k -range, only 15 parameters should have been used in the fit (Teo, 1986). Thus, although the proposed model for uranyl substitution into calcite is interesting, further experimental work is required for its confirmation.

The overall conclusion that the uranyl ion is more effectively incorporated into the aragonite than the calcite structure raises an environmental issue (Reeder *et al.*, 2000). Prevalent geological conditions at or near the Earth's surface favor the transformation of aragonite, which is metastable, into calcite. However, the uranyl ion does not fit into the calcite lattice as well as it does into the aragonite lattice. The UO_2^{2+} coordination environment is more clearly defined in the latter material, which is known to incorporate a significantly higher concentration of uranyl. Therefore the transformation of aragonite into calcite destabilizes the uranyl incorporated into the phase. As a result, CaCO_3 may not be an effective sequestering agent for U(VI) under geologic conditions and over long timescales.

28.3.3 Fe-bearing mineral phases

Iron and its compounds play an important environmental role in both biotic and abiotic processes. Its complex redox and solubility behavior is a function of solution Eh and pH, as sketched in Fig. 28.5 (Hem, 1985). Fe^{2+} is generally soluble in groundwater systems whereas most iron minerals and insoluble complexes contain Fe^{3+} . Iron oxides in particular are ubiquitous in soils and

sediments where they play an important, although not well understood, role in regulating metal-ion distribution through chemical, adsorption, and redox mechanisms. Iron sulfides also play a role in more anoxic environments. Oxidation state properties of Fe can play an important role in actinide speciation and transport, especially in reducing environments. Simple solution redox reactions may be directly affected by the presence of a redox-active surface, or they may be altered in the presence of a mineral surface that can preferentially adsorb, and thereby concentrate metal-ions at solution concentrations that are well below their solubility limits.

In order to understand the results of experiments designed to study actinide speciation on Fe surfaces, which are conducted at a macroscopic level, it is necessary to elucidate a molecular level model for the solid/surface reactivity. Several studies, using EXAFS spectroscopy, have been undertaken to probe actinide speciation on carefully prepared Fe samples, as listed in Table 28.12. Most, although not all of these experiments have focused on uranyl adsorption onto mineral phases, although the occlusion of U by Fe-oxide mineral coatings has also been reported (Jenne, 1977). In the absence of high solution concentrations of complexing ligands, U has been shown to complex to Fe minerals such

Table 28.12 *Published studies of uranium and neptunium binding to Fe mineral surfaces. These studies focus on inner- versus outer-sphere coordination of actinide with mineral surface as well as any evidence of redox chemistry.*

<i>Actinide</i>	<i>Mineral name</i>	<i>Chemical formula</i>	<i>References</i>	
uranium (VI)	hydrous Fe oxide, ferrihydrate	microcrystalline hydrous $\text{Fe}_2\text{O}_3 \cdot n\text{H}_2\text{O}$	Manceau <i>et al.</i> (1992)	
	goethite	$\alpha\text{-FeOOH}$	Waite <i>et al.</i> (1994); Reich <i>et al.</i> (1998b) Moyes <i>et al.</i> (2000); Reddon <i>et al.</i> (2001); Walter <i>et al.</i> (2003)	
	hematite	$\alpha\text{-Fe}_2\text{O}_3$	Reich <i>et al.</i> (1998b); Bargar <i>et al.</i> (1999a, 2000)	
	lepidocrocite	$\gamma\text{-FeOOH}$	Moyes <i>et al.</i> (2000)	
	mackinawite	FeS_{1-x}	Moyes <i>et al.</i> (2000)	
	schwertmannite	$\text{Fe}_{16}\text{O}_{16}(\text{OH})_{12-9}$ $(\text{SO}_4)_{2-3.5} \cdot 10\text{H}_2\text{O}$	Walter <i>et al.</i> (2003)	
uranium (VI)	green rust	mixed Fe(II)/Fe(III) hydroxides U-Fe oxide co-precipitates	O'Loughlin <i>et al.</i> (2003) Duff <i>et al.</i> (2002)	
	neptunium (V)	goethite	$\alpha\text{-FeOOH}$	Combes <i>et al.</i> (1992)
	mackinawite	FeS_{1-x}	Moyes <i>et al.</i> (2002)	

as hematite and goethite over a wide range of solution pH conditions (Hsi and Langmuir, 1985; Waite *et al.*, 1994; Duff and Amrhein, 1996), making these reactions of significant importance to its environmental behavior. For the most part, these studies involve Fe(III) phases and are therefore unlikely to involve redox activity because the studies have utilized the fully oxidized UO_2^{2+} ion in solution.

Among the relevant experiments are those that probe the interaction of uranyl with hydrous ferric oxide (HFO) because the enrichment factor for uranyl on the HFO surface is about 500 times greater than on well-crystallized goethite, and about 10^5 times greater than on clay surfaces (Szalay, 1991). EXAFS data, obtained from samples prepared at pH 5 with an 8.2% surface coverage (Manceau *et al.*, 1992), show uranyl coordination with about five equatorial oxygens at 2.2–2.4 Å and an additional broad peak corresponding to one Fe at about 3.4 Å and another 0.5 Fe at about 3.3 Å. These distances are consistent with uranyl bonding as a mononuclear bidentate inner-sphere complex, sharing edges with the Fe–O, OH surface octahedra. The authors note the excellent match between the unshared edges of the Fe–O octahedra and of the O–O distance of the equatorial uranyl ligands. They use this match to explain the unusually high affinity of uranyl for HFO as compared to crystalline phases such as goethite. The structural relationship between the sorbent and the sorbate is used to explain, at a molecular level, why uranyl complexes inhibit the HFO to crystalline oxide transformation (Manceau *et al.*, 1992).

A related study involved U L_3 -XAFS studies of U(VI) adsorption onto ferrihydrate over a wide range of solution and adsorption conditions (Waite *et al.*, 1994). Ferrihydrate is an amorphous or poorly crystalline hydrous Fe(III) oxide that exhibits a stoichiometry near $\text{Fe}_2\text{O}_3 \cdot \text{H}_2\text{O}$. EXAFS experiments were performed on ferrihydrite samples that had been aged for 65 h at 25°C and pH 6, after which the pH was adjusted to 5 or 5.5 and held for a further 24 h before adding U(VI). There were two samples made with U/Fe molar ratios of 0.044 and 0.077. Data, collected over a k -range of 3–16 Å⁻¹, required three U–O and one U–Fe shells to obtain the best fit. The results, using integral coordination numbers for the U–O fits, were two axial O at 1.80 Å, three equatorial O at 2.34 Å, two O at 2.52 Å, and about 0.5–1 Fe at a distance of approximately 3.4 Å. The authors conclude from their fits that the O at 2.52 Å is an inner-sphere O sorbed to the ferrihydrate surface. The Fe is coordinated in a bidentate fashion with the U, and, within a 10% error margin, there are no sorbed multinuclear uranyl complexes. These results are very similar to those reported in the previous study (Manceau *et al.*, 1992), although the latter study shows a split equatorial oxygen shell. The EXAFS results, supported by model simulations, suggest that the major U(VI) species at the ferrihydrite surface in the acidic pH range is an inner-sphere, bidentate complex that involves two surface hydroxyls of an Fe octahedral edge and the uranyl cation. Later work on very similar samples (Reich *et al.*, 1998b) failed to confirm the split oxygen shells at 2.34 and 2.52 Å, but instead found a single shell with five O coordinating at 2.36–2.39 Å

with a large Debye–Waller factor, consistent with the earlier work (Manceau *et al.*, 1992). Despite the absence of evidence for a split equatorial oxygen shell, inner-sphere complexation was proposed (Reich *et al.*, 1998b), and the authors noted that the difference in the equatorial oxygen coordination cannot be explained by the shorter k -range of their data.

Uranium uptake was studied from solutions at various pH values in the presence of the iron-bearing mineral phases goethite, lepidocrocite, and mackinawite (Moyes *et al.*, 2000). Refinements of EXAFS data show the U coordination at the surface to be very similar to those reported previously for U bound to other Fe–O and Fe–S mineral surfaces (Waite *et al.*, 1994; Reich *et al.*, 1998b). Binuclear, bidentate surface complexes are present together with monodentate, mononuclear coordination to the structural sulfate for the FeSO₄ oxide, schwertmannite (Walter *et al.*, 2003).

The EXAFS results from uranyl adsorbed on HFO and other mineral samples, together with modeling, show that the adsorbed complex is a unique product of the coordination environment at the surface, and appears independent of the predominant U(VI) speciation in solution, as was previously suggested (Waite *et al.*, 1994). A diffuse double-layer, two-site model with two proposed surface species provided excellent agreement with all data over a range of pH, U(VI) concentration, and two dissolved CO₂ concentrations. This conclusion contradicts several previously published modeling approaches to uranyl surface speciation (Hsi and Langmuir, 1985).

It has been previously reported that dissolved carbonate, ubiquitous in groundwater, plays a crucial role in the distribution of U(VI) between solution and Fe oxide surfaces (Ho and Doern, 1985; Hsi and Langmuir, 1985). EXAFS studies have focused on the molecular influence of carbonate complexation on U sorption onto Fe oxide surfaces. U complexed to ferrihydrite shows a U–C distance of 2.93(2) Å (Reich *et al.*, 1998b), which matches the U–C distance previously reported for a bidentate coordination of the CO₃²⁻ group to uranyl (Coda *et al.*, 1981; Allen *et al.*, 1995), and is consistent with the proposed formation of (=FeO₂)UO₂CO₃²⁻ (Waite *et al.*, 1994), an inner-sphere structure. U coordinated to hematite shows a similar behavior (Bargar *et al.*, 1999a,b). EXAFS fits indicate that U(VI) has five to six equatorial oxygens. Since two of these should be hematite-surface oxygens, it is argued that there are at most two carbonate ligands and the complex should have a composition similar to FeO₂UO₂(CO₃)_x, where $x \leq 2$. The absolute coordination numbers for carbonate in all samples imply that $\geq 50\%$ of adsorbed U was complexed, even at pH 4.75. This finding contradicts predictions that U(VI)–carbonate ternary complexes should predominate only above pH 6 (Waite *et al.*, 1994). In addition, at pH values ≤ 6.5 , there was no evidence from the EXAFS data for second-neighbor U(VI), indicating that the adsorbates were monomeric (Bargar *et al.*, 2000).

Also ubiquitous in the environment is the citrate anion. EXAFS was used to characterize the coordination environment of uranyl adsorbed onto goethite in

the presence of citrate under aqueous conditions where uranyl is strongly sorbed (Reddon *et al.*, 2001). A PCA showed that two major constituents should account for all the data. Unlike other Fe-mineral adsorption studies, there was no evidence of a Fe-neighbor in the U EXAFS. The authors concluded that the adsorption of uranyl does not follow a simple, stoichiometric relationship between the total U and citrate in the sample, and that under the conditions employed the adsorption of citrate on goethite appears to be favored over the formation of a uranyl–citrate–goethite complex.

In addition to the adsorption of uranyl onto mineral phases, EXAFS structural data were reported for U trapped in Fe-rich gels that are formed during the oxidative weathering of a granitic U deposit in the context of acid-mine drainage (Allard *et al.*, 1999). These natural samples, from the Massif Central in France, were in water that was close to saturation with respect to amorphous silica and crystalline-hydrated U-hydroxides and silicates. This effort addressed the elementary processes implied in U sorption and the trapping mechanism of U by natural short-range ordered phases. They investigated samples obtained at the fissure outlets on the walls of the galleries. These include hydrated amorphous products that are referred to as gels. XANES data confirm that the U was found to be present as hexavalent uranyl. The EXAFS on the Fe-rich gels found that uranyl is mainly present either as an outer-sphere complex or as an inner-sphere complex unresolved by EXAFS. No U–Fe, U–Si/Al, or U–U interactions were evident from the gel samples. The absence of U–Fe contributions to the data, despite the high affinity of uranyl for hydrous Fe oxides, suggests that U may be trapped in a two-step process involving the early complexation of U and Si/Al followed by the transport of Fe as ferrous in fissure water, with the ultimate precipitation of Fe in Si/Al-containing solutions at a redox front.

Green rusts, which are mixed Fe(II)/Fe(III) hydroxides, are formed by a number of abiotic and biotic processes under circumneutral to alkaline conditions in suboxic environments. The interaction of hydroxysulfate green rust, in which SO_4^{2-} is an interlayer anion was studied to examine its influence on the redox behavior of U(VI) (O'Loughlin *et al.*, 2003). L_3 -edge XANES spectra show that U(VI) was readily reduced to U(IV) at a pH of 7.3 in the presence of green rust. EXAFS data indicate an average U local environment similar to that in UO_2 . The decreased FT amplitude in the green rust sample compared to a UO_2 standard probably indicates small particle size and/or increased disorder.

The co-precipitation of uranium with iron-oxide minerals was studied with a series of co-precipitates with mole fractions of U in the range of 0.35–5.4% (Duff *et al.*, 2002). Although the XANES spectra are consistent with U(VI), EXAFS results show U to be in a highly distorted environment, in agreement with XRD, FT-infrared, XANES, and luminescence studies. Fits to the data for samples with <1 mol% U indicate no axial O, instead there are about four O at 2.21–2.36 Å. The model fits also indicate that at least one Fe atom exists in the uranium second-coordination shell at 3.19 Å. However, details of the fit suggest that there are multiple shell environments. Overall, the results are interpreted as

consistent with the incorporation of U(vi), minus the dioxo coordination, into the Fe oxides. This situation does not apply for co-precipitated samples with > 1 mol% U, which exhibit uranyl coordination and evidence of a second shell U backscatterer. These data are consistent with XRD, FT-infrared and luminescence data, which taken together show evidence of a U(vi) oxide hydrated phase such as schoepite, $\text{UO}_2(\text{OH})_2 \cdot 2\text{H}_2\text{O}$.

There have been few reports of synchrotron studies centered on the sorption of transuranics onto Fe-bearing mineral phases. Despite its low affinity for complexation, Np(v) has been reported to sorb onto mineral surfaces with the decreasing affinity: calcite > goethite >> $\text{MnO}_2 \approx$ clays. The sorption of Np(v) onto these phases may involve its reduction to yield the much less soluble Np^{4+} , which has much high binding affinities and generally lower solubility. An early study of Np(v) on an iron-bearing mineral involved goethite, which has fully oxidized Fe (Combes *et al.*, 1992). XANES spectra confirm the presence of neptunyl groups. Fitting the EXAFS data results in 2.2 O at 1.85 Å and 5.5 O at 2.51 Å for Np adsorbed onto goethite, compared with the fit obtained from Np(v) in solution of 1.6 O at 1.83 Å and 5.2 O at 2.52 Å. This coordination environment for solution Np(v) compares with more recent comparative studies of Np coordination in solution, which are listed in Table 28.4. The only observed difference between the spectra obtained directly from solution and the goethite-sorbed spectrum is the presence of high-amplitude structure between 2.5 and 4 Å in the FT of the latter. Although these data may indicate Np–Fe interactions, the short *k*-range prohibits a full analysis. The authors claim that their data rule out diffusion into the solid and precipitation or coprecipitation of ordered solids onto the goethite surface. A more recent study (Moyes *et al.*, 2002) looked at solution Np(v) sorption onto microcrystalline mackinawite (FeS) at pH values in the range 7–8 and 3, and Np solution concentrations of 0.27, 0.68, and 2.74 mM. XANES spectra indicate limited sorption coupled with a reduction to Np(IV) that is confirmed by EXAFS. The coordination environment of Np in all samples is indistinguishable, with four O at 2.25 Å, three S at 2.63 Å, two Fe at 3.92 Å, and six Fe at 4.15 Å. The absence of two axial O atoms at about 1.85 Å supports the XANES finding for the reduction of Np(v). The short Np–S distances suggest a direct coordination with mineral surface S.

28.3.4 Phosphates

The phosphate class of minerals are made up of $(\text{MO}_4)^{3-}$ units in which M^{5+} can be P, As, Sb, or V (Deer *et al.*, 1992). Although apatites are the most common subclass of the phosphates, monazites are important here because of the insolubility of rare-earth and actinide phases. Thorium and uranium are common impurity phases in monazite.

Uranium sorption on the surface of hydroxyapatite, $\text{Ca}_5(\text{PO}_4)_3\text{OH}$, was studied as a removal mechanism for heavy metals from groundwater, either

by precipitating as a phosphate or by ion-exchange for Ca^{2+} (Fuller *et al.*, 2002). Samples with less than 4700 ppm surface-sorbed uranium(vi) were studied by EXAFS and found to have the standard axial dioxo coordination. In addition, a broad equatorial shell was observed that, for two of the three samples studied could not be resolved by the fit. The single, unresolved shell was fit to a distance of about 2.313 Å by employing large Debye–Waller factors and fixing the coordination number to six. The most concentrated sample (4700 ppm) showed a resolvable two-shell equatorial coordination with 3.6(6) O at 2.338(8) Å and 2.1(2) O at 2.51 Å. Two of the three samples also had U–Ca interactions that fit to about one Ca at 3.8 Å, a distance consistent with bidentate edge sharing and/or monodentate corner-sharing coordination between the equatorial oxygens of the uranyl ion and the Ca–O polyhedra on the hydroxyapatite surface. In contrast, the U(vi) coordination environment is inconsistent with its incorporation into the mineral phase. One of the samples, exposed to dissolved carbonate, showed a U–C interaction implying U–carbonate ternary complexes. There were also indications of a more distant coordination shell that was fit as either a Ca atom at 4.55 Å or a U atom at 4.09 Å, with no independent evidence presented that could distinguish between the two fits. As the uranyl coverage on the hydroxyapatite surface increased above 4700 ppm, the EXAFS spectra began to resemble that of a U(vi) phosphate, notably chernikovite, $(\text{H}_3\text{O})_2(\text{UO}_2)_2(\text{PO}_4)_2 \cdot 6\text{H}_2\text{O}$. The uranyl uptake at the onset of chernikovite precipitation corresponds to a surface coverage of about 6% of a monolayer.

An independent study was also conducted on the incorporation of U(vi) into synthetic fluorapatite (Rakovan *et al.*, 2002). XAS together with luminescence and diffuse reflectance were used to determine the local structure of U(vi) in a powder sample. The sample had a concentration of 2.3 wt% U. Optical luminescence data, including lifetime measurements, combined with diffuse reflectance data indicate that although the U appears hexavalent in the fluorapatite sample, it does not have the standard dioxo coordination environment. This finding is supported by U L_3 -edge XANES spectra, which confirms that uranium is hexavalent. However, the XANES data do not show the small shoulder feature indicative of dioxo coordination about uranium (Hudson *et al.*, 1995a), but instead are similar to the spectra observed for U(vi) in Li_4UO_5 (Locock and Burns, unpublished) and Np(vii) in solution (Williams *et al.*, 2001). Both of these ions exhibit an unusual tetraoxo coordination environment of four short and two longer oxygen distances. This coordination environment is confirmed by a simple inspection of the U EXAFS data, which are also inconsistent with a dioxo coordination environment. An analysis revealed that U is coordinated to six equidistant oxygens at 2.06 Å. With respect to the host fluorapatite sample, the U EXAFS fit shows a similarity to the coordination environment of the Ca1 site (space group $P6_3/m$, No 176; Wyckoff position 4*f*; 3 symmetry) (Comodi *et al.*, 2001). Attempts to fit the data assuming Ca2 substitution (Wyckoff position 6*h*, *m* symmetry) were unsuccessful. The finding of 6 oxygen at 2.06 Å is in agreement with the average U–O distances for

six-coordinate, tetraoxo- (Hoekstra and Siegel, 1964) or near-cubic (Bawson *et al.*, 1956) coordination. This work clearly demonstrates that fluorapatite can accommodate large concentrations of U(VI) into the lattice, with a coordination environment that is very similar to that found in perovskites, another common mineral class. Therefore, the determination of significant uranium incorporation into fluorapatite may point to an important sequestration mechanism for high-valent actinides in the environment.

Uranyl sorption onto the lanthanide phosphates LaPO_4 and $\text{La}(\text{PO}_3)_3$ has also been studied as a function of pH (Ordóñez-Regil *et al.*, 2002). The study included pH values of 1, 2, and 3, which compare to the isoelectric point of about 4 for LaPO_4 and 3 for $\text{La}(\text{PO}_3)_3$. The fitted parameters for the EXAFS spectra from the two samples were statistically indistinguishable. In addition to the dioxo-shell, there were two equatorial O shells, with 2.4 O at 2.31 Å, and 1.8 O at 2.47 Å, distances consistent with bidentate, inner-sphere coordination. The observation of a U–P interaction at 2.74 Å is used to argue that the uranyl is complexed to a single surface phosphate group.

28.3.5 Natural soil samples

The understanding and prediction of actinide speciation in natural soil samples comes from a synthesis of the published studies of actinide speciation and coordination under laboratory conditions. The challenge encountered when characterizing naturally occurring samples is the length scale of potential inhomogeneities. Depending on their origins, soil samples can have fine grain sediments that present chemical inhomogeneities on the micron or smaller length scale. Micro techniques that have been used to study such samples, including scanning tunneling microscopy (STM) (Yanase *et al.*, 2002) uranyl fluorescence (Joergensen, 1977) and micro-Raman (Allen *et al.*, 1987; Biwer *et al.*, 1990; Palacios and Taylor, 2000) that produce important, but limited, information about uranium speciation.

Until the development of specialized μ -XAS and μ -SXRF capabilities, synchrotron-based spectroscopic studies were limited by beam sizes on the order of mm^2 or larger. Various micro-focusing techniques have reduced the beam size to about $50 \times 50 \mu\text{m}^2$ or larger, depending on energy ranges and flux requirements. Unfortunately, the focusing optics work over limited energy ranges, so that for work on the actinide L_3 -edges, XAS energy scans are limited to 200–300 eV, sufficient only for XANES spectroscopy. Nevertheless, information has been obtained by these μ -XAS techniques that have significantly broadened the knowledge of actinide speciation in these complex samples.

A conventional XAS study on uranium-contaminated soil samples showed the potential for XAS to contribute information necessary to the development of a rational remediation scheme (Morris *et al.*, 1996). This study examined samples from the Fernald Environmental Restoration Management Company, a U.S. DOE facility that once served as one of the principal processing centers

for uranium. The soil matrix consists primarily of quartz, calcite, dolomite, and the clay minerals illite and chlorite, with the pH of the topsoils in the range of about 5.4–6.3 (Elless and Lee, 1994). Background levels of U in uncontaminated reference topsoils near the production facility are typically about 3–5 ppm. There were many different source terms for the contaminants including both aqueous waste and airborne particulate. U concentrations from production range from about 10 to 8000 ppm at pH values of 7–8.5. Only about the top 0.25–0.3 m were contaminated.

XANES studies of both bulk and size-selected samples showed that most of the U exists in the hexavalent oxidation state, a finding that was confirmed by EXAFS. EXAFS data showed that the equatorial uranyl coordination varied significantly between samples and indicated variation in speciation. Independent optical, microscopy, and diffraction (Elless and Lee, 1994) data indicated the presence of autunite-like, $\text{Ca}(\text{UO}_2)_2(\text{PO}_4)_2 \cdot 2\text{--}6\text{H}_2\text{O}$, and schoepite-like, $\text{UO}_3 \cdot 2\text{H}_2\text{O}$, phases in the samples, consistent with the variation in EXAFS coordination. The goethite (FeOOH) that is naturally present in the soil should require U(vi) if equilibrium is reached because the Fe(III)/Fe(II) reduction potential is considerably lower than the corresponding U(vi)/U(iv) potential. The XAS used in this study, together with other spectroscopies, confirmed that 75–95% U was hexavalent. Based on this speciation, the authors were able to make specific recommendations about site remediation, including the need for near-term action based on the solubility and mobility of U(vi). A later study, in which U was added to natural subsurface soil samples from Hanford, SRS, and Oak Ridge produced similar results (Bostick and Fendorf, 2002).

Micro-XAS and synchrotron X-ray fluorescence (SXRF) studies on soil and sediment samples from Fernald and the Savannah River Site (SRS) offer a different perspective (Bertsch *et al.*, 1994; Hunter and Bertsch, 1998). The samples from the SRS differ from those of Fernald in that the U contamination was discharged as aqueous waste. This study used a micro-focused synchrotron beam with spot sizes that varied from 50×50 to $300 \times 300 \mu\text{m}^2$. The focusing optics utilized limit the energy range over which data was collected to approximately 200–300 eV, which restricted spectra to the XANES region only. Under the experimental configuration employed, it was possible to simultaneously collect a full SXRF spectrum to provide specific information on associated elemental distributions that is coupled to speciation data from XAS. The objective of the study was to determine U speciation in localized regions within inhomogeneous samples. XANES of clay fractions from both sites indicated > 90% hexavalent U, with no evidence of spatial variability of the U speciation within the clay fraction. This result was expected because the beam size was much bigger than individual clay particles and was consistent with the large number of size-fractionated sediment samples from SRS even though some of these latter samples were collected in seasonally reduced environments from wetland areas. No observation of significant biotic or abiotic U reduction was observed, as had been previously suggested (Lovley *et al.*, 1991; Nagy *et al.*, 1991), from samples

with high organic content that were in reducing environments. In contrast, sand and sediment fractions showed significant spatial variation using a 50 μm beam. The XRF signal was monitored, looking for areas concentrated in U, and then XANES spectra collected. Two types of populations were discernable: (1) those highly enriched in U and depleted in other elements such as Fe and Mn. For Fernald soil samples, U-rich regions were often relatively enriched in Ca, Cu, and Zn, whereas for SRS sediment these regions were highly enriched in Ni, and (2) U was concentrated and co-associated with regions relatively enriched in Fe and Mn. The U-rich region represented about 25% of the observations and may represent discrete U-containing phases either originally deposited as a component of the source term, or subsequently precipitated as a secondary phase. The zones of lower U concentration may represent either U co-precipitated with or sorbed to the Fe, Al, and Mn oxyhydroxides indigenous to the samples. XANES data, obtained using a 50 μm beam, from various regions within the sand fraction of Fernald soils provided evidence of varying oxidation states. Two of the 22 regions sampled showed predominantly U(IV) whereas other regions showed U(VI). There appeared to be discrete regions of U(IV) surrounded by a larger number of U(VI)-containing particles or surface-associated U(VI) phases. In contrast, when operating with a beam size of 300 μm , there was no evidence of pure or predominantly U(VI) speciation because of spatial averaging, pointing out the clear advantage of microprobe studies of natural, spatially inhomogeneous samples. The sand fractions from SRS did not display spectral differences indicative of varying oxidation states and were consistent with U(VI). However, post edge features indicated significant differences in the coordination environments within various regions of the sample.

During the 1999 global conflicts in the Balkan states, ammunitions were expended containing large amounts of depleted uranium (DU) that remains as an environmental pollutant with unknown health risks (Fetter and von Hippel, 1999; Priest, 2001; Bleise *et al.*, 2003). A series of studies was devised to investigate the oxidation state of particles dispersed into the geosphere in order to assess the fate and transport of this introduced pollutant (Shaughnessy *et al.*, 2003). The samples used in the analyses were collected at Ceja Mountain, Kosovo. Analytical results revealed U in soils with concentrations exceeding 2–3 ppm. Scanning electron microscopy (SEM) showed that most of the particles were present in the respiratory fraction, that is less than 5 μm (Danesi *et al.*, 2003). Micro-XANES data from the samples, obtained over an energy range of 300 eV using an X-ray beam spot size of $20 \times 20 \mu\text{m}^2$, were compared with U standards. SXRF data indicated the simultaneous presence of U and Ti, in accord with other analytical techniques and the known sample histories. The U L_{3-} edge data from the samples indicated that the U was oxidized, i.e. that there was no metal present. Depending on sample details, the U was consistent with either tetravalent U, as UO_2 , or U_3O_8 , or mixed samples. Hexavalent U was not observed. This finding is interpreted as DU particles with tetravalent

cores and oxidized surfaces, indicating weathering. This study revealed important factors for further assessing the environmental and health impacts of munitions-generated depleted U.

Elevated levels of U occur in natural soils and evaporation ponds that are associated with agricultural irrigation activities in the southwestern U.S. Evaporation ponds are periodically filled and evaporated to dryness, a process that can significantly influence redox processes. Most soils in the area are derived from marine Cretaceous shale that is known to contain high levels of U, with total concentrations as high as 280 ppm. A synchrotron-based study has been published that focuses on natural uranium speciation in evaporation ponds located in the San Joaquin Valley (SJV), CA (Duff *et al.*, 1997). Sediment samples, obtained from depths of 0–5 cm, were collected on two different occasions, one when the pond was nearly dry and the other when it was partially filled with drainage water. Suspension pH and Eh measurements were obtained at the time of sampling. There were no observable trends in U concentration with depth of sample, however the aqueous concentrations of U(IV) decreased with increasing Eh whereas dissolved U(VI) concentrations increased greatly with increasing Eh.

Micro-XANES data were obtained over a 130 eV range with a $200 \times 200 \mu\text{m}^2$ beam size and SXRF data were collected at the U L₃-edge energy. XANES spectra were fitted using those obtained from standard spectra to assess relative ratios of reduced to oxidized U. These data showed that the amount of reduced U relative to oxidized U increases with increasing sample depth. The deepest samples (about 5 cm) showed that about 25% of the U in the measured samples was tetravalent. No changes were observed in the U concentration as the beam was scanned across the sample. Whereas the samples did not appear to contain any U hotspots, it should be noted that the particle sizes less than 2 μm were considerably smaller than the beam size, which was about 200 μm . A scenario for the fate of U in the SJV evaporation pond was proposed based on XANES and SXRF data that were complemented by other analytical techniques. It was proposed that U enters the pond in the drainage water, probably as a carbonate anionic species. Some of the U is accumulated by algae that creates a biomass with reducing conditions in which U(VI) reduction takes place. The precipitation of mixed U(VI)/U(IV) in organic matter then brings the U into the sediment. Over time, with increasing burial, the increasingly anoxic environment further reduces the U(VI). As the ponds drain, the soil aerates and the reduced U is reoxidized, resolubilized, and thus remobilized. A follow-up study was published that addressed samples obtained over a wider depth range, 0–40 cm (Duff *et al.*, 2000). Microprobe (300 μm^2 spot size) XANES measurements, over a 140 eV range, were used to infer the relative amount of U(VI) by comparing edge position with known standards. This study found that the relative percentage of U(VI) appeared to decrease with increasing sampling depth and correlated with a decreasing total organic content.

The power of synchrotron-based microprobe spectroscopies to provide unique speciation information was clearly demonstrated in a series of experiments designed to probe plutonium adsorbed to natural tuff samples from the Yucca Mountain site (Duff *et al.*, 1999a,b, 2001). Tuff is rock composed of compacted volcanic ash that varies in size from fine particulate to gravel. These studies were performed to assist in the modeling of Pu speciation and groundwater transport in the event of a release of stored radioactive waste into the environment. The solubility of Pu in groundwater varies greatly, with 3+ and 4+ states being significantly more sorptive and less soluble than their higher valent counterparts. This discrepancy occurs because the higher valent ions form dioxo moieties, which have lower overall ionic charges. Under acidic conditions, Pu(v) undergoes disproportionation, to form Pu(iv) and Pu(vi), whereas in neutral to basic oxic solutions Pu(v)O₂⁺ dominates speciation. The synchrotron microprobe studies were designed to determine what Pu species are adsorbed to natural tuff samples using spatially resolved μ -SXRF to determine Pu distribution and μ -XANES to determine oxidation states. All oxidation states of Pu have been reported to sorb to smectites and iron- and manganese-bearing oxyhydroxides (Keeney-Kennicutt and Morse, 1985; Sanchez *et al.*, 1985). A question addressed by these studies is whether minerals, particularly those with redox-active surfaces, can influence the redox chemistry of Pu in solution. The tuff samples, analyzed by X-ray diffraction, were predominantly zeolitic phases, specifically clinoptilolite 80 wt%, smectite 2%, opal 8%, feldspar 7%, and quartz 3%. Further work on the smectite isolates showed them to contain rancieite, a mineral with mixed manganese content, (Ca, Mn²⁺) Mn₄⁴⁺O₉ · 3H₂O.

Information on the average oxidation state of sorbed Pu on tuff was obtained on the spatial scale of about 140 μm^2 . The Pu-sorbed samples were prepared using 10⁻⁴ M, ²³⁹Pu(v) spiked, synthetic groundwater meant to mimic deep tuffaceous aquifers such as those found below Yucca Mountain. About 92–98% of the initial Pu(v) in solution was sorbed to the samples. SXRF was done for elements with absorption energies below 18.5 keV. The problem in resolving the Pu and Sr signals was circumvented by obtaining one elemental map just below the Pu L₃-edge and another just above the edge. The Pu elemental map was then obtained by subtracting the images. Contrary to expectations based on previous work (Triay *et al.*, 1997), the mapping showed that Pu is predominately associated with manganese oxides, specifically rancieite, and smectites but not with iron oxides. Fractures and pore spaces from Yucca Mountain tuff samples contain highly reactive surfaces that can sorb a variety of differently charged and sized ions from fracture- and pore-space fluids. Rancieite comprises less than a percent of the mineral distribution in the tuff, but its presence at primary flow paths makes it highly accessible to dissolved species in the groundwater (Duff *et al.*, 2001). Several other elements in addition to Pu were co-associated with the manganese oxide and not with hematite. It is postulated that the iron mineral surfaces appear to be passivated and thus inaccessible to sorption.

Why the iron oxide, and not the manganese oxide, surfaces were passivated is not understood. Modeling and surface calculations based on experimentally determined concentrations suggest that multiple binding sites are present on the Mn–O/smectite phase.

μ -XANES was obtained from the same samples at two different $10 \times 15 \mu\text{m}^2$ spots that appeared to contain the highest level of Pu as determined by the SXRF mapping. Unfortunately, XANES was not definitive in determining the oxidation state. Although the Pu L_3 -edge position indicates the presence of primarily Pu(VI), the post edge feature associated with multiple-scattering from the plutonyl was not observed. The FT of a short EXAFS spectrum ($k_{\text{max}} = 8 \text{ \AA}^{-1}$) did not show evidence of the two-shell first coordination sphere that is expected for plutonyl coordination (Duff *et al.*, 1999b). A single peak at 1.65 \AA (uncorrected for phase shift) was observed but not fit. In addition, there was no evidence of a Pu–Pu interaction, which would have signaled Pu precipitation on the tuff surface. The authors conclude only that there may have been some oxidation of their Pu upon sorption to the Mn^{4+} -rich phase. It should be noted that tuff samples have been shown to oxidize Ce(III) to Ce(IV) (Vaniman *et al.*, 2002), an oxidation that was attributed to its association with rancieite, which contains an oxidized fraction of Mn.

These seminal papers clearly demonstrate the importance of a molecular level understanding of sorption on natural samples. That Pu should sorb preferentially to a Mn-oxide phase was not expected. Such information is very important in modeling actinide migration through the geosphere. In addition, it supports previous findings that actinide sorption is governed by the solid–water interface rather than solution speciation (Waite *et al.*, 1994). The results show that predictive remediation requires a more comprehensive understanding of Mn–Pu interactions.

Toward this end, a study was undertaken (Shaughnessy *et al.*, 2003) of interfacial reactions between aqueous Pu(VI) species and Mn oxyhydroxide mineral surfaces, notably manganite (MnOOH) and hausmannite (Mn_3O_4), which serve as representative examples of Mn phases typically found in the vadose zone. Note that manganite has a rutile-related structure, with trivalent Mn whereas hausmannite is a spinel-related structure with mixed di- and trivalent Mn. These two phases were from commercial stock and size selected for particles in the range of $63\text{--}212 \mu\text{m}$. The pH of the point of zero surface charge (pH_{pzc}) was determined to be 7.4(3) for manganite and greater than 10 for hausmannite. Sorption studies were done as a function of pH over the range 3–10, a function of Pu concentration, and as a function of solution exposure time at a fixed pH. Pu solution concentrations ranged from 1×10^{-7} to 1×10^{-4} M. There was an initial rapid sorption step that occurred within the first 24 h of contact, followed by a much slower sorption process. This two-step process for actinide adsorption onto mineral phases has been previously reported (Keeney-Kennicutt and Morse, 1985; Waite *et al.*, 1994). All XAS data reported in the Mn work were limited to samples that had a 24 h contact time with the soak-Pu

solutions. The sorbed Pu oxidation states were determined by a combination of optical absorption methods and XAS. A comparison of the Pu L₃-edge XANES data from the mineral-adsorbed phase with those from oxidation-state specific solution phases showed that the Pu sorbed to the Mn phases had been reduced from Pu(vi) in the initial solutions to Pu(iv) on the sorbed surface. Optical spectra on the remaining solutions determined the presence of Pu(v). In other words, all of the initial solution phase Pu(vi) had been reduced to either Pu(v), which remained in solution, or Pu(iv), which remained sorbed on manganite or hausmannite. There was no reduction observed for a blank Pu(vi) solution over the same time frame. The reductant in this redox reaction was not clearly evident from the experiment, but the authors conjecture that there may have been dissolved Mn(II) in solution. It should be noted that the reduction of Pu(vi) observed in this study is in contrast to the work on natural tuff, in which Pu(v) was seen to oxidize (Duff *et al.*, 1999a,b, 2001). The similarity in redox couples for Pu(iv), Pu(v), and Pu(vi) clearly complicates the chemistry in these redox-active mineral systems. EXAFS data from the same Mn samples (Shaughnessy *et al.*, 2003) were analyzed to determine the Pu coordination onto the mineral surfaces. The data were analyzed over a short *k*-range (2.5–10 Å⁻¹), significantly limiting the allowable number of variable parameters in the fitting. The data do not indicate dioxo coordination of the Pu, supporting the XANES interpretation of Pu reduction to tetravalent. The best fit was consistent with a single O shell at distances of 2.28–2.36 Å and with coordination numbers in the range of 7–9. The values may vary with the pH of the soak solution used for the sorption experiments. The fitted distances compare well with those expected for Pu(iv)–O interactions, as exemplified by the 2.337 Å one found in PuO₂ (Haschke *et al.*, 2000). In addition, Pu–Mn interactions were observed at about 3.37 Å for all samples, indicating that, like other adsorbed actinides, the sorbed Pu has an inner-sphere coordination with the mineral surface. These results support the finding that Mn-based mineral phases may serve to sequester Pu under natural groundwater conditions.

28.3.6 Bacterial interactions

It has been recently realized that microbes can actively influence actinide chemistry in the environment. Although much less studied than processes involving inorganic constituents, biotic interactions can have a marked influence on actinide speciation. Microbes are ubiquitous in the environment and therefore their influence must be included when developing predictive modeling for actinide fate and transport. Microbial processes can cause either mobilization or immobilization of radionuclides, that is actinides may be stabilized in solution or precipitated by direct processes, such as respiration, or indirect processes, such as the biotic modification of solution constituents.

XAS is developing into a cornerstone technique for discerning the influence of bacteria on actinide speciation, as indicated by the published work referenced in

Table 28.13. XAS is often used together with other physical techniques, such as optical and/or infrared spectroscopies, X-ray diffraction, microscopy (TEM, SEM), EDS (energy dispersive X-ray spectroscopy). These results augment the standard chemical analyses, such as titrations and solvent extraction. The advantage afforded by XAS is that it can probe metal-ion speciation *in situ*, that is in the presence of bacterial cells, cell growth media, and other metal-ions, with no necessity for chemical pretreatment. Its sensitivity to oxidation state is particularly important for probing redox effects of microbial interactions. Among its most significant disadvantages are its sensitivity, often requiring ppm or higher concentrations for meaningful data acquisition, and the propensity for beam-induced redox chemistry (Skanthakumar *et al.*, 2004) that can vitiate speciation, especially at low metal concentrations.

There are several questions that arise concerning microbial influence on actinide speciation. These all center on solubility and transport issues, and include precipitation, adsorption to the bacterial surface, incorporation into the cell, and solubilization of mineral phases. Precipitation can occur either through a change in redox state or through chelation. Generally, the higher oxidation states, including U(vi), Np(v), and Pu(v), (vi) are soluble in acidic and near-neutral pH, whereas their tetravalent analogs are relatively insoluble. Therefore, processes that control oxidation state are particularly important to quantify. Compounds or ions in solution may be used as electron acceptors in energy metabolism, a process referred to as dissimilative metabolism. The reduced species is excreted in the environment. Microbes are known to involve metal-ions, such as Fe(III) or Mn(III,IV), directly in their respiratory processes as electron acceptors. Aerobic respiration involves O₂ as the electron acceptor. Some microbes are capable of anaerobic respiration, in which they use nitrate, sulfate, carbonate, ferric iron or even certain organic compounds as the electron acceptor. Because these ions have lower reduction potentials than O₂, less energy is released. However, the use of alternate electron acceptors in their respiratory process allows microorganisms to live in environments that contain too little oxygen to support life.

Dissimilatory metal-reducing bacteria (DMRB) are able to couple the oxidation of organic matter to the reduction of Fe(III) or Mn(III/IV). Under anoxic conditions, DMRB have been shown to readily reduce U(vi) to precipitate UO₂ solid (Lovley *et al.*, 1991; Gorby and Lovley, 1992). XANES spectroscopy was used to probe U(vi) reduction, either as an aqueous species [UO₂(CO₃)_{3(aq)}]⁴⁻ or as metaschoepite [UO₃·2H₂O_(s)] (Fredrickson *et al.*, 2000). The results showed that the DMRB bacterium *Shewanella putrefaciens* reduced UO₂²⁺ in complex mineral suspensions via a combination of direct enzymatic or indirect mechanisms to insoluble U(IV) species. U reduction occurred whether the U(vi) was in solution or associated with a solid phase. The studies further showed that *S. putrefaciens* could reduce U(vi) in complex suspensions that included Fe(III) as an alternative electron acceptor, despite the lower standard potential of the U(vi) couple, as shown in Table 28.1. Further experiments, involving Mn K-edge

Table 28.13 Published studies of actinide-ion sorption onto bacterial surfaces. These studies involve actinide redox speciation studies and efforts to define active binding sites on bacterial surfaces.

	Strain	Gram	Growth conditions	pH	Comment	Metal	References
<i>Clostridium</i> sp.	ATCC 53464		anaerobe	6.8		U(VI)	Francis <i>et al.</i> (1994) Francis <i>et al.</i> (2002) Francis (2002) Suzuki <i>et al.</i> (2003)
<i>Clostridium</i> sp.			anaerobe		inactive uranium mine	U(VI)	
<i>Pseudomonas fluorescens</i>	ATCC 55241		aerobe	6.1	citrate, Fe(III) complexes	U(VI)	Dodge and Francis (1997)
<i>Halomonas</i> sp.	WIPPIA	+	(an)aerobe	about 9.1		U(VI)	Gillow <i>et al.</i> (1999) Francis <i>et al.</i> (2000)
<i>Desulfovibrio desulfuricans</i>	ATCC 29577		anaerobe	6.1		Np(V)	Soderholm <i>et al.</i> (2000)
<i>Shewanella putrefaciens</i>	CN32		aerobe	about 7		U(VI)	Fredrickson <i>et al.</i> (2000)
<i>Bacillus cereus</i>	JG-A30 4415	+	aerobe		vegetative cells, spores	U(VI)	Hennig <i>et al.</i> (2001a)
<i>Bacillus sphaericus</i>	JG-A12 9602	+	aerobe	2		U(VI)	Hennig <i>et al.</i> (2001a)
<i>Acidithiobacillus ferrooxidans</i>						U(VI)	Merroun <i>et al.</i> (2002a)
<i>Shewanella putrefaciens</i>	CN32		anaerobe		Mn(III,IV)	U(VI)	Fredrickson <i>et al.</i> (2002)
<i>Pseudomonas fluorescens</i>	ATCC 55241	-	aerobe	variable		Np(V)	Songkasiri <i>et al.</i> (2002)
<i>Bacillus sphaericus</i>	ATCC 14577	+	aerobe		vegetative, heat killed cells, spores	U(VI)	Panak <i>et al.</i> (2002b)
<i>Bacillus sphaericus</i>	ATCC 14577	+	aerobe	4.4	recovered from U mining waste	Pu(VI)	Panak <i>et al.</i> (2002a)
<i>Acidithiobacillus ferrooxidans</i>	D2					U(VI)	Merroun <i>et al.</i> (2002a)
<i>Pseudomonas stutzeri</i>	DSMZ 7136 DSMZ 5190					U(VI)	Merroun <i>et al.</i> (2002a)

Table 28.13 (Contd.)

	Strain	Gram	Growth conditions	pH	Comment	Metal	References
<i>Pseudomonas migulae</i>	CIP 105470					U(VI)	Merroun <i>et al.</i> (2002a)
<i>Desulfosporosinus</i> ssp.		+	anaerobe		inactive uranium mine	U(VI)	Suzuki <i>et al.</i> (2002, 2003)
<i>Bacillus subtilis</i>				variable		U(VI)	Kelly <i>et al.</i> (2002)
<i>Shewanella putrefaciens</i>	CN32		aerobe anaerobe			U(VI)	Brooks <i>et al.</i> (2003)
<i>Desulfovibrio desulfuricans</i>			anaerobe			U(VI)	Brooks <i>et al.</i> (2003)
<i>Geobacter sulfurreducens</i>			aerobe			U(VI)	Brooks <i>et al.</i> (2003)

XANES, showed that the presence of Mn(III/IV) oxides may impede the reduction of U(VI), by *S. putrefaciens* (Fredrickson *et al.*, 2002), in soils. Independent studies use U L₃ XANES to determine that *Desulfosporosinus* ssp, a Gram positive sulfate reducer, is able to reduce U(VI) to U(IV) (Suzuki *et al.*, 2002, 2003). These studies used organic substrates to create anaerobic conditions to stimulate growth of *Desulfosporosinus* ssp in natural U-contaminated sediments from the Midnight Mine, WA, USA. After 1 month, the U concentrations were reduced from 20 to 0.3 ppm. EXAFS-determined coordination numbers were used to infer an average particle size of about 1.5 nm. XAS, together with TEM data show the particles to be uraninite. The authors conclude that the small particle size of biogenic UO₂ may not significantly limit its mobility. This has important implications for the use of bacteria in environmental remediation.

A review of the standard reduction potentials listed in Table 28.1 shows that both Np(V) and Pu(VI), (V) are more easily reduced than is U(VI), suggesting that microbial reduction may play an important role in the aquatic environmental chemistry of dissolved or sorbed actinide ions. In addition, bacteria can be viewed as generating a biopotential through their surfaces and through enzymes, such as siderophores, that they excrete into their environment. In this way, bacteria compete with dissolved ions to influence the solution's effective reduction potential, or Eh. There are very few studies focused on their microbial reduction, even though Pu(VI) and (V) are both more easily reduced than Fe(III). Published work investigating Np(V) reduction by *Desulfovibrio desulfuricans* (Soderholm *et al.*, 2000) and by an anaerobic methanogenic microcosm (Banaszak *et al.*, 1999) indicate that Np(V) is reduced abiotically in the growth medium necessary to sustain the organism.

The solubility and mobility of actinide ions can also be significantly influenced by biosorption. In addition to living cells and spores, dead and decomposed cells are present in natural systems, and can play a role in complexation. Actinides can be complexed with the amino, carboxylate, hydroxyl, and phosphate functional groups that are present on the cell surface. These negatively charged groups are capable of complexation with actinide cations to form biocolloids that have their own chemistry and transport properties. EXAFS spectroscopy has been used to develop an understanding of the functional groups responsible for complexation. XAS studies of actinide biocolloid formation are largely limited to L₃-edge U data. EXAFS of biocolloids formed in brine by halophilic bacteria (WIPP 1A) indicate that bulk samples contain more than one U-containing phase (Francis *et al.*, 1998). TEM and EDS analyses supported this result, showing that U was accumulated intracellularly in addition to being bound to the cell surface. In another study (Hennig *et al.*, 2001a), Gram-positive strains of *Bacillus cereus* and *Bacillus sphaericus* were recovered from a U waste pile, the 'Haberlandhalde' in Germany. The vegetative cells and spores of these isolates were compared with cells and spores of two reference strains, *B. cereus* 4415 and *B. sphaericus* 9602. The structure of the spore coat is completely different from that of the cell wall. The studies showed that the

bacteria selectively accumulate a large variety of heavy metals, specifically these strains accumulate large amount of U. L_{3-} and L_{2-} edge XANES spectra obtained from all the bacilli samples were consistent with U(VI). The EXAFS parameters from all the samples, including both vegetative cells and spores, were very similar, indicating that a structurally similar U complex is formed in all cases. The structural parameters exclude the presence of hydrolysis species but coordination numbers and bond lengths compare well with inorganic 1:1 uranyl phosphate phases. U–P interactions at 3.61–3.63 Å in all samples, which are typical distances for monodentate-bound phosphate phases. After 8 weeks, vegetative cells of *B. sphaericus*, lysing cells, and the activity of enzymes lead to the release of $H_2PO_4^-$ that caused quantitative precipitation of bacterial U(VI) as $UO_2(H_2PO_4)_2$ (Panak *et al.*, 2002b). This complex differs significantly from those of the bacterial surface complexes. The results confirm that surface complexes are formed without metabolic activity.

Similar results were obtained from studies of U complexes formed by *Acidithiobacillus ferrooxidans* (Merroun *et al.*, 2002a), which accumulate U as phosphate compounds. EXAFS data, supported by EDX and infrared spectroscopy (Merroun *et al.*, 2002b) were used to suggest that U accumulates within extracellular polysaccharides and as dense granules in the cell cytoplasm. On the basis of these results it was suggested that these bacteria use polyphosphates to detoxify and remove U when it enters the cells and is present at toxic levels.

In order to quantitatively assess the effects of changing chemical conditions on actinide adsorption/desorption on bacterial surfaces, a surface complexation model for U complexation for Gram-positive cells has been developed (Fein *et al.*, 1997). This model treats surface complexation as a series of thermodynamic equilibria that are dependent on binding geometry and may be pH-dependent. XAS spectroscopy has been used to test this uranyl–bacterial surface speciation model (Kelly *et al.*, 2002). In general, the data are consistent with the model, although a large number of parameters were used to treat the EXAFS data.

Np(V) was determined to adsorb on the facultative, gram negative soil bacterium *Pseudomonas fluorescens* without significant reduction (Songkasiri *et al.*, 2002). The adsorption of 15–20% of the available NpO_2^+ onto the bacterial surface at pH 7 is contrary to expectations based on solution Np(V) chemistry. The situation is more complex for Pu. Sorption studies with Pu(VI) on aerobic soil bacteria showed the reduction of Pu upon complexation, as determined by optical absorption spectroscopy and solvent extraction techniques (Panak and Nitsche, 2001). Follow-up studies, employing XANES spectroscopy in conjunction with solvent extraction, showed that after 9 days of contact with *B. sphaericus*, 32(10)% of the Pu(VI) remained, whereas 28(12)% and 40(6)% were reduced to Pu(V) and Pu(IV), respectively (Panak *et al.*, 2002a). EXAFS data were used to show that Pu(VI) forms strong surface complexes with *B. sphaericus*. These complexes mainly involve phosphate groups, similar to earlier U work (Panak *et al.*, 2000). These results are consistent with a model of

the different interaction processes of Pu(VI) with aerobic soil bacteria (Panak and Nitsche, 2001). This process involves (i) the complexation of Pu(VI) with phosphate groups on the cell wall, (ii) reduction of Pu(VI) followed by the dissolution of Pu(V), and (iii) disproportionation of Pu(V) to tetravalent and hexavalent Pu, followed by the complexation of Pu(IV) with the biomass. These interactions may have important implications for the migration behavior of Pu in natural systems.

Overall, the role of bacteria on the chemistry of actinides and their impact on speciation and transport remains unclear. There is certainly evidence of actinide reduction and precipitation; it remains unclear if these small particles remain mobile through some biocolloid transportation mechanisms. In addition, the particles are so small that re-dissolution reactions may be important. The development of predictive models for the mechanisms of actinide complexation with bacterial surfaces (Fein *et al.*, 1997) and actinide redox reactions (Panak and Nitsche, 2001) are important steps toward a predictive understanding of bacterial influences on actinide mobility. XAS is playing a crucial role in the development and testing of these models.

28.4 FUTURE DIRECTION

XAS and μ -SXRF capabilities have proven to be important synchrotron tools applied to the study of actinide chemistry. The information obtained has significantly improved, and is still improving, our understanding of environmental actinide chemistry. The direction of future actinide studies is closely tied with the operation of existing synchrotrons and with the development of the so-called fourth generation facilities. The availability of new beamlines will open scientific vistas heretofore unavailable with regard to time, energy, and spatial resolution, including the study of dynamic processes and reactions with unprecedented temporal sensitivity; high-energy resolution measurements throughout the electromagnetic spectrum from the infrared through the visible, vacuum ultraviolet, and deep into the X-ray region; and microanalysis of materials on the nanometer length scale.

There are a variety of other synchrotron techniques that are currently under development and are beginning to find use for answering outstanding issues in environmental science (Fenter *et al.*, 2002). Although XAS and microprobe experiments are expected to continue playing a central role in discerning actinide speciation, several relatively new synchrotron techniques, including small-angle X-ray scattering (SAXS), high-energy X-ray scattering (HES), standing wave, and reflectivity measurements are expected to play a growing role in unraveling ever more complex problems posed by actinides in the environment.

Although it is always more convenient to conduct experiments in one's own laboratory than at a synchrotron radiation facility, conventional tube-sources

of X-rays do not provide properties, such as polarization and pulsed-time structure to name just two, that arise naturally from the continuum radiation produced at bending magnets and from the tuned radiation produced from insertion devices. Without exception, synchrotron light is a probe with which actinide science will advance in ways that would be impossible otherwise.

ACRONYMS, ABBREVIATIONS, AND SYMBOLS

An	actinide
Ar	aromatic/aryl functional group
ATCC	American-Type Culture Collection
B	empirical constant, 0.37, in Brown's BVS equation
B3LYP	hybrid Hamiltonian of Becke's 3 parameter exchange functional and correlation functional of Lee-Yang-Parr
BET	Brunauer-Emmett-Teller, adsorption method for surface area measurement
BVS	bond-valence sum
COSMO	conductor-like screening model
CPCM	conductive polarizable continuum model
CN	coordination number
DFT	density functional theory
DMRB	dissimilatory metal-reducing bacteria
DU	depleted uranium
e^-	electron
E	X-ray energy, eV
E_p	applied/controlled electrode potential, V
E°	standard electrode potential, V
$E^{\circ'}$	formal electrode potential, V
E_0	energy threshold for k -space conversion, eV
ΔE_0	energy scale parameter
Eh	redox potential
EDS	energy dispersive X-ray spectroscopy
EDX	energy dispersive X-ray analysis
EXAFS	extended X-ray absorption fine structure
F	Faraday's constant
$F(k, r)$	back-scattering amplitude function
FEFF	effective curved-wave scattering amplitude, $F_{\text{eff}}(k, r)$, computer code
FT	Fourier transform
\hbar	Planck's constant
HES	high-energy X-ray scattering
HFO	hydrrous ferric oxide

ICP-MS	inductively coupled plasma-mass spectrometry
IR	ionic radius/radii
k	photoelectron wave vector, \AA^{-1}
λ_e	photoelectron wavelength
m	electron mass
MCD	magnetic circular dichroism
MP2	2 nd order Moller Plesset perturbation theory
n	number of electrons
N	coordination number
N_p	number of independent parameters
μ -SXRF	micro synchrotron-X-ray fluorescence
μ -XANES	micro X-ray absorption near-edge structure
$\varphi(k, r)$	backscattering atom phase function
$\varphi_c(k)$	central atom phase function
pH	negative log of the hydrogen ion concentration
PCA	principal component analysis
R	aliphatic/alkyl functional group
r	interatomic distance
R	gas constant
R_0	empirical radius parameter in Brown's BVS equation
\mathfrak{R}_{ox}	oxidized form of reagent
\mathfrak{R}_{d}	reduced form of reagent
σ	Debye-Waller factor
S_0^2	amplitude reduction factor
SJV	San Joaquin Valley
SRS	Savannah River Site
SEM	scanning electron microscopy
S/N	signal to noise
SAXS	small-angle X-ray scattering
SHE	standard hydrogen electrode
SXRF	synchrotron X-ray fluorescence
T	temperature
TEM	transmission electron microscopy
WIPP	waste isolation pilot plant
XANES	X-ray absorption near-edge structure
XAS	X-ray absorption spectroscopy
$\chi(k)$	EXAFS signal

ACKNOWLEDGMENTS

This work is supported by the U.S. DOE, OBES – Chemical Sciences, under Contract W-31-109-ENG-38.

REFERENCES

- Aberg, M. (1970) *Acta Chem. Scand.*, **24**, 2901–15.
- Aberg, M., Ferri, D., Glaser, J., and Grenthe, I. (1983) *Inorg. Chem.*, **22**, 3986–9.
- Allard, T., Ildefonse, P., Beaucaire, C., and Calas, G. (1999) *Chem. Geol.*, **158**, 81–103.
- Allen, G. C., Butler, I. S., and Tuan, N. A. (1987) *J. Nucl. Mater.*, **144**, 17–19.
- Allen, P. G., Bucher, J. J., Clark, D. L., Edelstein, N. M., Ekberg, S. A., Gohdes, J. W., Hudson, E. A., Kaltsoyannis, N., Lukens, W. W., Neu, M. P., Palmer, P. D., Reich, T., Shuh, D. K., Tait, C. D., and Zwick, B. D. (1995) *Inorg. Chem.*, **34**, 4797–807.
- Allen, P. G., Shuh, D. K., Bucher, J. J., Edelstein, N. M., Reich, T., Denecke, M. A., and Nitsche, H. (1996a) *Inorg. Chem.*, **35**, 784–7.
- Allen, P. G., Veirs, D. K., Conradson, S. D., Smith, C. A., and Marsh, S. F. (1996b) *Inorg. Chem.*, **35**, 2841–5.
- Allen, P. G., Bucher, J. J., Shuh, D. K., Edelstein, N. M., and Reich, T. (1997) *Inorg. Chem.*, **36**, 4676–83.
- Allen, P. G., Bucher, J. J., Shuh, D. K., Edelstein, N. M., and Craig, I. (2000) *Inorg. Chem.*, **39**, 595–601.
- Ankudinov, A. L., Conradson, S. D., de Leon, J. M., and Rehr, J. J. (1998) *Phys. Rev. B*, **57**, 7518–25.
- Antonio, M. R., Teo, B. -K., Cleland, W. E., and Averill, B. A. (1983) *J. Am. Chem. Soc.*, **105**, 3477–84.
- Antonio, M. R., Soderholm, L., and Song, I. (1997) *J. Appl. Electrochem.*, **27**, 784–92.
- Antonio, M. R., Soderholm, L., Williams, C. W., Blaudeau, J. P., and Bursten, B. E. (2001) *Radiochim. Acta*, **89**, 17–25.
- Antonio, M. R., Williams, C. W., and Soderholm, L. (2002) *Radiochim. Acta*, **90**, 851–6.
- Archer, M. D. (1989) *ACS Symp. Ser.*, **390**, 115–26.
- Babu, C. S. Lim, C. and (1999) *J. Phys. Chem. B*, **103**, 7958–68.
- Baes, C. E. and Mesmer, R. F. (1976) *The Hydrolysis of Cations*, John Wiley, New York.
- Bailey, E. H., Mosselmans, J. F. W., and Schofield, P. F. (2004) *Geochim. Cosmochim. Acta*, **68**, 1711–22.
- Banaszak, J. E., Webb, S. M., Rittmann, B. E., Gaillard, J. F., and Reed, D. T. (1999) *Mater. Res. Soc. Symp. Proc.*, **556**, 1141–9.
- Bardin, N., Rubini, P., and Madic, C. (1998) *Radiochim. Acta*, **83**, 189–94.
- Bargar, J. R., Reitmeyer, R., and Davis, J. A. (1999a) *Environ. Sci. Technol.*, **33**, 2481–4.
- Bargar, J. R., Reitmeyer, R. L., and Davis, J. A. (1999b) *Abstr. Pap. Am. Chem. Soc.*, **217**, 143-NUCL
- Bargar, J. R., Reitmeyer, R., Lenhart, J. J., and Davis, J. A. (2000) *Geochim. Cosmochim. Acta*, **64**, 2737–49.
- Barnes, C. E., Shin, Y., Saengkerdsub, S., and Dai, S. (2000) *Inorg. Chem.*, **39**, 862–4.
- Bawson, J. K., Wait, Z., Alcock, K., and Chilton, D. R. (1956) *J. Chem. Soc.*, **1956**, 3531–40.
- Bernhard, G., Geipel, G., Brendler, V., and Nitsche, H. (1996) *Radiochim. Acta*, **74**, 87–91.
- Bernhard, G., Geipel, G., Reich, T., Brendler, V., Amayri, S., and Nitsche, H. (2001) *Radiochim. Acta*, **89**, 511–18.
- Bertagnolli, H. and Ertel, T. S. (1994) *Angew. Chem. Int. Edn. Engl.*, **33**, 45–66.

- Bertsch, P. M., Hunter, D. B., Sutton, S. R., Bajt, S., and Rivers, M. L. (1994) *Environ. Sci. Technol.*, **28**, 980–4.
- Biwer, B. M., Ebert, W. L., and Bates, J. K. (1990) *J. Nucl. Mater.*, **175**, 188–93.
- Biwer, B. M., Soderholm, L., Greggor, R. B., and Lytles, F. W. (1997) *Mater. Res. Soc. Symp. Proc.*, **465**, 229–36.
- Blaudeau, J. P., Zygmunt, S. A., Curtiss, L. A., Reed, D. T., and Bursten, B. E. (1999) *Chem. Phys. Lett.*, **310**, 347–54.
- Bleise, A., Danesi, P. R., and Burkart, W. (2003) *J. Environ. Radioact.*, **64**, 93–112.
- Bolvin, H., Wahlgren, U., Moll, H., Reich, T., Geipel, G., Fanghaenel, T., and Grenthe, I. (2001) *J. Phys. Chem. A*, **105**, 11441–5.
- Bostick, B. C. and Fendorf, S. (2002) *Soil Sci. Soc. Am. J.*, **66**, 99–108.
- Brannon, J. C., Cole, S. C., Podosek, F. A., Ragan, V. M., Coveney, R. M. J., Wallace, M. W., and Bradley, A. J. (1996) *Science*, **271**, 491–3.
- Bratsch, S. G. (1989) *J. Phys. Chem. Ref. Data*, **18**, 1–21.
- Breit, G. N. (1995) *Econ. Geol.*, **90**, 407–17.
- Bridgeman, A. J. and Cavigliasso, G. (2003) *Faraday Discuss.*, **124**, 239–58.
- Brooks, S. C., Fredrickson, J. K., Carroll, S. L., Kennedy, D. W., Zachara, J. M., Plymale, A. E., Kelly, S. D., Kemner, K. M., and Fendorf, S. (2003) *Environ. Sci. Technol.*, **37**, 1850–8.
- Brown, I. D. (1981) in *Structure and Bonding in Crystals*, vol. 2 (eds. M. O'Keeffe and A. Navrotsky), Academic Press, New York, pp. 1–52.
- Brown, I. D. (1987) *Phys. Chem. Miner.*, **15**, 30–4.
- Brown, I. D. (1996) *J. Appl. Crystallogr.*, **29**, 479–80.
- Brown, I. D. (2002) *The Chemical Bond in Inorganic Chemistry: The Bond Valence Model*, Oxford University Press, Oxford.
- Burns, J. H., Baldwin, W. H., and Stokely, J. R. (1973) *Inorg. Chem.*, **12**, 466–9.
- Burns, P. C., Ewing, R. C., and Hawthorne, F. C. (1997) *Can. Mineral.*, **35**, 1551–70.
- Calas, G., Brown, G. E. Jr, Waychunas, G. A., and Petiau, J. (1987) *Phys. Chem. Miner.*, **15**, 19–29.
- Carroll, S. A. and Bruno, J. (1991) *Radiochim. Acta*, **52–53**, 187–93.
- Carroll, S. A., Bruno, J., Petit, J. C., and Dran, J. C. (1992) *Radiochim. Acta*, **58–59**, 245–52.
- Charpin, P., Dejean, A., Folcher, G., Rigny, P., and Navaza, P. (1985) *J. Chim. Phys. Phys.-Chim. Biol.*, **82**, 925–32.
- Chiang, M.-H., Soderholm, L., and Antonio, M. R. (2003) *Eur. J. Inorg. Chem.*, 2929–36.
- Chisholm-Brause, C., Conradson, S., Eller, P. G., and Morris, D. E. (1992) *Mater. Res. Soc. Symp. Proc.*, **257**, 315–22.
- Chisholm-Brause, C., Conradson, S. D., Buscher, C. T., Eller, P. G., and Morris, D. E. (1994) *Geochim. Cosmochim. Acta*, **58**, 3625–31.
- Clark, D. L., Hobart, D. E., and Neu, M. P. (1995) *Chem. Rev.*, **95**, 25–48.
- Clark, D. L., Conradson, S. D., Ekberg, S. A., Hess, N. J., Janecky, D. R., Neu, M. P., Palmer, P. D., and Tait, C. D. (1996a) *New J. Chem.*, **20**, 211–20.
- Clark, D. L., Conradson, S. D., Ekberg, S. A., Hess, N. J., Neu, M. P., Palmer, P. D., Runde, W., and Tait, C. D. (1996b) *J. Am. Chem. Soc.*, **118**, 2089–90.
- Clark, D. L., Conradson, S. D., Neu, M. P., Palmer, P. D., Runde, W., and Tait, C. D. (1997) *J. Am. Chem. Soc.*, **119**, 5259–60.

- Clark, D. L., Conradson, S. D., Keogh, D. W., Palmer, P. D., Scott, B. L., and Tait, C. D. (1998) *Inorg. Chem.*, **37**, 2893–9.
- Clark, D. L., Conradson, S. D., Donohoe, R. J., Keogh, D. W., Morris, D. E., Palmer, P. D., Rogers, R. D., and Tait, C. D. (1999) *Inorg. Chem.*, **38**, 1456–66.
- Coda, A., Giusta, A. D., and Tazzoli, V. (1981) *Acta Crystallogr. B*, **37**, 1496–500.
- Cohen, D. and Hindman, J. C. (1952) *J. Am. Chem. Soc.*, **74**, 4679–82.
- Combes, J. M., Chisholm-Brause, C. J., Brown, G. E. Jr, Parks, G. A., Conradson, S. D., Eller, P. G., Triay, I. R., Hobart, D. E., and Miejer, A. (1992) *Environ. Sci. Technol.*, **26**, 376–82.
- Comodi, P., Liu, Y., Zanazzi, P. F., and Montagnoli, M. (2001) *Phys. Chem. Miner.*, **28**, 219–24.
- Conradson, S. D. (1998) *Appl. Spectrosc.*, **52**, 252A–79A.
- Conradson, S. D., Al Mahamid, I., Clark, D. L., Hess, N. J., Hudson, E. A., Neu, M. P., Palmer, P. D., Runde, W. H., and Tait, C. D. (1998) *Polyhedron*, **17**, 599–602.
- Conradson, S. D., Begg, B. D., Clark, D. L., Den Auwer, C., Espinosa-Faller, F. J., Gordon, P. L., Hess, N. J., Hess, R., Keogh, D. W., Morales, L. A., Neu, M. P., Runde, W., Tait, C. D., Veirs, D. K., and Vilella, P. M. (2003) *Inorg. Chem.*, **42**, 3715–17.
- Conradson, S. D., Abney, K. D., Begg, B. D., Brady, E. D., Clark, D. L., Den Auwer, C., Ding, M., Dorhout, P. K., Espinosa-Faller, F. J., Gordon, P. L., Haire, R. G., Hess, N. J., Hess, R. F., Keogh, D. W., Lander, G. H., Lupinetti, A. J., Morales, L. A., Neu, M. P., Palmer, P. D., Paviet-Hartmann, P., Reilly, S. D., Runde, W. H., Tait, C. D., Veirs, D. K., and Wastin, F. (2004) *Inorg. Chem.*, **43**, 116–31.
- Cossy, C., Helm, L., Powell, D. H., and Merbach, A. E. (1995) *New J. Chem.*, **19**, 27–35.
- Cotton, F. A., Wilkinson, G., Murillo, C., and Bochmann, M. (1999) *Advanced Inorganic Chemistry*, John Wiley, New York.
- Daehn, R., Scheidegger, A. M., Manceau, A., Curti, E., Baeyens, B., Bradbury, M. H., and Chateigner, D. (2002) *J. Colloid Interface Sci.*, **249**, 8–21.
- Dal Negro, A. and Ungaretti, L. (1971) *Am. Mineral.*, **56**, 768–72.
- Danesi, P. R., Markowicz, A., Chinea-Cano, E., Burkart, W., Salbu, B., Donohue, D., Ruedenauer, F., Hedberg, M., Vogt, S., Zahradnik, P., and Ciurapinski, A. (2003) *J. Environ. Radioact.*, **64**, 143–54.
- David, F., Revel, R., Fourest, B., Hubert, S., Le Du, J. F., Den Auwer, C., Madic, C., Morss, L. R., Ionova, G., Mikhalko, V., Vokhmin, V., Nikonov, M., Berthet, J. C., and Ephritikhine, M. (1998) in *Speciation, Techniques and Facilities for Radioactive Materials at Synchrotron Light Sources*, Nuclear Energy Agency: Organisation for Economic Co-Operation and Development, Grenoble, France, pp. 95–100.
- David, F. H. and Vokhmin, V. (2003) *New J. Chem.*, **27**, 1627–32.
- de Leon, J. M., Rehr, J. J., Zabinsky, S. I., and Albers, R. C. (1991) *Phys. Rev.*, **B44**, 4146–56.
- de Villiers, J. P. R. (1971) *Am. Mineral.*, **56**, 758–66.
- Deer, W. A., Howie, R. A., and Zussman, J. (1992) *The Rock Forming Minerals*, Longman Scientific and Technical, Hong Kong.
- Den Auwer, C., Grégoire-Kappenstein, A. C., and Moisy, P. (2003a) *Radiochim. Acta*, **91**, 773–6.
- Den Auwer, C., Simoni, E., Conradson, S., and Madic, C. (2003b) *Eur. J. Inorg. Chem.*, 3843–59.

- Denecke, M. A., Pompe, S., Reich, T., Moll, H., Bubner, M., Heise, K. H., Nicolai, R., and Nitsche, H. (1997a) *Radiochim. Acta*, **79**, 151–9.
- Denecke, M. A., Reich, T., Pompe, S., Bubner, M., Heise, K. H., Nitsche, H., Allen, P. G., Bucher, J. J., Edelstein, N. M., and Shuh, D. K. (1997b) *J. Phys. IV*, **7**, 637–8.
- Denecke, M. A., Reich, T., Bubner, M., Pompe, S., Heise, K. H., Nitsche, H., Allen, P. G., Bucher, J. J., Edelstein, N. M., and Shuh, D. K. (1998a) *J. Alloy. Compd.*, **271**, 123–7.
- Denecke, M. A., Reich, T., Pompe, S., Bubner, M., Heise, K. H., Nitsche, H., Allen, P. G., Bucher, J. J., Edelstein, N. M., Shuh, D. K., and Czerwinski, K. R. (1998b) *Radiochim. Acta*, **82**, 103–8.
- Denecke, M. A., Bublitz, D., Kim, J. I., Moll, H., and Farkes, I. (1999) *J. Synchrotron. Radiat.*, **6**, 394–6.
- Denecke, M. A., Marquardt, C. M., Rothe, J., Dardenne, K., and Jensen, M. P. (2002) *J. Nucl. Sci. Technol.*, **Suppl. 3**, 410–13.
- Denecke, M. A., Rothe, J., Dardenne, K., and Lindqvist-Reis, P. (2003) *Phys. Chem. Chem. Phys.*, **5**, 939–46.
- Dent, A. J., Ramsay, J. D. F., and Swanton, S. W. (1992) *J. Colloid Interface Sci.*, **150**, 45–60.
- Djogic, R. and Branica, M. (1991) *Mar. Chem.*, **36**, 121–35.
- Docrat, T. I., Mosselmans, J. F. W., Charnock, J. M., Whiteley, M. W., Collison, D., Livens, F. R., Jones, C., and Edmiston, M. J. (1999) *Inorg. Chem.*, **38**, 1879–82.
- Dodge, C. J. and Francis, A. J. (1997) *Environ. Sci. Technol.*, **31**, 3062–7.
- Dodge, C. J. and Francis, A. J. (2003) *Radiochim. Acta*, **91**, 525–32.
- Duff, M. C. and Amrhein, C. (1996) *Soil Sci. Soc. Am. J.*, **60**, 1393–400.
- Duff, M. C., Amrhein, C., Bertsch, P. M., and Hunter, D. B. (1997) *Geochim. Cosmochim. Acta*, **61**, 73–81.
- Duff, M. C., Hunter, D. B., Triay, I. R., Bertsch, P. M., Reed, D. T., Sutton, S. R., Shear-Mccarthy, G., Kitten, J., Eng, P., Chipera, S. J., and Vaniman, D. T. (1999a) *Environ. Sci. Technol.*, **33**, 2163–9.
- Duff, M. C., Newville, M., Hunter, D. B., Bertsch, P. M., Sutton, S. R., Triay, I. R., Vaniman, D. T., Eng, P., and Rivers, M. L. (1999b) *J. Synchrotron. Radiat.*, **6**, 350–2.
- Duff, M. C., Morris, D. E., Hunter, D. B., and Bertsch, P. M. (2000) *Geochim. Cosmochim. Acta*, **64**, 1535–50.
- Duff, M. C., Hunter, D. B., Triay, I. R., Bertsch, P. M., Kitten, J., and Vaniman, D. T. (2001) *J. Contam. Hydrol.*, **47**, 211–18.
- Duff, M. C., Coughlin, J. U., and Hunter, D. B. (2002) *Geochim. Cosmochim. Acta*, **66**, 3533–47.
- Effenberger, H., Mereiter, K., and Zemmann, H. (1981) *Z. Kristallogr.*, **156**, 233–43.
- Efurd, D. W., Runde, W., Banar, J. C., Janecky, D. R., Kaszuba, J. P., Palmer, P. D., Roensch, F. R., and Tait, C. D. (1998) *Environ. Sci. Technol.*, **32**, 3893–900.
- Egami, T. and Aur, S. (1987) *J. Non-Cryst. Solids*, **89**, 60–74.
- Eller, P. G., Jarvinen, G. D., Purson, J. D., Penneman, R. A., Ryan, R. R., Lytle, F. W., and Gregor, R. B. (1985) *Radiochim. Acta*, **39**, 17–22.
- Elless, M. P. and Lee, S.-Y. (1994) *Physicochemical and Mineralogical Characterization of Transuranic Contaminated Soils for Uranium Soil Integrated Demonstration*, ORNL/TM-12848, Oak Ridge National Laboratory, Oak Ridge, TN.
- Evans, H. T. Jr (1963) *Science*, **141**, 154–8.

- Fahey, J. A. (1986) in *The Chemistry of the Actinide Elements*, vol. 1 (eds. J. J. Katz, G. T. Seaborg, and L. R. Morss), Chapman & Hall, London, pp. 443–98.
- Farges, F. (1991) *Geochim. Cosmochim. Acta*, **55**, 3303–19.
- Farley, N. R. S., Gurman, S. J., and Hillman, A. R. (1999) *Electrochem. Commun.*, **1**, 449–52.
- Fein, J. B., Daughney, C. J., Yee, N., and Davis, T. A. (1997) *Geochim. Cosmochim. Acta*, **61**, 3319–28.
- Felmy, A. R., Rai, D., Sterner, S. M., Mason, N. J., Hess, N. J., and Conradson, S. D. (1997) *J. Solution Chem.*, **26**, 233–48.
- Fenter, P. A., Rivers, M. L., Sturchio, N. C., and Sutton, S. R. (eds.) (2002) *Applications of Synchrotron Radiation in Low-Temperature Geochemistry and Environmental Science*, Reviews in Mineralogy and Geochemistry, Mineralogical Society of America, Washington DC.
- Fetter, S. and von Hippel, F. N. (1999) *Sci. Globe Security*, **8**, 125–61.
- Filipponi, A. (2001) *J. Phys.: Condens. Matter*, **13**, R23–R60.
- Fourest, B., Morss, L. R., Blain, G., David, F., and M'Halla, J. (1995) *Radiochim. Acta*, **69**, 215–19.
- Francis, A. J., Dodge, C. J., Lu, F. L., Halada, G. P., and Clayton, C. R. (1994) *Environ. Sci. Technol.*, **28**, 636–9.
- Francis, A. J., Gillow, J. B., Dodge, C. J., Dunn, M., Mantione, K., Strietelmeier, B. A., Pansoy-Hjelvik, M. E., and Papenguth, H. W. (1998) *Radiochim. Acta*, **82**, 347–54.
- Francis, A. J., Dodge, C. J., Gillow, J. B., and Papenguth, H. W. (2000) *Environ. Sci. Technol.*, **34**, 2311–17.
- Francis, A. J. (2002) in *Uranium in the Aquatic Environment* (eds. B. J. Merkel, B. Planer-Friedrich, and C. Wolkersdorfer), Springer-Verlag, Berlin, pp. 451–8.
- Francis, A. J., Joshi-Tope, G. A., and Dodge, C. J., Gillow, J. B. (2002) *J. Nucl. Sci. Technol.*, **Suppl. 3**, 935–8.
- Fredrickson, J. K., Zachara, J. M., Kennedy, D. W., Duff, M. C., Gorby, Y. A., Li, S.-M. W., and Krupka, K. M. (2000) *Geochim. Cosmochim. Acta*, **64**, 3085–98.
- Fredrickson, J. K., Zachara, J. M., Kennedy, D. W., Liu, C., Duff, M. C., Hunter, D. B., and Dohnalkova, A. (2002) *Geochim. Cosmochim. Acta*, **66**, 3247–62.
- Fuller, C. C., Bargar, J. R., Davis, J. A., and Piana, M. J. (2002) *Environ. Sci. Technol.*, **36**, 158–65.
- Gale, R. J. (ed.) (1988) *Spectroelectrochemistry: Theory and Practice*, Plenum Press, New York.
- Garnov, A. Y., Krot, N. N., Bessonov, A. A., and Perminov, V. P. (1996) *Radiochem., Engl. Transl.*, **38**, 402–6.
- Geipel, G., Reich, T., Brendler, V., Bernhard, G., and Nitsche, H. (1997) *J. Nucl. Mater.*, **248**, 408–11.
- Giaquinta, D. M., Soderholm, L., Yuchs, S. E., and Wasserman, S. R. (1997a) *J. Alloys. Compd.*, **249**, 142–5.
- Giaquinta, D. M., Soderholm, L., Yuchs, S. E., and Wasserman, S. R. (1997b) *Radiochim. Acta*, **76**, 113–21.
- Gillow, J. B., Francis, A. J., Dodge, C. J., Harris, R., Beveridge, T. J., Brady, P. V., and Papenguth, H. W. (1999) *Mater. Res. Soc. Symp. Proc.*, **556**, 1133–40.
- Giordano, T. H. (1994) in *Organic Acids in Geological Processes* (eds. E. D. Pittman and M. D. Lewan), Springer-Verlag, Berlin, pp. 319–54.

- Glebov, V. A., Nikitina, T. M., and Tikhonov, M. R. (1977) *Sov. Radiochem., Engl. Transl.* **19**, 231–2.
- Gorby, Y. A. and Lovley, D. R. (1992) *Environ. Sci. Technol.*, **26**, 205–7.
- Görller-Walrand, C. and Colen, W. (1982) *Chem. Phys. Lett.*, **93**, 82–5.
- Goulon, J., Goulon-Ginet, C., Friant, P., Poncet, J. L., Guillard, R., and Battioni, J. P., Mansuy, D. (1983) *Proc. 4th Int. Conf. on Organic Chemistry of Selenium and Tellurium*, Birmingham, England, 1983: pp. 379–90.
- Greathouse, J. A., O'Brian, R. J., Bemis, G., and Pabalan, R. T. (2002) *J. Phys. Chem. B*, **106**, 1546–655.
- Greaves, G. N., Barrett, N. T., Antonini, G. M., Thronley, F. R., Willis, B. T. M., and Steel, A. (1989) *J. Amer. Chem. Soc.*, **111**, 4313–20.
- Gregor, R. B., Pingitore, N. E. Jr., and Lytle, F. W. (1997) *Science*, **275**, 1452–5.
- Guilbaud, P. and Wipff, G. (1993) *J. Phys. Chem.*, **97**, 5685–92.
- Habenschuss, A. and Spedding, F. H. (1980) *J. Chem. Phys.*, **73**, 442–50.
- Hanchar, J. M. (1999) in *Uranium: Mineralogy, Geochemistry and the Environment*, vol. 38 (eds. P. C. Burns and R. Finch), Mineralogical Society of America, Washington DC, pp. 500–19.
- Haschke, J. M., Allen, T. H., and Morales, L. A. (2000) *Science* **287**, 285–7.
- Haschke, J. M., Allen, T. H., and Morales, L. A. (2001) *J. Alloys Compd.*, **314**, 78–91.
- Haschke, J. M. and Allen, T. H. (2002) *J. Alloys Compd.*, **336**, 124–31.
- Haschke, J. M. and Oversby, V. M. (2002) *J. Nucl. Mater.*, **305**, 187–201.
- Hay, P. J., Martin, R. L., and Schreckenbach, G. (2000) *J. Phys. Chem. A*, **104**, 6259–70.
- Hem, J. D. (1985) Study and Interpretation of the Chemical Characteristics of Natural Water, U.S. Geological Survey Water Supply Paper 2254, U.S. Geological Survey.
- Hennig, C., Panak, P. J., Reich, T., Rossberg, A., Raff, J., Selenska-Pobell, S., Matz, W., Bucher, J. J., Bernhard, G., and Nitsche, H. (2001a) *Radiochim. Acta*, **89**, 625–31.
- Hennig, C., Reich, T., Funke, H., Rossberg, A., Rutsch, M., and Bernhard, G. (2001b) *J. Synchrotron. Radiat.*, **8**, 695–7.
- Hennig, C., Reich, T., Daehn, R., and Scheidegger, A. M. (2002) *Radiochim. Acta*, **90**, 653–7.
- Hess, N. J., Felmy, A. R., Rai, D., and Conradson, S. D. (1997) *Mater. Res. Soc. Symp. Proc.*, **465**, 729–34.
- Hess, N. J., Weber, W. J., and Conradson, S. (1998) *J. Alloys Compd.*, **271–273**, 240–3.
- Ho, C. H. and Doern, D. C. (1985) *Can. J. Chem.*, **63**, 1100–4.
- Hoekstra, H. and Siegel, S. (1964) *J. Inorg. Nucl. Chem.*, **26**, 693–700.
- Hsi, C. K. D. and Langmuir, D. (1985) *Geochim. Cosmochim. Acta*, **49**, 1931–41.
- Hudson, E. A., Rehr, J. J., and Bucher, J. J. (1995a) *Phys. Rev. B*, **52**, 13815–26.
- Hudson, E. A., Terminello, L. J., Viani, B. E., Reich, T., Bucher, J. J., Shuh, D. K., and Edelstein, N. M. (1995b) *Mater. Res. Soc. Symp. Proc.*, **375**, 235–40.
- Hudson, E. A., Allen, P. G., Terminello, L. J., Denecke, M. A., and Reich, T. (1996) *Phys. Rev. B*, **54**, 156–65.
- Hudson, E. A., Terminello, L. J., Viani, B. E., Denecke, M., Reich, T., Allen, P. G., Bucher, J. J., Shuh, D. K., and Edelstein, N. M. (1999) *Clays Clay Miner.*, **47**, 439–57.
- Hunter, D. B. and Bertsch, P. M. (1998) *J. Radioanal. Nucl. Chem.*, **234**, 237–42.

- Hursthouse, A. S., Baxter, M. S., Livens, F. R., and Duncan, H. J. (1991) *J. Environ. Radioact.*, **14**, 147–74.
- Igo, D. H., Elder, R. C., Heineman, W. R., and Dewald, H. D. (1991) *Anal. Chem.*, **63**, 2535–9.
- Jenne, E. A. (1977) in *Molybdenum in the Environment* (eds. W. Chappel and K. Peterson), Marcel Dekker, New York, pp. 425–553.
- Jiang, J., Rao, L., Bernardo, P. D., Zanonato, P., and Bismondo, A. (2002) *J. Chem. Soc., Dalton Trans.*, 1832–8.
- Joergensen, C. K. (1977) *Rev. Chim. Miner.*, **14**, 127–38.
- Johansson, G. and Wakita, H. (1985) *Inorg. Chem.*, **24**, 3047–52.
- Johansson, G., Magini, M., and Ohtaki, H. (1991) *J. Solution Chem.*, **20**, 775–92.
- Karim, D. P., Georgopoulos, P., and Knapp, G. S. (1980) *Nucl. Technol.*, **51**, 162–8.
- Kaszuba, J. P. and Runde, W. H. (1999) *Environ. Sci. Technol.*, **33**, 4427–33.
- Keeney-Kennicutt, W. L. and Morse, J. W. (1985) *Geochim. Cosmochim. Acta*, **49**, 2577–88.
- Kelly, S. D., Kemner, K. M., Fein, J. B., Fowle, D. A., Boyanov, M. I., Bunker, B. A., and Yee, N. (2002) *Geochim. Cosmochim. Acta*, **66**, 3855–71.
- Kelly, S. D., Newville, M. G., Cheng, L., Kemner, K. M., Sutton, S. R., Fenter, P., Sturchio, N. C., and Spoetl, C. (2003) *Environ. Sci. Technol.*, **37**, 1284–7.
- Kitano, Y. and Oomori, T. J. (1971) *J. Oceanogr. Soc. Jpn.*, **27**, 34–42.
- Koningsberger, D. C. and Prins, R. (1988) *X-Ray Absorption: Principles, Applications, Techniques of EXAFS, SEXAFS, and XANES*, John Wiley, New York.
- Krot, N. N. and Gelman, A. D. (1967) *Dokl. Akad. Nauk. SSSR, Engl. Transl.*, **177**, 124–6.
- Ku, T.-L., Knauss, K. G., and Mathieu, G. G. (1977) *Deep-Sea Res.*, **24**, 1005–17.
- Langmuir, D. (1978) *Geochim. Cosmochim. Acta*, **42**, 547–69.
- Latrous, H. and Oliver, J. (1999) *J. Mol. Liq.*, **81**, 115–21.
- Leciejewicz, J., Alcock, N. W., and Kemp, T. J. (1995) *Struct. Bond.*, **82**, 43–84.
- Lee, P. A., Citrin, P. H., Eisenberger, P., and Kincaid, B. M. (1981) *Rev. Mod. Phys.*, **53**, 769–806.
- Li, Y., Kato, Y., and Yoshida, Z. (1993) *Radiochim. Acta*, **60**, 115–19.
- Lieser, K. H. (1995) *Radiochim. Acta*, **70–71**, 355–75.
- Locock, A. J. and Burns, P. C. unpublished data.
- Lovley, D. R., Phillips, E. J. P., Gorby, Y. A., and Landa, E. R. (1991) *Nature*, **350**, 413–16.
- Lytle, F. W. (1999) *J. Synchrotron. Radiat.*, **6**, 123–34.
- Manceau, A., Charlet, L., Boisset, M. C., Didier, B., and Spadini, L. (1992) *Appl. Clay Sci.*, **7**, 201–23.
- Martens, G., Rabe, P., and Wenck, P. (1985) *Phys. Status Solidi A: Appl. Res.*, **88**, 103–11.
- Mashirov, L. G., Suglobov, D. N., and Shcherbakov, V. A. (1975) *Sov. Radiochem., Engl. Transl.*, **17**, 768–70.
- Mauerhofer, E., Zhernosekov, K., and Rösch, F. (2004) *Radiochim. Acta*, **92**, 5–10.
- Maya, L. (1982) *Radiochim. Acta*, **31**, 147–51.
- Meece, D. E. and Benninger, I. K. (1993) *Geochim. Cosmochim. Acta*, **57**, 1447–58.
- Merroun, M., Hennig, C., Rossberg, A., Geipel, G., Reich, T., and Selenska-Pobell, S. (2002a) *Biochem. Soc. Trans.*, **30**, 669–72.

- Merroun, M., Hennig, C., Rossberg, A., Reich, T., Nicolai, R., Heise, K. H., and Selenska-Pobell, S. (2002b) in *Uranium in the Aquatic Environment* (eds. B. J. Merkel, B. Planer-Friedrich, and C. Wolkersdorfer), Springer-Verlag, Berlin, pp. 509–15.
- Michard, P., Guibal, E., Vincent, T., and Le Cloirec, P. (1996) *Microporous Mater.*, **5**, 309–24.
- Moll, H., Farkas, I., Jalilehvand, F., Sandström, M., Szabó, Z., Grenthe, I., Denecke, M. A., and Wahlgren, U. (1998) in *Speciation, Techniques and Facilities for Radioactive Materials at Synchrotron Light Sources*, Organisation for Economic Co-Operation and Development, Nuclear Energy Agency, Grenoble, France: pp. 261–8.
- Moll, H., Denecke, M. A., Jalilehvand, F., Sandstrom, M., and Grenthe, I. (1999) *Inorg. Chem.*, **38**, 1795–9.
- Moll, H., Reich, T., Hennig, C., Rossberg, A., Szabo, Z., and Grenthe, I. (2000a) *Radiochim. Acta*, **88**, 559–66.
- Moll, H., Reich, T., and Szabo, Z. (2000b) *Radiochim. Acta*, **88**, 411–15.
- Moll, H., Geipel, G., Reich, T., Bernhard, G., Fanghänel, T., and Grenthe, I. (2003) *Radiochim. Acta*, **91**, 11–20.
- Morris, D. E., Allen, P. G., Berg, J. M., Chisholm-Brause, C., Conradson, S., Donohoe, R. J., Hess, N. J., Musgrave, J. A., and Tait, C. D. (1996) *Environ. Sci. Technol.*, **30**, 2322–31.
- Morris, D. E. (2002) *Inorg. Chem.*, **41**, 3542–7.
- Morss, L. R. (1994) in *Handbook on the Physics and Chemistry of Rare Earths*, vol. 18 (eds. K. A. Gschneidner Jr, L. Eyring, G. R. Choppin, and G. H. Lander), Elsevier Science, Amsterdam, pp. 239–91.
- Mosselmans, J. F., Bailey, E., and Schofield, P. (2001) *J. Synchrotron Radiat.*, **8**, 660–2.
- Moyes, L. N., Parkman, R. H., Charnock, J. M., Vaughan, D. J., Livens, F. R., Hughes, C. R., and Braithwaite, A. (2000) *Environ. Sci. Technol.*, **34**, 1062–8.
- Moyes, L. N., Jones, M. J., Reed, W. A., Livens, F. R., Charnock, J. M., Mosselmans, J. F. W., Hennig, C., Vaughan, D. J., and Patrick, R. A. D. (2002) *Environ. Sci. Technol.*, **36**, 179–83.
- Musikas, C. and Narten, A. H. (1978) *Inorg. Nucl. Chem. Lett.*, **14**, 283–5.
- Nace, R. L. (1967) *Are We Running Out of Water?*, U.S. Geological Survey Circular 536.
- Nagy, B., Gauthier-Lafaye, F., Holliger, P., Davis, D. W., Mossman, D. J., Leventhal, J. S., Rigali, M. J. and Parnell, J. (1991) *Nature*, **354**, 472–4.
- Neck, V. and Kim, J. I. (2001) *Radiochim. Acta*, **89**, 1–16.
- Neck, V., Müller, R., Bouby, M., Altmaier, M., Rothe, J., Denecke, M. A., and Kim, J. I. (2002) *Radiochim. Acta*, **90**, 485–94.
- Neilson, G. W., Schioberg, D., and Luck, W. A. P. (1985) *Chem. Phys. Lett.*, **122**, 475–9.
- Newville, M., Sutton, S., Rivers, M., and Eng, P. (1999) *J. Synchrotron. Radiat.*, **6**, 353–5.
- Nitsche, H. (1997) in *The Robert A. Welch Foundation*, Proc. 41st Conf. on Chemical Research. The Transactinide Elements, Robert A. Welch Foundation, Houston, TX, ch. 5.
- Nitsche, H., Silva, R. J., Brendler, V., Geipel, G., Reich, T., Teterin, Y. A., Thieme, M., Baraniak, L., and Bernhard, G. (1999) in *Actinide Speciation in High Ionic Strength Media* (eds. D. T. Reed, S. B. Clark, and L. Rao), Kluwer Academic Publishers, New York, pp. 11–38.

- Oesthols, E. (1995) *Geochim. Cosmochim. Acta*, **59**, 1235–49.
- Oesthols, E., Manceau, A., Farges, F., and Charlett, L. (1997) *J. Colloid Interface Sci.*, **194**, 12–21.
- O'Loughlin, E. J., Kelly, S. D., Cook, R. E., Csencsits, R., and Kemner, K. M. (2003) *Environ. Sci. Technol.*, **37**, 721–7.
- Ordenez-Regil, E., Drot, R., Simoni, E., and Ehrhardt, J. J. (2002) *Langmuir*, **18**, 7977–84.
- Paciolla, M. D., Davies, G., and Jansen, S. A. (1999) *Environ. Sci. Technol.*, **33**, 1814–18.
- Palacios, M. L. and Taylor, S. H. (2000) *Appl. Spectrosc.*, **54**, 1372–8.
- Panak, P. J., Raff, J., Selenska-Pobell, S., Geipel, G., Bernhard, G., and Nitsche, H. (2000) *Radiochim. Acta*, **88**, 71–6.
- Panak, P. J. and Nitsche, H. (2001) *Radiochim. Acta*, **89**, 499–504.
- Panak, P. J., Booth, C. H., Caulder, D. L., Bucher, J. J., Shuh, D. K., and Nitsche, H. (2002a) *Radiochim. Acta*, **90**, 315–21.
- Panak, P. J., Knopp, R., Booth, C. H., and Nitsche, H. (2002b) *Radiochim. Acta*, **90**, 779–83.
- Pauling, L. (1929) *J. Am. Chem. Soc.*, **51**, 1010–26.
- Pingitore, N. E. Jr., Iglesias, A., Lytle, F., and Wellington, G. M. (2002) *Microchem. J.*, **71**, 261–6.
- Pittman, E. D. and Lewan, M. D. (eds) (1994) *Organic Acids in Geological Processes*, Springer-Verlag, Berlin.
- Pocov, S. and Johansson, G. (1973) *Acta Chem. Scand.*, **27**, 2146–60.
- Pompe, S., Bubner, M., Denecke, M. A., Reich, T., Brachmann, A., Geipel, G., Nicolai, R., Heise, K. H., and Nitsche, H. (1996) *Radiochim. Acta*, **74**, 135–40.
- Pourbaix, M. (1974) *Atlas of Electrochemical Equilibria in Aqueous Solutions*, Cebelcor, Brussels.
- Priest, N. D. (2001) *Lancet*, **357**, 244–6.
- Quinn, B. M., Ding, Z., Moulton, R., and Bard, A. J. (2002) *Langmuir*, **18**, 1734–42.
- Rai, D., Felmy, A. R., Hess, N. J., Moore, D. A., and Yui, M. (1998) *Radiochim. Acta*, **82**, 17–25.
- Rai, D., Hess, N. J., Felmy, A. R., Moore, D. A., and Yui, M. (1999a) *Radiochim. Acta*, **84**, 159–69.
- Rai, D., Hess, N. J., Felmy, A. R., Moore, D. A., Yui, M., and Vitorge, P. (1999b) *Radiochim. Acta*, **86**, 89–99.
- Rakovan, J., Newville, M., and Sutton, S. (2001) *Am. Mineral.*, **86**, 697–700.
- Rakovan, J., Reeder, R. J., Elzinga, E. J., Cherniak, D. J., Tait, C. D., and Morris, D. E. (2002) *Environ. Sci. Technol.*, **36**, 3114–17.
- Rao, L., Jiang, D. L., Zanonato, P., Di Bernardo, P., Bismondo, A., and Garnov, A. Y. (2002) *Radiochim. Acta*, **90**, 581–8.
- Reddon, G., Bargar, J. R., and Bencheikh-Latmani, R. (2001) *J. Colloid. Interface Sci.*, **244**, 211–19.
- Reeder, R. J. (1983) in *Reviews of Mineralogy*, vol. 23 (ed. R. J. Reeder), Mineralogical Society of America, Washington DC, pp. 1–47.
- Reeder, R. J., Nugent, M., Lamble, G. M., Tait, C. D., and Morris, D. E. (2000) *Environ. Sci. Technol.*, **34**, 638–44.

- Reeder, R. J., Nugent, M., Tait, C. D., Morris, D. E., Heald, S. M., Beck, K. M., and Hess, W. P. (2001) *Geochim. Cosmochim. Acta*, **65**, 3491–503.
- Rehr, J. J., de Leon, J. M., Zabinsky, S. I., and Albers, R. C. (1991) *J. Am. Chem. Soc.*, **113**, 5135–40.
- Rehr, J. J., Albers, R. C., and Zabinsky, S. I. (1992) *Phys. Rev. Lett.*, **69**, 3397–400.
- Rehr, J. J. and Albers, R. C. (2000) *Rev. Mod. Phys.*, **72**, 621–54.
- Reich, T., Denecke, M. A., Pompe, S., Bubner, M., Heise, K.-H., Schmidt, M., Brendler, V., Baraniak, L., Nitsche, H., Allen, P. G., Bucher, J. J., Edelstein, N. M., and Shuh, D. K. (1996a) in *Synchrotron Radiation Techniques in Industrial, Chemical, and Materials Science* (eds. K. L. D'Amico, L. J. Terminello, and D. K. Shuh), Plenum Press, New York, pp. 215–28.
- Reich, T., Moll, H., Denecke, M. A., Geipel, G., Bernhard, G., Nitsche, H., Allen, P. G., Bucher, J. J., Kaltsoyannis, N., Edelstein, N. M., and Shuh, D. K. (1996b) *Radiochim. Acta*, **74**, 219–23.
- Reich, T., Hudson, E. A., Denecke, M. A., Allen, P. G., and Nitsche, H. (1998a) *Poverkhnost (4–5)*, 1997, pp 149–57 **13**, 557–68.
- Reich, T., Moll, H., Arnold, T., Denecke, M. A., Hennig, C., Geipel, G., Bernhard, G., Nitsche, H., Allen, P. G., Bucher, J. J., Edelstein, N. M., and Shuh, D. K. (1998b) *J. Electron Spectrosc. Relat. Phenom.*, **96**, 237–43.
- Reich, T., Bernhard, G., Geipel, G., Funke, H., Hennig, C., Rossberg, A., Matz, W., Schell, N., and Nitsche, H. (2000) *Radiochim. Acta*, **88**, 633–7.
- Revel, R., Den Auwer, C., Madic, C., David, F., Fourest, B., Hubert, S., Le Du, J. F., and Morss, L. R. (1999) *Inorg. Chem.*, **38**, 4139–41.
- Riglet, C., Robouch, P., and Vitorge, P. (1989) *Radiochim. Acta*, **46**, 85–94.
- Roehler, J. (1992) in *Lattice Effects in High-Tc Superconductors: Proceedings of the Conference: Santa Fe, New Mexico, January 13–15, 1992* (eds. Y. Bar-Yam, T. Egami, J. Mustre-de Leon, and A. R. Bishop) World Scientific, Singapore, pp. 77–83.
- Rossberg, A., Baraniak, L., Reich, T., Hennig, C., Bernhard, G., and Nitsche, H. (2000) *Radiochim. Acta*, **88**, 593–7.
- Rossberg, A., Reich, T., and Bernhard, G. (2003) *Anal. Bioanal. Chem.*, **376**, 631–8.
- Rothe, J., Denecke, M. A., Neck, V., Mueller, R., and Kim, J. I. (2002) *Inorg. Chem.*, **41**, 249–58.
- Runde, W., Neu, M. P., Conradson, S. D., Clark, D. L., Palmer, P. D., Reilly, S. D., Scott, B. L., and Tait, C. D. (1997) *Mater. Res. Soc. Symp. Proc.*, **465**, 693–703.
- Runde, W., Neu, M. P., and Reilly, S. D. (1999) in *Actinide Speciation in High Ionic Strength Media* (eds. D.T. Reed, S. B. Clark, and L. Rao), Kluwer Academic Publishers, New York, pp. 141–51.
- Russell, A. D., Emerson, S., Nelson, B. K., Erez, J., and Lea, D. W. (1994) *Geochim. Cosmochim. Acta*, **58**, 671–81.
- Rykov, A. G., Andreichuk, N. N., and Vasil'ev, V. Y. (1973) *Sov. Radiochem., Engl. Transl.*, **15**, 350–5.
- Sanchez, A. L., Murray, J. W., and Silbley, T. H. (1985) *Geochim. Cosmochim. Acta*, **49**, 2297–307.
- Sayers, D. E., Stern, E. A., and Lytle, F. W. (1971) *Phys. Rev. Lett.*, **27**, 1204–7.
- Schmeide, K., Sachs, S., Bubner, M., Reich, T., Heise, K. H., and Bernhard, G. (2003) *Inorg. Chim. Acta*, **351**, 133–40.

- Schofield, P. F., Bailey, E. H., and Mosselmans, J. F. W. (1999) in *Geochemistry of the Earth's Surface* (ed. H. Armannsson), Proc. 5th Int. Symp. on Geochemistry of the Earth's Surface Balkema, Rotterdam, pp. 465–8.
- Schreckenbach, G., Hay, P. J., and Martin, R. L. (1998) *Inorg. Chem.*, **37**, 4442–51.
- Sémon, L., Boehme, C., Billard, I., Hennig, C., Lutzenkirchen, K., Reich, T., Rossberg, A., Rossini, I., and Wipff, G. (2001) *Chem. Phys. Chem.*, **2**, 591–8.
- Shannon, R. D. (1976) *Acta Crystallogr.*, **A32**, 751–67.
- Sharpe, L. R., Heineman, W. R., and Elder, R. C. (1990) *Chem. Rev.*, **90**, 705–22.
- Shaughnessy, D. A., Nitsche, H., Booth, C. H., Shuh, D. K., Waychunas, G. A., Wilson, R. E., Gill, H., Cantrell, K. J., and Serne, R. J. (2003) *Environ. Sci. Technol.*, **37**.
- Shcherbakov, V. A., Iorga, E. V., and Mashirov, L. G. (1974) *Sov. Radiochem., Engl. Transl.*, **16**, 286–7.
- Shcherbakov, V. A. and Iorga, E. V. (1975) *Sov. Radiochem., Engl. Transl.*, **17**, 763–7.
- Shen, G. T. and Dunbar, R. B. (1995) *Geochim. Cosmochim. Acta*, **59**, 2009–24.
- Shilov, V. P. (1998) *Radiochem., Engl. Transl.*, **40**, 11–16.
- Shilov, V. P. and Yusov, A. B. (2002) *Russ. Chem. Rev., Engl. Transl.*, **71**, 465–88.
- Silva, R. J. and Nitsche, H. (1995) *Radiochim. Acta*, **70–71**, 377–96.
- Skanthakumar, S., Gorman-Lewis, D., Locock, A., Chiang, M.-H., Jensen, M. P., Burns, P. C., Fein, J. B., Jonah, C. D., Attenkofer, K., and Soderholm, L. (2004) *Mater. Res. Soc. Symp. Proc.*, **802**, 151–6.
- Smith, D. A., Heeg, M. J., Heineman, W. R., and Elder, R. C. (1984) *J. Am. Chem. Soc.*, **106**, 3053–4.
- Soderholm, L., Antonio, M. R., Williams, C., and Wasserman, S. R. (1999) *Anal. Chem.*, **71**, 4622–8.
- Soderholm, L., Williams, C. W., Antonio, M. R., Tischler, M. L., and Markos, M. (2000) *Mater. Res. Soc. Symp. Proc.*, **590**, 27–32.
- Songkasiri, W., Reed, D. T., and Rittmann, B. E. (2002) *Radiochim. Acta*, **90**, 785–9.
- Sonnenberg, L. B., Johnson, J. D., and Christman, R. F. (1989) in *Aquatic Humic Substances. Influence on Fate and Treatment of Pollutants* (eds. I. H. Suffet and P. MacCarthy) (ACS Symp. Ser. 219), American Chemical Society, Washington, DC, pp. 3–23.
- Spencer, S., Gagliardi, L., Handy, N. C., Ioannou, A. G., Skylaris, C.-K., Willetts, A., and Simper, A. M. (1999) *J. Phys. Chem. A*, **103**, 1831–7.
- Spitsyn, V. I., Gelman, A. D., Krot, N. N., Mefodiyeva, M. P., Zakharova, F. A., Komkov, Y. A., Shilov, V. P., and Smirnova, I. V. (1969) *J. Inorg. Nucl. Chem.*, **31**, 2733–45.
- Spoetl, C., Unterwurzacher, M., Mangini, A., and Longstaffe, F. J. (2002) *J. Sediment. Res.*, **72**, 793–808.
- Sposito, G. (1984) *The Surface Chemistry of Soils*, Oxford University Press, Oxford.
- Sposito, G. (1990) in *Reviews in Mineralogy*, vol. 23 (eds. M. F. Hochella and A. F. White), Mineralogical Society of America, Washington DC, pp. 259–79.
- Sterne, P. A., Gonis, A., and Borovoi, A. A. (eds.) (1998) *Actinides and the Environment*, Kluwer Academic Publishers, Dordrecht.
- Stevenson, F. J. (1994) *Humus Chemistry: Genesis, Composition, Reactions*, John Wiley, New York.
- Stumpf, T., Hennig, C., Bauer, A., Denecke, M. A., and Fanghaenel, T. (2004) *Radiochim. Acta*, **92**, 133–8.

- Sturchio, N. C., Antonio, M. R., Soderholm, L., Sutton, S. R., and Brannon, J. C. (1998) *Science*, **281**, 971–3.
- Suzuki, Y., Kelly, S. D., Kemner, K. M., and Banfield, J. F. (2002) *Nature (London)*, **419**, 134.
- Suzuki, Y., Kelly, S. D., Kemner, K. M., and Banfield, J. F. (2003) *Appl. Environ. Microbiol.*, **69**, 1337–46.
- Sylwester, E. R., Hudson, E. A., and Allen, P. G. (2000) *Geochim. Cosmochim. Acta*, **64**, 2431–8.
- Szabo, Z., Moll, H., and Grenthe, I. (2000) *J. Chem. Soc., Dalton Trans.*, 3158–61.
- Szalay, A. (1991) *Geochim. Int.*, **6**, 1605–14.
- Templeton, D. H. and Templeton, L. K. (1982) *Acta Crystallogr.*, **A38**, 62–7.
- Teo, B. K. (1986) *EXAFS: Basic Principles and Data Analysis*, Springer-Verlag, Berlin.
- Teo, B. K. and Lee, P. A. (1979) *J. Am. Chem. Soc.*, **101**, 2815–32.
- Thompson, H. A., Brown, G. E., and Parks, G. A. (1995) *Physica B*, **209**, 167–8.
- Thompson, H. A., Brown, G. E., and Parks, G. A. (1997) *Am. Mineral.*, **82**, 483–96.
- Thompson, H. A., Parks, G. A., and Brown, G. E. (1998) in *Adsorption of Metals by Geomedia* (ed. E. A. Jenne), Academic Press, San Diego, pp. 349–70.
- Triay, I. R., Meijer, A., Conca, J. L., Kung, K. S., Rundberg, R. S., Strietelmeier, B. A., and Tait, C. D. (1997) *Summary and Synthesis Report on Radionuclide Retardation for the Yucca Mountain Site Characterization Project*, LA-13262, Los Alamos National Laboratory.
- Tsushima, S. and Suzuki, A. (2000) *J. Mol. Struct. (Theochem)*, **529**, 21–5.
- Tsushima, S. and Reich, T. (2001) *Chem. Phys. Lett.*, **347**, 127–32.
- Tsushima, S., Uchida, Y., and Reich, T. (2002) *Chem. Phys. Lett.*, **357**, 73–7.
- Vallet, V., Wahlgren, U., Schimmelpfennig, B., Moll, H., Szabo, Z., and Grenthe, I. (2001) *Inorg. Chem.*, **40**, 3516–25.
- Vallet, V., Moll, H., Wahlgren, U., Szabo, Z., and Grenthe, I. (2003) *Inorg. Chem.*, **42**, 1982–93.
- Vaniman, D. T., Chipera, S. J., Bish, D. L., Duff, M. C., and Hunter, D. B. (2002) *Geochim. Cosmochim. Acta*, **66**, 1349–74.
- Vasil'ev, V. Y., Andreichuk, N. N., and Rykov, A. G. (1974) *Sov. Radiochem., Engl. Transl.*, **16**, 583–6.
- Vazquez, J., Bo, C., Poblet, J. M., de Pablo, J., and Bruno, J. (2003) *Inorg. Chem.*, **42**, 6136–41.
- Veirs, D. K., Smith, C. A., Berg, J. M., Zwick, B. D., Marsh, S. F., Allen, P., and Conradson, S. D. (1994) *J. Alloys Compd.*, **213**, 328–32.
- Viswanathan, H. S., Robinson, B. A., Valocchi, A. J., and Triay, I. R. (1998) *J. Hydrol.*, **209**, 251–80.
- Wahlgren, U., Moll, H., Grenthe, I., Schimmelpfennig, B., Maron, L., Vallet, V., and Gropen, O. (1999) *J. Phys. Chem. A*, **103**, 8257–64.
- Waite, T. D., Davis, J. A., Payne, T. E., Waychunas, G. A., and Xu, N. (1994) *Geochim. Cosmochim. Acta*, **58**, 5465–78.
- Walter, M., Arnold, T., Reich, T., and Bernhard, G. (2003) *Environ. Sci. Technol.*, **37**, 2898–904.
- Wasserman, S. R. (1997) *J. Phys. IV*, **7**, 203–5.
- Wasserman, S. R., Allen, P. G., Shuh, D. K., Bucher, J. J., and Edelstein, N. M. (1999) *J. Synchrotron Radiat.*, **6**, 284–6.

- Wasserman, S. R., Soderholm, L., and Giaquinta, D. M. (2000) *Mater. Res. Soc. Symp. Proc.*, **590**, 39–44.
- Weiland, E., Wanner, H., Albinsson, Y., Wersin, P., and Karnland, O. (1994) SKB Technical Report 94-26, 64 pp.
- Williams, C. W., Blaudeau, J.-P., Sullivan, J. C., Antonio, M. R., Bursten, B. E., and Soderholm, L. (2001) *J. Am. Chem. Soc.*, **123**, 4346–7.
- Winick, H. and Nuhn, H.-D. (2003) <http://www.lightsources.org>
- Yanase, N., Isobe, H., Sato, T., Sanada, Y., Matsunaga, T., and Amano, H. (2002) *J. Radioanal. Nucl. Chem.*, **252**, 233–9.
- Yang, T., Tsushima, S., and Suzuki, A. (2001) *J. Phys. Chem. A*, **105**, 10439–45.
- Zabinsky, S. I., Rehr, J. J., Ankudinov, A., Albers, R. C., and Eller, M. J. (1995) *Phys. Rev.*, **B52**, 2995–3009.
- Zachara, J. M. and McKinley, J. P. (1993) *Aquat. Sci.*, **55**, 250–61.
- Zhang, L., Crossley, M. J., Dixon, N. E., Ellis, P. J., Fisher, M. L., King, G. F., Lilley, P. E., Mac Lachlan, D., Pace, R. J., and Freeman, H. C. (1998) *J. Biol. Inorg. Chem.*, **3**, 470–83.
- Zielen, A. J. and Cohen, D. (1970) *J. Phys. Chem.*, **74**, 394–405.
- Zubavichus, Y. V. and Slovokhotov, Y. L. (2001) *Russ. Chem. Rev., Engl. Transl.*, **70**, 373–403.